

ESCUELA TÉCNICA SUPERIOR DE INGENIERÍA DE
TELECOMUNICACIÓN
UNIVERSIDAD POLITÉCNICA DE CARTAGENA



Proyecto Fin de Carrera

Lowpass filter design for space applications in waveguide technology using alternative topologies



AUTOR: Diego Correas Serrano

DIRECTOR: Alejandro Álvarez Melcón

CODIRECTOR: Fernando Quesada Pereira

Cartagena, Enero 2013

Author	Diego Correas Serrano
Author's email	diego.correas.serrano@gmail.com
Director	Alejandro Álvarez Melcón
Director's email	alejandro.alvarez@upct.es
Co-director	Fernando Quesada Pereira
Title	Lowpass filter design for space applications in waveguide technology using alternative topologies
Summary	
<p>The main goal of this project is to study the possibility of utilizing topologies based on curved surfaces (metallic posts) to realize low pass filters in waveguide technologies, as an alternative to the traditional implementation based on rectangular irises, in order to obtain devices that present a higher multipaction threshold. In the first chapters, the theoretical synthesis techniques utilized are explained. Understanding the synthesis of the different types of filter polynomials and prototype networks is necessary in order to precisely design filters with a predictable frequency response. The commercial package HFSS will be used for the design and verification of the filters, controlling its operation with scripts in order to automate the design process.</p>	
Degree	Ingeniero de Telecomunicación
Department	Tecnologías de la Información y la Comunicación
Submission date	January 2013

Contents

1	Introduction	13
2	Synthesis of the filter function	17
2.1	Polynomial forms of the transfer and reflection parameters.	17
2.2	Alternating pole method for determination of the denominator polynomial $E(s)$	21
2.3	Chebyshev filter functions of the first kind	23
2.3.1	Recursive Technique	28
2.4	Chebyshev filter functions of the second kind	30
2.4.1	Recursive Technique	32
2.5	Achieser-Zolotarev Functions	35
2.6	Chained Functions	36
3	Synthesis of the prototype network	41
3.1	Commensurate-Line Building Elements	42
3.2	Synthesis of the Distributed Stepped Impedance lowpass filter	45
3.2.1	Mapping the Transfer Function S_{21} from the ω Plane to the θ Plane	47
3.2.2	Network Synthesis	50
3.3	Synthesis of Tapered-Corrugated lowpass filter.	55
3.3.1	Network Synthesis	60

4	Realization using alternative topologies	65
4.1	Design Technique	66
4.2	Example of filter design	71
4.3	Analysis of Results	81
4.3.1	Variation of the prescribed Return Loss level.	82
4.3.2	Variation of the Commensurate Line length θ_c	83
4.3.3	Comparison of different post topologies	86
4.3.4	Comparison of the different types of filtering functions	90
4.3.5	Using MATLAB-HFSS interaction to optimize the filter design	95
4.3.6	Effect of manufacturing errors	101
4.4	Additional topologies using conducting posts	103
4.4.1	Post-based filter with reduced waveguide heights	103
4.4.2	Multiple post implementation introducing a displacement to some of the posts	105
4.5	Realization of the Tapered-Corrugated LPF	107
5	Conclusions	113

List of Figures

2.1	Determination of roots of $E(s)$ using the alternating pole method . . .	23
2.2	Example of $x_n(\omega)$ with a prescribed transmission zero at $\omega_n = 1.2$. . .	25
2.3	Transfer and reflection of a sixth-degree Chebyshev function of the first kind with two transmission zeros	31
2.4	Transfer and reflection of Chebyshev functions of first and second kind	34
2.5	Zolotarev response with $x_1 = 0.3$ (left) and with $x_1 = 0.4$ (right) . . .	36
2.6	6th-degree all-pole Chebyshev response	37
2.7	Chained function: 3rd-degree seed function, multiplicity 2	38
2.8	Chained function: 2nd-degree seed function, multiplicity 3	38
2.9	Chained functions rejection performance	39
3.1	Commensurate-line equivalent for lumped inductor and lumped ca- pacitor	44
3.2	Unit element	44
3.3	Transfer and reflection response of a 6th-degree Chebyshev filter (nor- malized frequency)	46
3.4	Mapping of an all-pole transfer and reflection function to the θ plane. $\theta_c = 22^\circ$ (left) and $\theta_c = 30^\circ$ (right)	46
3.5	Introduction of Impedance Inverters in the Stepped Impedance LPF .	53
3.6	Stepped Impedance filter using non-unity Impedance Inverters and transmission lines of constant characteristic impedance	54

3.7	Basic element of the lumped/distributed filter	56
3.8	Eleventh-degree Chebyshev function of the second kind in the ω and θ plane.	57
4.1	Low pass filter network	67
4.2	Circuit Segment: Impedance inverter with input and output transmission lines	67
4.3	Circuit Segment realized using a conducting post	68
4.4	Ideal transfer and reflection function of the filter designed	72
4.5	Waveguide section containing two conducting posts	73
4.6	Variation of $ S_{21} $ with R (radius of posts)	74
4.7	Variation of $\angle S_{21}$ with length of WG section for each value of R	75
4.8	Sixth degree LPF realized using conducting posts pairs.	76
4.9	Frequency response of sixth degree Chebyshev LPF realized using conducting posts pairs.	77
4.10	Pass band of sixth degree Chebyshev LPF realized using conducting posts pairs.	78
4.11	LPF using traditional capacitive irises	79
4.12	Comparison of double post based filter and capacitive iris filter	80
4.13	Twelfth degree LPF using elliptical posts	80
4.14	Frequency response of twelfth degree LPF using elliptical posts	81
4.15	Comparison of frequency response varying the prescribed Return Loss	84
4.16	Comparison of frequency response varying the Commensurate Line length θ_c	86
4.17	Different post topologies to realize the LPF	87
4.18	Low pass filter using single circular posts as impedance inverters	88
4.19	Low pass filter using single elliptical posts (axis ratio 0.75) as impedance inverters	88
4.20	Low pass filter using circular posts pairs as impedance inverters	89
4.21	Low pass filter using three circular posts as impedance inverters	89

4.22	Comparison of frequency responses using different topologies	90
4.23	Ideal frequency response of sixth-degree Zolotarev filter	91
4.24	Ideal frequency response of sixth-degree (2^3) Chained Chebyshev filter	92
4.25	Frequency response of sixth-degree Zolotarev filter	93
4.26	Frequency response of sixth-degree (2^3) Chained Chebyshev filter . .	94
4.27	Comparison of frequency response using different filtering function types	94
4.28	Frequency response of three filters with the same rejection performance	97
4.29	Designated frequency point of equal rejection for the three filters . . .	97
4.30	Zolotarev and Chained filters with reduced usable bandwidth to achieve better rejection than a Chebyshev filter	99
4.31	Regular Chebyshev filter compared to reduced-bandwidth Zolotarev and Chained filters	99
4.32	Yield analysis of sixth degree Zolotarev, Chebyshev and Chained fil- ters with the same rejection performance (different prescribed Return Loss).	102
4.33	Yield analysis of sixth degree Chebyshev filter using circular posts pairs	102
4.34	Yield analysis of sixth degree K-band filter	103
4.35	Lowpass filter using reduced waveguide height	104
4.36	Frequency response of reduced waveguide height filter, compared with single post and double post filters in constant height waveguide. . . .	105
4.37	Lowpass filter using non-aligned posts	106
4.38	Frequency response of filter with non-aligned posts, compared with aligned double and triple post equivalent.	107
4.39	Tapered Corrugated prototype network	108
4.40	Basic network element of the tapered-corrugated filter	108
4.41	Basic network element of the tapered-corrugated filter (HFSS)	109
4.42	Tapered Corrugated filter using standard capacitive irises	110
4.43	Tapered Corrugated filter using curved capacitive irises	110

4.44 Frequency response of the Tapered Corrugated filters designed 111

List of Tables

2.1	Poles and zeros of a sixth-degree Chebyshev function with two transmission zeros	30
2.2	Zeros of a sixth-degree Chebyshev function with a half-zero pair . . .	34
3.1	Poles and zeros of a sixth-degree Chebyshev function in the s and t planes	54
3.2	Element values of sixth-degree Stepped Impedance Lowpass Filter . .	55
3.3	Poles and zeros of a eleventh degree Chebyshev function of the second kind in the s and t planes	63
3.4	Element values of eleventh degree Corrugated Lowpass Filter	63
4.1	Filter specification of the first filter designed	72
4.2	Inverter values and associated $ S_{21} $ for first filter designed	73
4.3	Radius values (mm) for each of the conducting posts pairs	74
4.4	Length of waveguide sections for each inverter	76
4.5	Filter specification of the first filter designed	82
4.6	Inverters values for filter designs with different prescribed Return Loss	82
4.7	Radius values (mm) for filter designs with different prescribed Return Loss	83
4.8	Computed distance between posts (mm) for filter designs with different prescribed Return Loss	83

4.9	Inverter values for filter designs with different prescribed transmission line length θ_c	85
4.10	Radius values (mm) for filter designs with different prescribed transmission line length θ_c	85
4.11	Computed distance between posts (mm) for filter designs with different prescribed transmission line length θ_c	85
4.12	Radius values (mm) for filter designs using different topologies	87
4.13	Computed distance between posts (mm) for filter designs using different topologies	88
4.14	Inverter values for filter designs using different filtering functions types	91
4.15	Radius values (mm) for filter designs using different filtering functions types	92
4.16	Computed distance between posts (mm) for filter designs using different filtering functions types	92
4.17	Computed values of Return Loss to achieve a prescribed value of attenuation	96
4.18	Radius values (mm) for filter designs using different filtering functions types, after iterative optimization	96
4.19	Computed distance between posts for filter designs using different filtering functions types, after iterative optimization	96
4.20	Usable bandwidth (return loss of 20 dB) for each type of filtering function	100
4.21	Filter specification of Tapered Corrugated Filter	110

Introduction

A filter is a frequency selective two-port network with low levels of attenuation or insertion loss in its passband and specified high levels of attenuation in its stopband. It is used to control the frequency response at a certain point in a microwave system. Typical frequency responses include low-pass, high-pass, bandpass, and band-reject characteristics. Applications can be found in virtually any type of microwave communication, radar, or test and measurement system.

This work is focused on the design of microwave lowpass filters in waveguide technology, which are of great importance in space applications since they are required to suppress the harmonics generated by the high-power amplifiers. These filters require bandwidths in the GHz range, and for this reason, the lumped-element prototypes that are commonly used for realizing narrow band bandpass and band stop filters are not applicable, and different synthesis techniques, based on distributed elements, have to be used.

Generally speaking, filter design can be summarized in three steps

1. Synthesis of the transfer and reflection polynomials for a given specification. Chebyshev functions (first or second kind) and Achieser-Zolotarev functions represent the prime candidates for derivation of the characteristic polynomials

for a lowpass filter design.

2. Synthesis of a network able to implement this filtering function.
3. Realization of the previous network, using whatever technology is most suitable for the application.

Among the vast amount of published literature on the design of microwave filters, the theory most directly related to the filters designed in this work is explained in chapters 2 and 3, corresponding to the first two steps mentioned. Chapter 4 details the utilization of alternative topologies to realize the distributed low pass filter in waveguide technology, explaining the design technique used and software developed and analyzing the results.

In waveguide low-pass filters, capacitive rectangular windows are typically employed. The presence of corners and edges causes strong singularities in the proximities (fringing fields), which can induce negative high-power effects such as multipactor and corona. This is critical for high power applications in communication satellites, since they limit the power level that a microwave filter can handle without triggering destructive phenomena. In this work we focus on exploring topologies that would improve the power handling capabilities of waveguide filters. Multipaction occurs when electrons accelerated by electromagnetic fields are self-sustained in a vacuum (or near vacuum) via electron avalanche caused by secondary electron emission. The impact of an electron to a surface can, depending on its energy and angle, release one or more secondary electrons into the vacuum. These electrons can be accelerated again by the EM fields and impact with the same or another surface. Should the impact energies, number of electrons released and timing of the impacts be such that a sustained multiplication of the number of electrons occurs, the phenomenon can grow exponentially and may lead to operational problems of the system such as distortion, high losses, or even permanent damage to the device. Traditional waveguide low pass filters are realized using capacitive irises, requiring

small distances between parallel plates, which favors the critical electron avalanche.

One of the techniques that can be employed to increase the multipactor breakdown power thresholds is to introduce modifications in the traditional rectangular waveguide filter geometry, avoiding the presence of parallel plates where the electron avalanche can take place due to the continuous "bouncing" of electrons caused by the electromagnetic fields. For instance, in [1], a bandpass filter composed of wedge waveguide sections was designed and showed better power handling thresholds than a classical rectangular waveguide implementation. This is true due to the effect produced by the slanting waveguide walls on the electron trajectories. The electrons are moved away from the critical gap regions when they impact on the wedge waveguide walls, and therefore the multipactor breakdown threshold is increased. There is some recent work on the multipactor breakdown between cylinders, works have proved that multipactor is less likely to happen between two

The same concept is applied here, where we explore the design of low pass filters based on circularly-shaped conducting posts, avoiding the presence of parallel plates. Recent works prove that multipactor breakdown is less likely to happen between cylinders than it is between parallel plates [2], [3], due to the geometrical spreading of the emitted electrons, caused by the curvature of the emitting surfaces. For the realization of filters based in these topologies, a method based on the scattering parameters of each impedance inverter will be used, adjusting the absolute value and phase of S_{11} or S_{21} in a two step design technique, using the commercial packages HFSS and MATLAB. The software developed allows the complete automation of the process for multiple topologies, most of them based on conducting posts, starting from the filtering polynomials for normalized frequency. The input parameters include the waveguide dimensions, cutoff frequency, type of filtering function, degree of the filter, maximum return loss allowed in the passband, and electric length of the transmission lines used in the distributed prototype circuit. The required HFSS

projects are automatically generated and analyzed, completing the process in a few minutes. Due to modular nature of the software, it can be easily modified to adapt the design technique to any topology. Multiple designs have been realized, starting from the mathematical synthesis of the transfer and reflection polynomials. This will allow the comparison of different type of functions and structures, in terms of passband performance, rejection, spurious response and sensitivity to manufacturing errors.

Synthesis of the filter function

In this chapter we explain the synthesis techniques for various types of frequently utilized polynomials, which will later serve as the starting point for the synthesis of the filter. The chapter starts with some theoretical background and then explains the synthesis of multiple types of filtering functions: Chebyshev of the first and second kind, Zolotarev and Chained function. For the synthesis procedure, the design parameters are the degree of the filter, the desired return loss and the transmission zeros. The software developed takes these parameters as input in order to calculate the corresponding polynomials and frequency response for each type of function, as the first step in the filter design.

2.1 Polynomial forms of the transfer and reflection parameters.

For the majority of filter circuits, we shall initially consider two-port networks, consisting of a source port and a load port. For a two-port network, the scattering matrix is represented by a 2×2 matrix

$$\begin{bmatrix} b_1 \\ b_2 \end{bmatrix} = \begin{bmatrix} S_{11} & S_{12} \\ S_{21} & S_{22} \end{bmatrix} \quad (2.1)$$

where b_1 and b_2 are the power waves propagating away from ports 1 and 2, respectively, and a_1 and a_2 are the power waves incident at ports 1 and 2, respectively. If the network is passive, lossless, and reciprocal, the previous S-parameter matrix yields two conservation of energy equations

$$S_{11}(s)S_{11}(s)^* + S_{21}(s)S_{21}(s)^* = 1 \quad (2.2)$$

$$S_{22}(s)S_{22}(s)^* + S_{12}(s)S_{12}(s)^* = 1 \quad (2.3)$$

and one orthogonality equation

$$S_{11}(s)S_{12}(s)^* + S_{21}(s)S_{22}(s)^* = 0 \quad (2.4)$$

The S parameters are assumed to be functions of the frequency variable $s = j\omega$. The reflection parameter S_{11} at port 1 is expressed as the ratio of two finite-degree polynomials $E(s)$ and $F(s)$ and the constant ε_R .

$$S_{11}(s) = \frac{F(s)/\varepsilon_R}{E(s)} \quad (2.5)$$

where $E(s)$ is an N th-degree polynomial with complex coefficients $e_0, e_1, e_2, \dots, e_N$, where N is the degree of the filter network. $F(s)$ is an N th degree polynomial with complex coefficients $f_0, f_1, f_2, \dots, f_N$. The constant ε_R allows the normalization of the highest degree coefficients of $E(s)$ and $F(s)$ to unity. Since we will consider the filter a lossless passive network, $E(s)$ is strictly Hurwitz [4], that is, all the roots of $E(s)$ are in the left half of the complex plane. The polynomial $F(s)$, for lowpass and bandpass filters is also of degree N . For band-stop filters the degree of $F(s)$ can be lower than N . The roots of $F(s)$ are the points of zero reflected power, or points of perfect transmission. By reorganizing the equation (2.2) and substituting the $S_{11}(s)$ formula, we obtain

$$S_{21}(s)S_{21}(s)^* = 1 - \frac{F(s)F(s)^*/\varepsilon_R^2}{E(s)E(s)^*} = \frac{E(s)E(s)^* - F(s)F(s)^*/\varepsilon_R^2}{E(s)E(s)^*} \quad (2.6)$$

if we call $P(s)P(s)^*/\varepsilon^2 = E(s)E(s)^* - F(s)F(s)^*/\varepsilon_R^2$

$$S_{21}(s)S_{21}(s)^* = \frac{P(s)P(s)^*/\varepsilon^2}{E(s)E(s)^*} \quad (2.7)$$

and finally the parameter $S_{21}(s)$ can be expressed as the ratio of two polynomials

$$S_{21}(s) = \frac{P(s)/\varepsilon}{E(s)} \quad (2.8)$$

It is clear from equations (2.5) and (2.8) that $S_{11}(s)$ and $S_{21}(s)$ share a common denominator polynomial $E(s)$. The numerator of $S_{21}(s)$ is a polynomial $P(s)/\varepsilon$ whose zeros are the transmission zeros of the filtering function, established as one of the design parameters of the filter. The degree n_{fz} of the polynomial $P(s)$ corresponds to the number of finite-position Tx zeros that the transfer function incorporates. This also implies that $n_{fz} \leq N$, since otherwise, it would be of a higher degree than $E(s)$, which would imply that as $s \rightarrow \infty$ $S_{21}(s)$ would be greater than unity, which is obviously impossible for a passive network.

We distinguish between *finite-position transmission zeros* and *transmission zeros at infinity*. Finite position zeros occur when the frequency variable s coincides with a root of $P(s)$. For each each root s_i that is complex there must be a second root $-s_i^*$ to make up a pair having symmetry about the imaginary axis. This ensures that polynomial $P(s)$ has coefficients that alternate between purely real and purely imaginary as the power of s increases. This is a condition that must hold if the filter is to be realized with purely reactive components. In addition, when the quantity $(N - n_{fz})$ is even, the $P(s)$ polynomial must be multiplied by j . This rule, associated with the orthogonality condition, won't be demonstrated here but a detailed explanation can be found in [4].

When $n_{fz} \leq N$, at $s = \infty$, $S_{21}(s) = 0$, and this is what we call transmission zeros at infinity. When there are no finite-position transmission zeros, the filtering

function is known as an all-pole response.

The real constant ε is determined by evaluating $P(s)/E(s)$ at a convenient value of s , where $|S_{11}(s)|$ or $|S_{21}(s)|$ are known, for instance, at $s = \pm j$, where the equiripple return loss level for Chebyshev filters is known (the maximum passband value of return loss prescribed in the synthesis)

$$\varepsilon = \frac{1}{\sqrt{10^{RL/10} - 1}} \left| \frac{P(\omega)}{F(\omega)/\varepsilon_R} \right|_{\omega=\pm 1} \quad (2.9)$$

If $n_{fz} < N$, $|S_{21}(s)| = 0$ at infinite frequency. When $|S_{21}(s)|$, the conservation of energy condition (2.2) dictates:

$$S_{11}(j\infty)S_{11}(j\infty)^* = 1 \quad (2.10)$$

which means that

$$S_{11}(j\infty) = \frac{1}{\varepsilon_R} \left| \frac{F(j\infty)}{E(j\infty)} \right| = 1 \quad (2.11)$$

and because the highest degree coefficients of $E(s)$ and $F(s)$ are unity, it is easily seen that $\varepsilon_R = 1$.

In the case of a fully canonical filter, $n_{fz} = N$, the attenuation at $s = \pm j\infty$ is different from 0 and we must obtain the expression for ε_R again. Using the same conservation of energy condition (2.2):

$$S_{11}(j\infty)S_{11}(j\infty)^* + S_{21}(j\infty)S_{21}(j\infty)^* = 1 \quad (2.12)$$

$$\frac{F(j\infty)F(j\infty)^*}{\varepsilon_R^2 E(j\infty)E(j\infty)^*} + \frac{P(j\infty)P(j\infty)^*}{\varepsilon^2 E(j\infty)E(j\infty)^*} = 1 \quad (2.13)$$

and since we're in the fully canonical case, all three polynomials are of degree N , with the highest-power coefficients being unity. Therefore, at $s = \pm j\infty$

$$\frac{1}{\varepsilon_R^2} + \frac{1}{\varepsilon^2} = 1 \longrightarrow \varepsilon_R = \frac{\varepsilon}{\sqrt{\varepsilon^2 - 1}} \quad (2.14)$$

It also follows that for the fully canonical case

$$S_{21}(\pm j\infty) = \frac{1}{\varepsilon} \quad (2.15)$$

$$S_{11}(\pm j\infty) = \frac{1}{\varepsilon_R} \quad (2.16)$$

2.2 Alternating pole method for determination of the denominator polynomial $E(s)$

In this section we explain how the polynomial $E(s)$ is generally obtained. The way it is determined is common for all the function types, since it is based on the conservation of energy condition. In the synthesis methods to be explained later, transmission zeros are prescribed in the complex plane, which immediately defines the $S_{21}(s)$ numerator polynomial $P(s)$. Then, the coefficients of the $S_{11}(s)$ numerator polynomial $F(s)$ are found using an analytic or recursive method. Finally only the common denominator $E(s)$ remains to be found. Writing the conservation of energy equation (2.2) in terms of the three polynomials, as done earlier:

$$\frac{F(s)F(s)^*}{\varepsilon_R^2 E(s)E(s)^*} + \frac{P(s)P(s)^*}{\varepsilon^2 E(s)E(s)^*} = 1 \quad (2.17)$$

$$\frac{F(s)F(s)^*}{\varepsilon_R^2} + \frac{P(s)P(s)^*}{\varepsilon^2} = E(s)E(s)^* \quad (2.18)$$

it is clear that the roots of the polynomial $E(s)E(s)^*$ can be found by using the $P(s)$ and $F(s)$ polynomials. The $2N$ roots of the polynomial $E(s)E(s)^*$ form a symmetric pattern about the imaginary axis in the complex plane, so that at any frequency s the product $E(s)E(s)^*$ is scalar. Since $E(s)$ is strictly Hurwitz, those roots that are in the left-half plane belong to $E(s)$, with the ones in the right-hand

plane belonging to $E(s)^*$, and thus, the $E(s)$ polynomial can be formed.

This method, however, implies that we have to work with polynomials of degree $2N$, which can cause imprecisions for higher degree filter functions, and thus, the *alternating pole method* is usually utilized, since it allows the root-finding directly using the $P(s)$ and $F(s)$, that is, N th-degree polynomials. A detailed demonstration can be found in [4], starting by expanding equation (2.18). This method is only usable when all the zeros of $F(s)$ lie on the imaginary axis and are coincident with those of $F_{22}(s)$, which is usually the case for most filtering functions. If this condition is fulfilled, we can find $E(s)$ by means of the following equation

$$\varepsilon^2 \varepsilon_R^2 E(\omega) E(\omega)^* = [\varepsilon_R P(\omega) - j \varepsilon F(\omega)] [\varepsilon_R P(\omega) - j \varepsilon F(\omega)]^* \quad (2.19)$$

Rooting one of the two terms on the right-hand side of (2.19) results in a pattern of singularities alternating between the left-half and right-half planes. Rooting the other term will give the complementary set of singularities, completing the symmetry of the pattern about the imaginary axis and ensuring that the RHS of (2.19) is properly scalar as the LHS demands. Knowing that the polynomial $E(s)$ must be Hurwitz, we can find its roots by calculating only one of the terms, and reflecting to the left half-plane any singularity lying in the right-half plane. Finally, the polynomial $E(s)$ can be formed.

Figure 2.1 shows an example of usage of this method, to determine the roots of the $E(s)$ polynomial for an arbitrary *8th – degree* Chebyshev function.

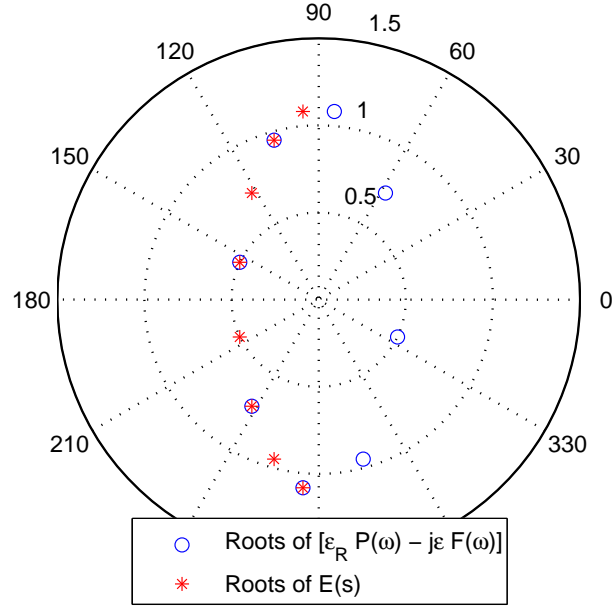


Figure 2.1: Determination of roots of $E(s)$ using the alternating pole method

2.3 Chebyshev filter functions of the first kind

For convenience, we will work in the ω variable, where $s = j\omega$

$$S_{11}(\omega) = \frac{F(\omega)/\varepsilon_R}{E(\omega)} \quad (2.20)$$

$$S_{21}(\omega) = \frac{P_N(\omega)}{\varepsilon E_N(\omega)} \quad (2.21)$$

$$\varepsilon = \frac{1}{\sqrt{10^{RL/10} - 1}} \left| \frac{P(\omega)}{F(\omega)/\varepsilon_R} \right|_{\omega=\pm 1} \quad (2.22)$$

As seen earlier, it is assumed that the polynomials $P(\omega)$, $F(\omega)$, and $E(\omega)$ are normalized such that their highest degree coefficients are unity. $S_{11}(\omega)$ and $S_{21}(\omega)$ share a common denominator $E(\omega)$, and the polynomial $P(\omega) = \prod_{n=1}^{n_{fz}} (\omega - \omega_n)$ carries n_{fz} transfer function finite-position transmission zeros. For a Chebyshev filter

function ε is a constant normalizing S_{21} to the equiripple level at $\omega = \pm 1$.

Let us define the function $C_N(\omega) = \frac{F(\omega)}{P(\omega)}$. This function is known as the filtering function of degree N , and its poles and zeros are the roots of $P(\omega)$ and $F(\omega)$, respectively. For the general Chebyshev characteristic, it has the form

$$C_N(\omega) = \cosh \left[\sum_{n=1}^N \cosh^{-1}(x_n(\omega)) \right] \quad (2.23)$$

or, by using the identity $\cosh \theta = \cos j\theta$, the alternative expression for $C_N(\omega)$ is given by

$$C_N(\omega) = \cos \left[\sum_{n=1}^N \cos^{-1}(x_n(\omega)) \right] \quad (2.24)$$

To properly represent a Chebyshev function, $x_n(\omega)$ requires the following properties:

- At $\omega = \omega_n$ where ω_n is a finite-position prescribed transmission zero, or where ω_n is at infinite frequency ($\omega_n = \pm\infty$), $x_n(\omega = \pm\infty)$
- At $\omega = \pm 1$, $x_n(\omega) = \pm 1$
- Between $\omega = -1$ and $\omega = 1$ (in-band), $1 \geq x_n(\omega) \geq -1$

The first condition is satisfied if $x_n(\omega)$ is a rational function with its denominator equal to $(\omega - \omega_n)$

$$x_n(\omega) = \frac{f(\omega)}{\omega - \omega_n} \quad (2.25)$$

if we use this equation for the second condition

$$x_n(\omega)|_{\omega=\pm 1} = \frac{f(\omega)}{\omega - \omega_n} \Big|_{\omega=\pm 1} = \pm 1 \quad (2.26)$$

This condition is satisfied if $f(1) = 1 - \omega_n$ and $f(-1) = 1 + \omega_n$, giving $f(\omega) = 1 - \omega\omega_n$. Therefore

$$x_n(\omega) = \frac{1 - \omega\omega_n}{\omega - \omega_n} \quad (2.27)$$

For the previous expression of $x_n(\omega)$ there are no turning or inflection points between $\omega = -1$ and $\omega = 1$, which implies that the third condition is also satisfied,

considering that $x_n(\omega) = -1$ at $\omega = -1$ and $x_n(\omega) = 1$ at $\omega = 1$. Finally, we divide by ω_n to deal with any transmission zeros at $\omega_n = \pm\infty$, obtaining the final expression for $x_n(\omega)$

$$x_n(\omega) = \frac{\omega - 1/\omega_n}{1 - \omega/\omega_n} \quad (2.28)$$

In equation (2.28), the transmission zero ω_n in the ω plane, as expected, relates to each of the prescribed transmission zeros in the s plane by $\omega_n = s_n/j$.

Figure 2.2 shows an example of the $x_n(\omega)$ function, with a prescribed transmission zero at $\omega = 1.2$.

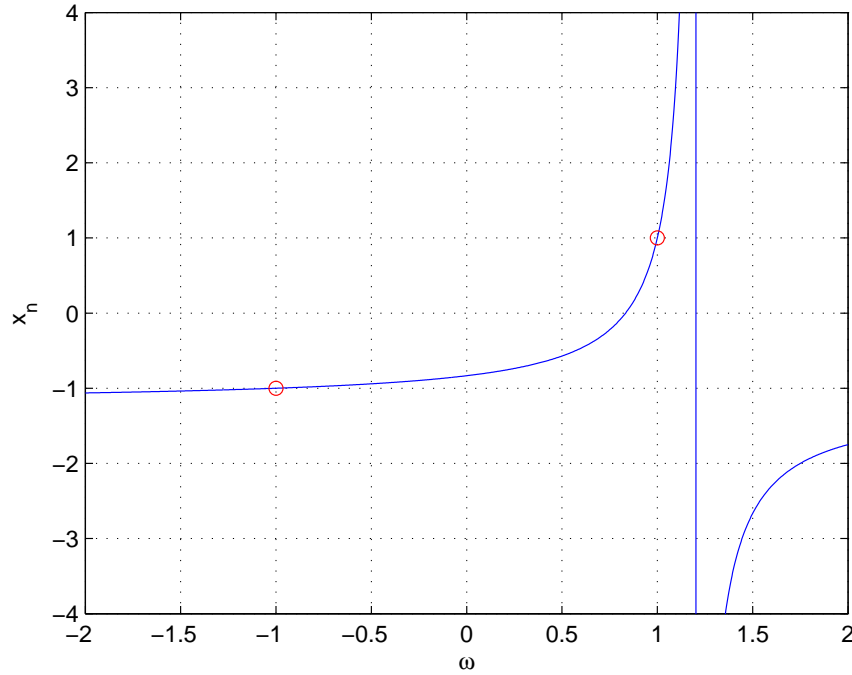


Figure 2.2: Example of $x_n(\omega)$ with a prescribed transmission zero at $\omega_n = 1.2$

As mentioned in an earlier section, the rule in prescribing the positions of the transmission zeros are that symmetry must be preserved about the imaginary axis ($j\omega$) of the complex s plane, to ensure that the unitary conditions are preserved.

If all N transmission zeros w_n approach infinity (all-pole response), $C_N(\omega)$ takes the following form

$$C_N(\omega)|_{\omega_n \rightarrow \infty} = \cosh [N \cosh^{-1}(\omega)] \quad (2.29)$$

Knowing the expression of the filtering function $C_N(\omega)$ from equation (2.23), the normalizing constant ε from equation (2.22) and the prescribed polynomial $P(\omega) = \prod_{n=1}^{n_{fz}} (\omega - \omega_n)$, the next step is to find the numerator of $C_N(\omega)$, to obtain $F(\omega)$, in order to be able to use the alternating pole method to obtain $E(\omega)$, completing the transfer and reflection Chebyshev functions.

Writing equation (2.23) in a different form, applying the \cosh^{-1} identity

$$\operatorname{acosh}(x) = \ln \left(x + \sqrt{x^2 - 1} \right) \quad (2.30)$$

we obtain

$$C_N(\omega) = \cosh \left[\sum_{n=1}^N \ln \left(x_n(\omega) + \sqrt{x_n(\omega)^2 - 1} \right) \right] \quad (2.31)$$

let us define

$$a_n = x_n(\omega) \text{ and } b_n = (x_n(\omega)^2 - 1)^{1/2}. \quad (2.32)$$

Then

$$C_N(\omega) = \cosh \left[\sum_{n=1}^N \ln(a_n + b_n) \right] \quad (2.33)$$

Applying the *cosh* exponential formula

$$\begin{aligned} C_N(\omega) &= \frac{1}{2} \left[e^{\sum_{n=1}^N \ln(a_n + b_n)} + e^{-\sum_{n=1}^N \ln(a_n + b_n)} \right] \\ &= \frac{1}{2} \left[\prod_{n=1}^N (a_n + b_n) + \frac{1}{\prod_{n=1}^N (a_n + b_n)} \right] \end{aligned} \quad (2.34)$$

By multiplying the second term in equation (2.34) top and bottom by $\prod_{n=1}^N (a_n - b_n)$ we obtain

$$C_N(\omega) = \frac{1}{2} \left[\prod_{n=1}^N (a_n + b_n) + \prod_{n=1}^N (a_n - b_n) \right] \quad (2.35)$$

since the product $\prod_{n=1}^N (a_n + b_n) \cdot \prod_{n=1}^N (a_n - b_n) = \prod_{n=1}^N (a_n^2 - b_n^2) = 1$ (see form of a_n and b_n in (2.32)). Finally, substituting a_n , b_n and x_n expressions from equations (2.32) and (2.28) in equation (2.35), the final expression of $C_N(\omega)$ is found

$$C_N\omega = \frac{1}{2} \left[\frac{\prod_{n=1}^N (c_n + d_n) + \prod_{n=1}^N (c_n - d_n)}{\prod_{n=1}^N (1 - \omega/\omega_n)} \right] \quad (2.36)$$

where

$$c_n = \left(\omega - \frac{1}{\omega_n} \right) \quad \text{and} \quad d_n = \omega' \sqrt{1 - \frac{1}{\omega_n^2}} \quad (2.37)$$

and ω' is a transformed frequency variable

$$\omega' = \sqrt{(\omega^2 - 1)} \quad (2.38)$$

comparing (2.36) with the general expression of $C_N(\omega) = \frac{F(\omega)}{P(\omega)}$, it is clear that the denominator of (2.36) corresponds to $P(\omega)$, the polynomial containing the transmission zeros. The numerator corresponds to $F(\omega)$, the numerator of $S_{11}(\omega)$. The numerator of (2.36) appears to be a mixture of two polynomials in two different variables, ω and ω' , but it can be proven that the terms in the ω' variable cancel each other when equation (2.36) is expanded. This can be seen with an example

$$\begin{aligned} \text{For } N = 1, \text{ Num}[C_1(\omega)] &= \frac{1}{2} \left[\prod_{n=1}^1 (c_n + d_n) + \prod_{n=1}^1 (c_n - d_n) \right] = c_1. \\ \text{For } N = 2, \text{ Num}[C_2(\omega)] &= c_1 c_2 + d_1 d_2. \\ \text{For } N = 2, \text{ Num}[C_3(\omega)] &= (c_1 c_2 + d_1 d_2) c_3 + (c_2 d_1 + c_1 d_2) d_3. \end{aligned} \quad (2.39)$$

A product of an even number of d_n elements will always eliminate the ω' form of the polynomial, since $\omega' = \sqrt{(\omega^2 - 1)}$. In the cases where we have a product of an odd number of d_n elements, they will cancel out because of the different sign in the two product terms in equation (2.36). As a result of this, the numerator of $C_N(\omega)$ will be a polynomial purely in the variable ω , and its roots will be exactly those of the polynomial $F(\omega)$. Next we will explain the recursive technique used to obtain this polynomial.

2.3.1 Recursive Technique

The numerator of equation (2.36) can be written as

$$Num[C_N(\omega)] = \frac{1}{2} [G_N(\omega) + G'_N(\omega)] \quad (2.40)$$

where

$$G_N(\omega) = \prod_{n=1}^N [c_n + d_n] = \prod_{n=1}^N \left[\left(\omega - \frac{1}{\omega_n} \right) + \omega' \sqrt{1 - \frac{1}{\omega_n^2}} \right] \quad (2.41)$$

and

$$G'_N(\omega) = \prod_{n=1}^N [c_n - d_n] = \prod_{n=1}^N \left[\left(\omega - \frac{1}{\omega_n} \right) - \omega' \sqrt{1 - \frac{1}{\omega_n^2}} \right] \quad (2.42)$$

In the method used to compute the coefficients of the numerator of $C_N(\omega)$, the solution for the n th degree is constructed from the results of the $(n-1)$ th degree polynomials. Let us define the polynomial $G_N(\omega)$ as a sum of two polynomials $U_N(\omega)$ and $V_N(\omega)$, where the $U_N(\omega)$ polynomial contains purely coefficients of the terms in the variable ω , whereas each coefficient of the auxiliary polynomial $V_N(\omega)$ is multiplied by the variable ω' .

$$G_N(\omega) = U_N(\omega) + V_N(\omega) \quad (2.43)$$

$$U_N(\omega) = u_0 + u_1\omega + u_2\omega^2 + \dots + u_N\omega^N \quad (2.44)$$

$$V_N(\omega) = \omega'(v_0 + v_1\omega + v_2\omega^2 + \dots + v_N\omega^N) \quad (2.45)$$

Starting with the first prescribed transmission zero, ω_1 :

$$\begin{aligned} G_1(\omega) &= c_1 + d_1 = \left(\omega - \frac{1}{\omega_1}\right) + \omega' \sqrt{\left(1 - \frac{1}{\omega_1^2}\right)} \\ &= U_1(\omega) + V_1(\omega) \end{aligned} \quad (2.46)$$

In the next iteration, $G_1(\omega)$ has to be multiplied by the term corresponding to the second prescribed zero ω_2 .

$$\begin{aligned} G_2(\omega) &= G_1(\omega) \cdot (c_2 + d_2) = [U_1(\omega) + V_1(\omega)] \left[\left(\omega - \frac{1}{\omega_2}\right) + \omega' \sqrt{\left(1 - \frac{1}{\omega_2^2}\right)} \right] \\ &= U_2(\omega) + V_2(\omega) \end{aligned} \quad (2.47)$$

If we multiply out this equation, we obtain

$$U_2(\omega) = \omega U_1(\omega) - \frac{U_1(\omega)}{\omega_2} + \omega' \sqrt{\left(1 - \frac{1}{\omega_2^2}\right)} V_1(\omega) \quad (2.48)$$

$$V_2(\omega) = \omega V_1(\omega) - \frac{V_1(\omega)}{\omega_2} + \omega' \sqrt{\left(1 - \frac{1}{\omega_2^2}\right)} U_1(\omega) \quad (2.49)$$

This process is repeated with the rest of prescribed zeros. If the same process is repeated for $G'_N(\omega) = U'_N(\omega) + V'_N(\omega)$, it can be shown that $U'_N(\omega) = U_N(\omega)$ and $V'_N(\omega) = -V_N(\omega)$. Therefore, we conclude that

$$Num[C_N(\omega)] = \frac{1}{2} [G_N(\omega) + G'_N(\omega)] = \frac{1}{2} \cdot (2 \cdot U_N(\omega)) = U_N(\omega) \quad (2.50)$$

This equation demonstrates that the numerator of $C_N(\omega)$ is equal to $F(\omega)$ when the recursive method has been completed. Rooting this polynomial, the roots of

Roots of $F(s)$	Roots of $E(s)$	Roots of $P(s)$
$-0.9522j$	$-0.2482 - 1.2160j$	$+j1.45$
$-0.6041j$	$-0.6239 - 0.7445j$	$+j2.3$
$-0.0643j$	$-0.7175 - 0.0388j$	$j\infty$
$+0.8135j$	$-0.2961 + 0.9525j$	$j\infty$
$+0.4557j$	$-0.0856 + 1.0893j$	$j\infty$
$+0.9802j$	$-0.5523 + 0.5862j$	$j\infty$
$\varepsilon = 4.3871$		$\varepsilon_R = 1$

Table 2.1: Poles and zeros of a sixth-degree Chebyshev function with two transmission zeros

$F(\omega)$ are found, and since $P(\omega)$ is formed directly from the prescribed transmission zeros, the only polynomial left to obtain is $E(\omega)$, which can be immediately calculated using the alternating pole method explained in the previous section. The software implemented, as the first part of the filter design, takes as input the degree of the filter, the prescribed return loss, and the prescribed transmission zeros. Then, using the recursive technique, and then applying the alternating pole method, all three polynomials that define the transfer and reflection functions are obtained.

As an example, Table 2.1 shows the roots of all three polynomials for an arbitrary 6th degree filter with an equiripple return loss of 26 dB and prescribed zeros at $+j1.45$ and $+j2.3$. Figure 2.3 shows the frequency response of this filter.

2.4 Chebyshev filter functions of the second kind

The tapered-corrugated lowpass filter functions require Chebyshev polynomials of the second kind, with one symmetric half-zero pair of transmission zeros, due to the structure of the circuit used to implement the filtering function. A more detailed explanation is given in the next chapter. The transfer and reflection functions of the

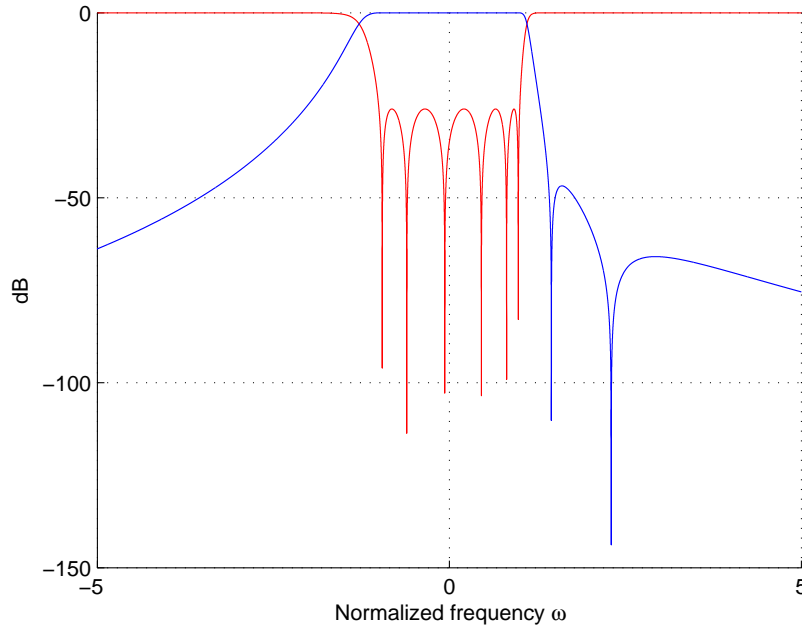


Figure 2.3: Transfer and reflection of a sixth-degree Chebyshev function of the first kind with two transmission zeros

Chebyshev filter function of the second kind have the form

$$S_{11}(\omega) = \frac{F(\omega)}{E(\omega)} \quad (2.51)$$

$$S_{21}(\omega) = \frac{P(\omega)}{\varepsilon E(\omega)} = \frac{\sqrt{\omega^2 - a^2}}{\varepsilon E(\omega)} \quad (2.52)$$

The $P(\omega)$ polynomial can be formed immediately from the prescribed transmission zeros. The N th-degree filtering function for the Chebyshev function of the second kind for up to N half-zero pairs is generated by a zero-mapping formula and recursive method, similar to that used for the generation of the Chebyshev function of the first kind

$$C_N(\omega) = \frac{F(\omega)}{P(\omega)} = \cosh \left[\sum_{n=1}^N \cosh^{-1}(x_n) \right] \quad (2.53)$$

where

$$x_n = \omega \sqrt{\frac{(1 - 1/\omega_n^2)}{(1 - \omega^2/\omega_n^2)}} \quad (2.54)$$

$$a_n = x_n \quad (2.55)$$

$$b_n = \sqrt{x_n^2 - 1} = \frac{\omega'}{\sqrt{(1 - \omega^2/\omega_n^2)}} \quad (2.56)$$

where ω' is the transformed frequency variable, as before

$$\omega' = \sqrt{\omega^2 - 1} \quad (2.57)$$

Using the previous notation, the C_N polynomial is formed

$$\begin{aligned} C_N(\omega) &= \frac{\prod_{n=1}^N [\omega \sqrt{(1 - 1/\omega_n^2)} + \omega'] + \prod_{n=1}^N [\omega \sqrt{(1 - 1/\omega_n^2)} - \omega']}{2 \prod_{n=1}^N \sqrt{(1 - \omega^2/\omega_n^2)}} \\ &= \frac{\prod_{n=1}^N [c_n + d_n] + \prod_{n=1}^N [c_n - d_n]}{2 \prod_{n=1}^N \sqrt{(1 - \omega^2/\omega_n^2)}} \end{aligned} \quad (2.58)$$

where

$$c_n = \omega \sqrt{(1 - 1/\omega_n^2)} \quad (2.59)$$

$$d_n = \omega' \quad (2.60)$$

2.4.1 Recursive Technique

The recursive method is very similar as that shown for the Chebyshev functions of the first kind. Using the same terminology, where U_n are the polynomials in the ω variable and V_n are in the ω' variable

$$G_N(\omega) = \prod_{n=1}^N [c_n + d_n] = U_N(\omega) + V_N(\omega) \quad (2.61)$$

For the first iteration

$$U_1(\omega) = \omega \sqrt{(1 - 1/\omega_n^2)} \quad (2.62)$$

$$V_1 = \omega' \quad (2.63)$$

In the second iteration

$$G_2(\omega) = (U_1(\omega) + V_1(\omega)) \cdot (\omega \sqrt{1 - 1/\omega_2^2} + \omega') \quad (2.64)$$

To find $U_2(\omega)$ and $V_2(\omega)$ we have to expand the product and separate the polynomials in the two variables ω and ω'

$$U_2(\omega) = U_1(\omega) \cdot \omega \sqrt{1 - 1/\omega_2^2} + \omega' \cdot V_1(\omega) \quad (2.65)$$

$$V_2(\omega) = V_1(\omega) \cdot \omega \sqrt{1 - 1/\omega_2^2} + \omega' \cdot U_1(\omega) \quad (2.66)$$

notice how the product of the $V_1(\omega)$ polynomial and ω' yields a ω polynomial, belonging to $U_2(\omega)$, since $\omega' = \sqrt{\omega^2 - 1}$. Similarly, the term $\omega' \cdot U_1(\omega)$ belongs to the ω' polynomial $V(\omega)$ because it has all its elements multiplied by ω' . The same is repeated until all zeros (including those at infinity) are used. Finally, the roots of the polynomial $U_N(\omega)$ are the same as those of $F(\omega)$ and only the $E(\omega)$ polynomial remains to be found. For odd numbers of half-zero pairs the alternating-pole method cannot be used directly to create the coefficients of $E(\omega)$, due to the square root in the numerator of $S_{21}(\omega)$. However, it is shown in the next chapter, in the section on tapered-corrugated LPFs, that in this case, after transformation to the t -plane

$S_{21}(t)$ will always have an even number of half-zeros, meaning that in the t plane the square root disappears and the polynomial $P(t)$ can be formed, enabling the use of the alternating pole method to find $E(t)$.

As an example, we apply the synthesis procedure for a seventh degree filter with $RL = 26dB$ and a symmetric half-zero pair at $\pm j2.4$.

Roots of $F(s)$
$\pm 0.9762j$
$\pm 0.7901j$
$\pm 0.4433j$
0

Table 2.2: Zeros of a sixth-degree Chebyshev function with a half-zero pair

Figure 2.4 shows the frequency response corresponding to this filter and compares it with a first kind Chebyshev filter with a zero pair at the same frequency $\pm j2.4$

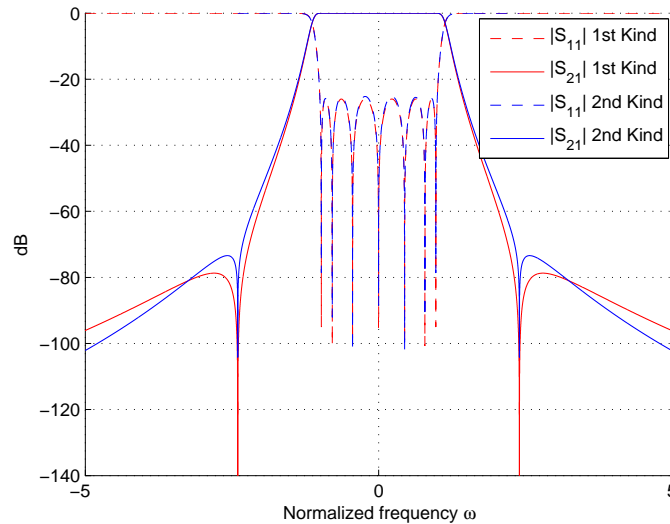


Figure 2.4: Transfer and reflection of Chebyshev functions of first and second kind

We see that the Chebyshev function of the second kind presents thinner zeros

than the first kind, resulting in less close to band selectivity for zeros in the same position, although the far out of band rejection is slightly better.

2.5 Achieser-Zolotarev Functions

Achieser-Zolotarev functions are similar to the Chebyshev functions in that they have an equiripple characteristic. The difference is that they possess an extra design parameter that allows the peak nearest to the origin to exceed the preset equiripple level. The reason that the Zolotarev function is valuable in the design of LPFs is that it tends to yield better element values with less abrupt transitions and greater internal gap dimensions that help with high power design. The out-of-band rejection is slightly better than that of the Chebyshev functions.

The all-pole even-degree Achieser-Zolotarev function is easily generated from the zeros of the Chebyshev function of the first kind, of the same degree and prescribed return loss level through the following mapping formula

$$s'_k = \pm \sqrt{s_k^2(1 - x_1^2) - x_1^2} \quad (2.67)$$

where s_k is the original position of the singularity in the complex s plane, s'_k is the transformed position, and x_1 ($|x_1| < 1$) is the frequency point in the band at which the equiripple behavior starts.

The mapping formula is applied to the roots of $F(s)$ of the original Chebyshev polynomial (first or second kind), obtained through the use of the recursive technique. Then, the polynomial $E(s)$ is formed using the alternating pole method. When $x_1 = 0$, the even-degree Zolotarev function degenerates to the pure all-pole Chebyshev function.

Figure 2.5 shows two Zolotarev responses, for an arbitrary 8th degree filter for two values of the parameter x_1 , 0.3 and 0.4

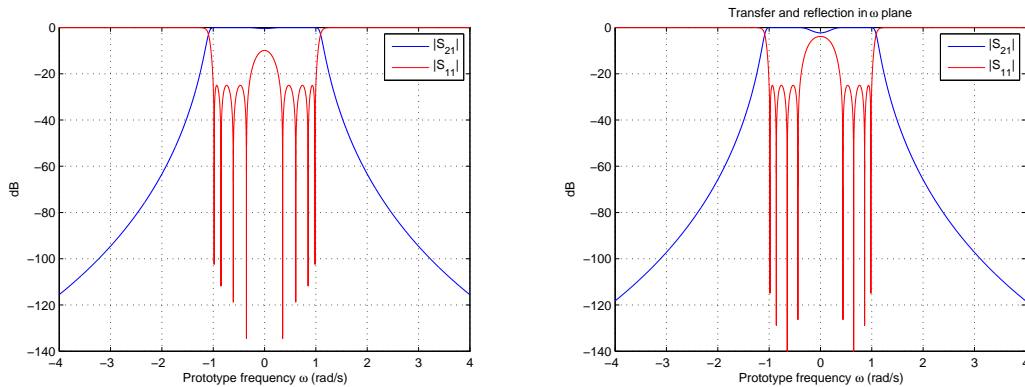


Figure 2.5: Zolotarev response with $x_1 = 0.3$ (left) and with $x_1 = 0.4$ (right)

For higher values of x_1 we will get slightly better rejection at the cost of usable bandwidth, since the high reflection central lobe becomes wider.

2.6 Chained Functions

This family of filters exhibits a reduced sensitivity to manufacturing errors while maintaining a maximum inband return loss. Chained functions are formed by combining filtering polynomials of lower degree (seed function) [5]

$$G_m(\omega) = \prod_{i=1}^k C_{n_i}(\omega) \quad (2.68)$$

where $G_m(\omega)$ is an m th-degree Chained function and $C_{n_i} = \frac{F(\omega)}{P(\omega)}$ is the n th-degree seed function i . By chaining a seed function with itself k times we obtain zeroes of multiplicity k . Knowing $G_m(\omega)$, which contains two of the three characteristic polynomials, the remaining polynomial $E(\omega)$ can be easily obtained using the Alternating Pole Method. These filters present a reduced sensitivity since they are based on lower degree polynomials, and are realizable as long as the seed functions are realizable. However, chained filters present a worse rejection performance compared to regular functions of the same total degree.

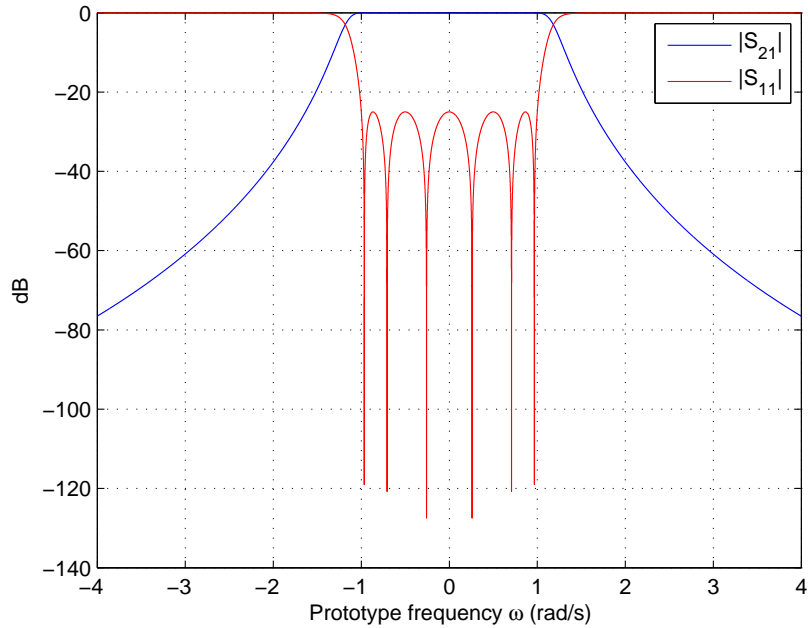


Figure 2.6: 6th-degree all-pole Chebyshev response

As an example, we will compare a regular 6th-degree all-pole Chebyshev filter (Figure 2.6) with the equivalent 6th-degree Chained functions, built with Chebyshev polynomials of lower degree: 3rd and 2nd degree, multiplicity 2 and 3 respectively (Figures 2.7 and 2.8). It is clearly appreciated that despite all filters being of degree 6, the number of reflection zeros corresponds to that of the seed function, with different multiplicity. Figure 2.9 shows the different rejection performances. As expected, seed functions of lower degree present worse out of band rejection.

When designing lowpass filters, it is not usually required that the entire pass band presents the same level of Return Loss, since the range of frequencies that will actually be used is only a fraction of the passband. Knowing this, and depending on the bandwidth required, we can design a Chained filter with a higher return loss than the specifications allows (which translates into better rejection), as long as one of the zeros falls on the desired range of frequencies. Doing this we can design a filter that presents better rejection performance than a Chebyshev or Zolotarev

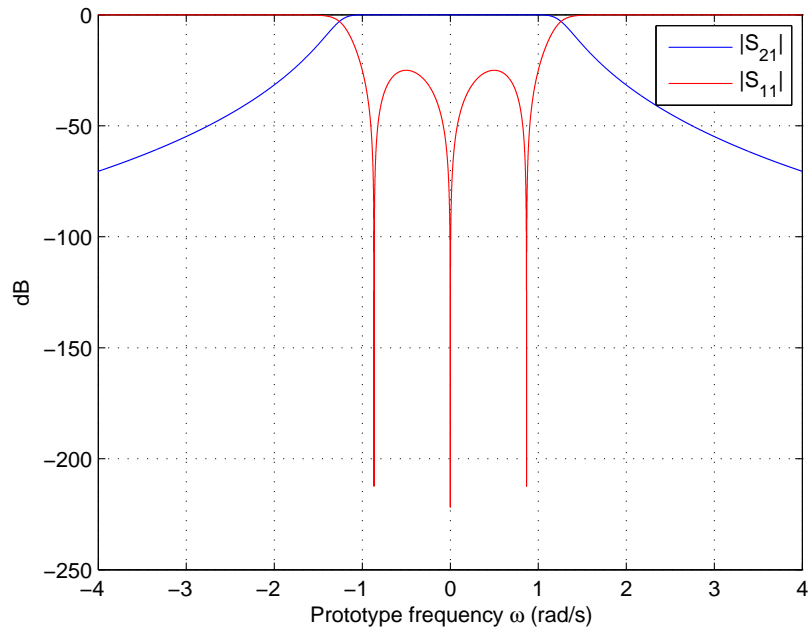


Figure 2.7: Chained function: 3rd-degree seed function, multiplicity 2

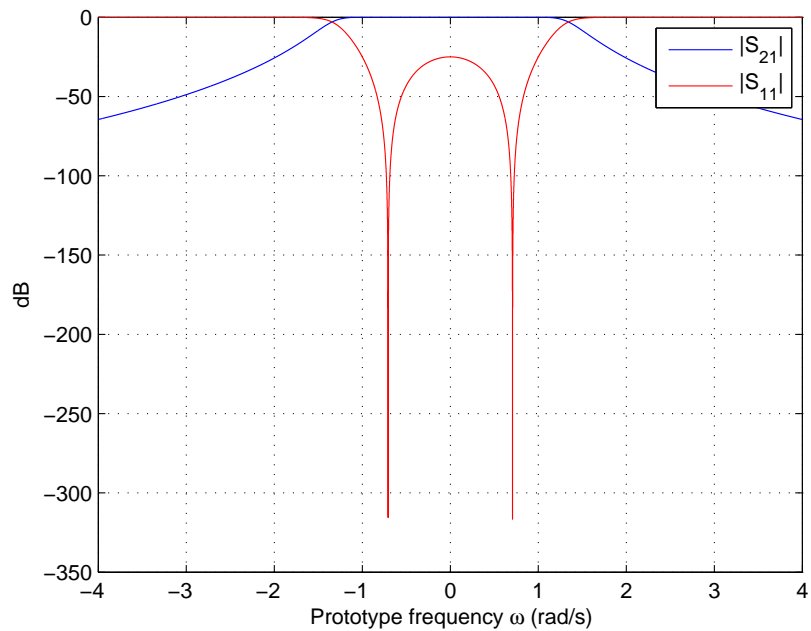


Figure 2.8: Chained function: 2nd-degree seed function, multiplicity 3

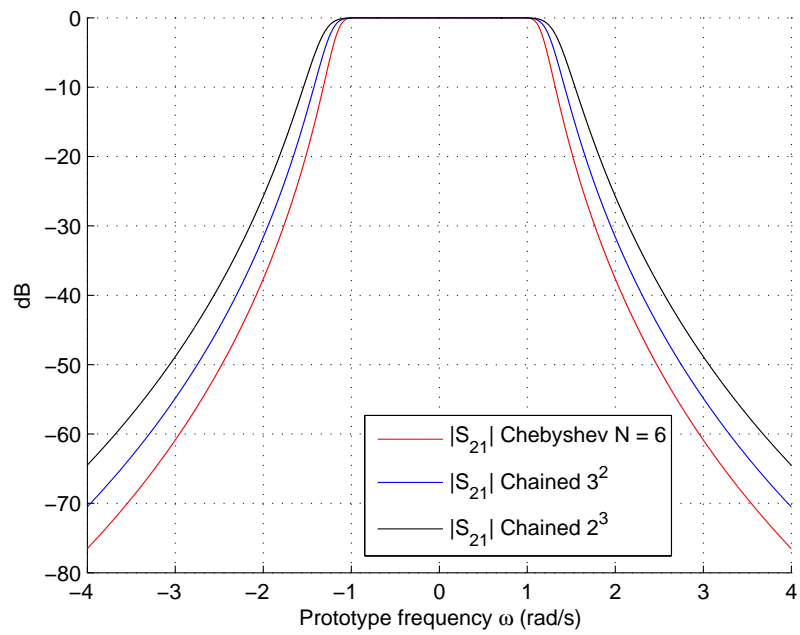


Figure 2.9: Chained functions rejection performance

filter. Examples of this concept can be found in chapter 4.

Chapter 3

Synthesis of the Distributed Low Pass Filter Prototype Network

The polynomials obtained in the previous chapter will be used here to synthesize a distributed LPF prototype circuit, which can then be realized in rectangular waveguide, coaxial transmission-line, or planar (TEM) technology. The different steps in the realization of the final lowpass filter, automated by the software developed, are explained in detail. We will review the synthesis of the the Stepped Impedance and the Tapered-Corrugated LPF prototype networks. These structures can support only certain types of filter functions [4]:

Stepped Impedance

- All-pole functions (no transmission zeros)
- Even or odd degree functions

Tapered Corrugated

- Only odd-degree polynomials can be realized
- One pair of half-zeros necessary in the transfer polynomials
- Chebyshev functions of the second kind with a half zero pair

- Zolotarev functions, also with a half-zero pair

For the stepped impedance filters, all-pole Chebyshev functions of the first kind or Zolotarev functions are most suitable (including Chained versions), whereas for the tapered-corrugated filters, Chebyshev polynomials of the second kind with one pair of half-zeros will be used, due to the prototype circuit presenting a half-zero pair.

First, the transmission line elements that go will go into the lowpass prototype network are examined and explained. Then, we study the transforms that are used in the synthesis of the Stepped Impedance lowpass filter, deduce the transfer polynomials that model this structure, and match them with the polynomials corresponding to the filtering function, obtaining the values of the network elements that give the desired frequency response. Finally, a similar procedure is applied to the tapered corrugated lowpass prototype. Most of the theory explained here can be found in [4].

3.1 Commensurate-Line Building Elements

The commensurate-line element is an essential component in the realization of microwave filters. These are short-lengths transmission lines, all of the same electrical length θ_c . With these elements, the distributed equivalents of lumped capacitors and inductors may be created. Commensurate elements have the same sign and value as those of their lumped equivalents, but their frequency dependence varies as $t = j \tan \theta$ instead of $s = j\omega$, where $\theta = \frac{\omega l}{v_p} = \frac{2\pi l}{\lambda} = \beta l$ is the electrical length of the element at frequency ω , l is the physical length of the commensurate line, and v_p is the velocity of propagation in the transmission-line.

Assuming that v_p is constant at all frequencies, $\theta_0 = \omega_0 l / v_p$, where θ_0 is the electrical length at a reference frequency ω_0 . This yields $\theta = (\omega / \omega_0) \cdot \theta_0$, the frequency variable θ , in terms of ω . The transform $t = j \cdot \tan \theta$ is known as *Richard's*

transform, and is used extensively as the frequency variable in commensurate-line networks.

A given lumped element and its commensurate-line equivalent have the same value of impedance or admittance at the frequency f_c at which the length of line is θ_c radians, but as the frequency moves away from f_c the values start to differ. The difference is a very important one, as the lumped element's reactance changes monotonically with frequency, whereas the distributed component's reactance is cyclic, repeating every π radians. The equivalence between these Commensurate-Line elements and the lumped counterparts can be easily proved if we take the known expression of the input impedance of a transmission line of characteristic impedance Z_0 ended in an impedance Z_L :

$$Z_{in} = Z_0 \cdot \frac{Z_L + jZ_0 \tan \theta}{Z_0 + jZ_L \tan \theta} \quad (3.1)$$

If we assume a short-circuited stub, $Z_L = 0$

$$Z_{in} = Z_0 \cdot \frac{jZ_0 \tan \theta}{Z_0} = jZ_0 \tan \theta = tZ_0 \quad (3.2)$$

which has the same form as the impedance of a series inductor $Z = j\omega L$, with a different frequency variation (repeating every π radians), as mentioned before.

Now, if we assume an open-circuited stub, $Z_L = \infty$

$$Z_{in} = Z_0 \cdot \frac{Z_L}{jZ_L \tan \theta} = -jZ_0 \cdot \frac{1}{\tan \theta}$$

$$Y_{in} = jY_0 \tan \theta = tY_0 \quad (3.3)$$

which has the same form as the admittance of a shunt capacitor.

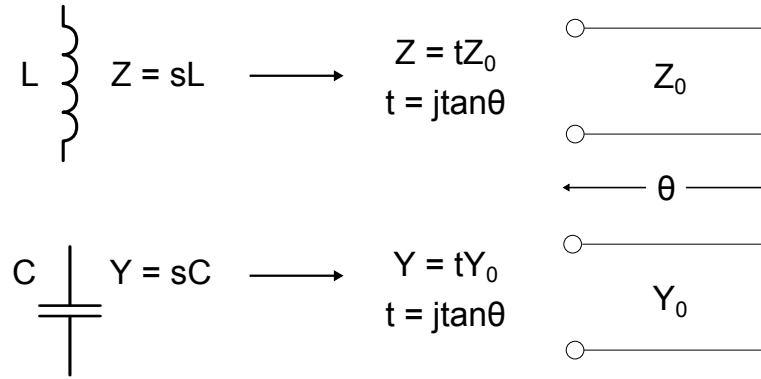


Figure 3.1: Commensurate-line equivalent for lumped inductor and lumped capacitor

In principle, then, the inductors and capacitors of a lumped-element filter design can be replaced with short-circuited and open-circuited stubs.

From now on, we will refer to the generic transmission line element of length θ and characteristic impedance Z with the term *unit element (UE)*. Its associated $[ABCD]$ matrix is shown in (3.4)

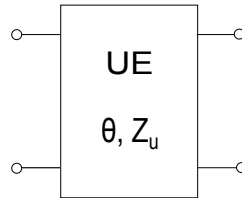


Figure 3.2: Unit element

$$\begin{bmatrix} A & B \\ C & D \end{bmatrix} = \begin{bmatrix} \cos \theta & jZ_u \sin \theta \\ j \sin \theta / Z_u & \cos \theta \end{bmatrix} \quad (3.4)$$

$$\begin{bmatrix} A & B \\ C & D \end{bmatrix} = \frac{1}{\sqrt{(1-t^2)}} \cdot \begin{bmatrix} 1 & Z_u t \\ t / Z_u & 1 \end{bmatrix} \quad (3.5)$$

Equation (3.5) is immediately obtained by using the identities $\cos \theta = 1/\sqrt{1 + \tan^2 \theta}$ and $\sin \theta = \tan \theta/\sqrt{1 + \tan^2 \theta}$ and then applying $t = j \tan \theta$.

3.2 Synthesis of the Distributed Stepped Impedance lowpass filter

The stepped-impedance filter is an approximation to the low-pass filter using the commensurate line elements seen in the previous section (open and short circuited stubs). This filter is realized by cascading transmission lines of the same electrical length θ_c (a prescribed value) and alternately very high and very low characteristic impedance. When the synthesis is complete, this cascade of transmission lines is transformed into a series of impedance inverters connected by lines of arbitrary impedance. In chapter 4 we will realize this network using multiple topologies.

Therefore, the objective of this section is to demonstrate that the polynomials that represent the transfer and reflection characteristics of such a cascade of commensurate elements of different impedances, are in the same form as the polynomials that represent certain filtering functions, transformed by the ω -plane to θ -plane mapping function

$$\omega = \frac{\sin \theta}{\sin \theta_c} = a \sin \theta \tag{3.6}$$

where θ_c is the commensurate-line length and $a = \frac{1}{\sin \theta_c}$.

The effect of applying this mapping function is shown in Figure 3.4, where the 6th-degree Chebyshev function of Figure 3.3 has been transformed to the θ plane using $\theta_c = 22^\circ$ and $\theta_c = 30^\circ$.

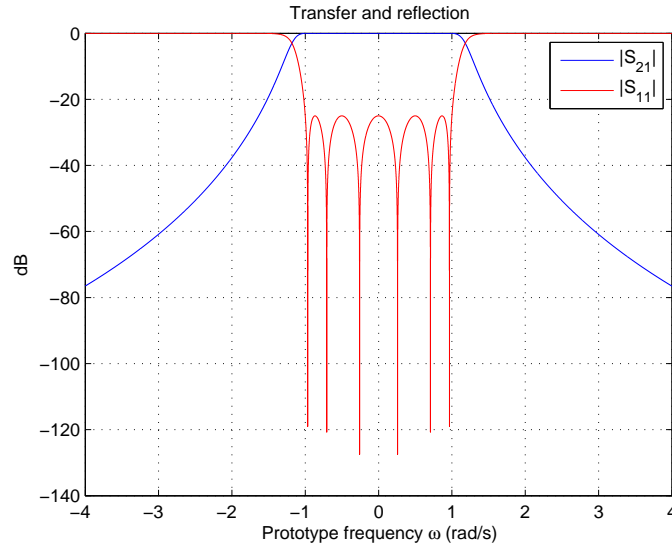


Figure 3.3: Transfer and reflection response of a 6th-degree Chebyshev filter (normalized frequency)

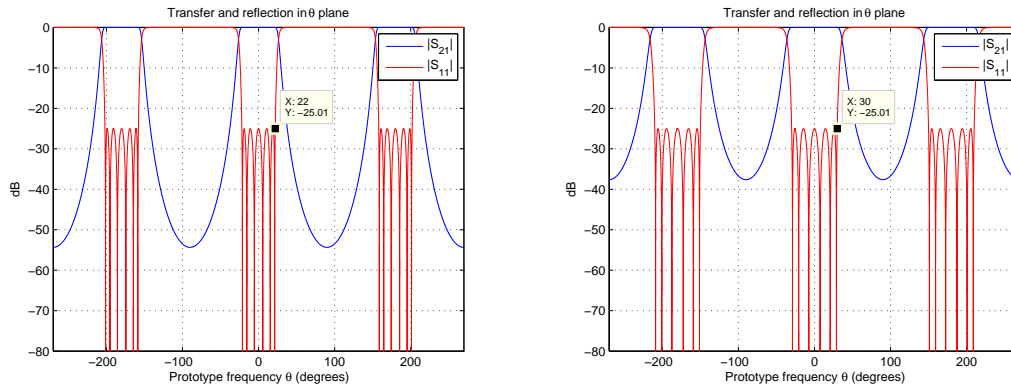


Figure 3.4: Mapping of an all-pole transfer and reflection function to the θ plane. $\theta_c = 22^\circ$ (left) and $\theta_c = 30^\circ$ (right)

It is seen that as θ increases from zero, the corresponding frequency variable in the ω plane increases, reaching band edge at $\omega = \pm 1$ when $\theta = \theta_c$. The range $\theta_c \leq \theta \leq 90^\circ$ maps into the range $1 \leq \omega \leq a$, with $a = \frac{1}{\sin \theta_c}$. As θ increases beyond 90° towards 180° , ω retraces its path back to zero and then on to $-a$ as θ reaches 270° . Therefore, it is seen that the repeating pattern in the θ plane corresponds to

the portion of the ω -plane characteristic between $\omega = \pm a$. In the next section we will detail the process necessary to obtain the polynomials in the t plane.

3.2.1 Mapping the Transfer Function S_{21} from the ω Plane to the θ Plane

We will use the transformation (3.6) as the first step towards finding the expression of S_{21} in the θ plane. Using the identity $\sin \theta = \frac{\tan \theta}{\sqrt{1+\tan^2 \theta}}$:

$$\omega = \frac{a \tan \theta}{\sqrt{1 + \tan^2 \theta}} \quad (3.7)$$

When we examined the commensurate-line elements in a previous section, we saw that the frequency dependence of these components varied as $t = j \tan \theta$. Using this in the previous equation, it follows that

$$s = j\omega = \frac{at}{\sqrt{1 - t^2}} \quad (3.8)$$

$$t = \frac{\pm s}{\sqrt{a^2 + s^2}} = \frac{\pm s \sin \theta_c}{\sqrt{1 + (s \sin \theta_c)^2}} \quad (3.9)$$

Now we can finally determine the expression of S_{21} in the t variable. As seen in the previous chapter, the s-plane all-pole transfer function has the form $S_{21}(s) = \frac{1}{\varepsilon E(s)}$. By changing the frequency variable from s to t we obtain:

$$S_{21}(t) = \frac{1}{\varepsilon E\left(\frac{at}{\sqrt{1-t^2}}\right)} = \frac{[\sqrt{1-t^2}]^N}{\varepsilon_t E(t)} \quad (3.10)$$

Where $E(t)$ is another Nth-degree polynomial in the variable $t = j \tan \theta$. The numerator $[\sqrt{1-t^2}]^N$ appears as a result of extracting this term from the denominator polynomial $E\left(\frac{at}{\sqrt{1-t^2}}\right)$ after the variable change, and the constant a is absorbed

into ε_t . To calculate $E(t)$ we will transform the N s -plane singularities of $E(s)$ to the t plane using (3.9), allowing to build the $E(t)$ immediately after. The normalizing constant is found by evaluating it at $\theta = \theta_c$, since, as explained in a previous section, this point corresponds to $\omega = 1$, where the return loss level is known (defined by the filter specifications). The polynomial $F(t)$ is found the same way.

Having obtained the general expression for $S_{21}(t)$, we will analyze the Stepped Impedance prototype circuit, to prove that it can be used to realize this transfer function. As seen in (3.5), the $[ABCD]$ matrix for a single UE is:

$$\begin{bmatrix} A & B \\ C & D \end{bmatrix} = \frac{1}{\sqrt{(1-t^2)}} \cdot \begin{bmatrix} 1 & Zt \\ t/Z & 1 \end{bmatrix} \quad (3.11)$$

The Stepped Impedance circuit will consist of N UE. If we cascade two UE of Impedances Z_1 and Z_2 (multiply their $[ABCD]$ matrices), we obtain:

$$\begin{aligned} \begin{bmatrix} A & B \\ C & D \end{bmatrix} &= \left[\frac{1}{\sqrt{(1-t^2)}} \right]^2 \cdot \begin{bmatrix} 1 + t^2 \cdot Z_1/Z_2 & t \cdot (Z_1 + Z_2) \\ t \cdot (1/Z_2 + 1/Z_1) & 1 + t^2 \cdot Z_2/Z_1 \end{bmatrix} \\ &= \left[\frac{1}{\sqrt{(1-t^2)}} \right]^2 \cdot \begin{bmatrix} A_2(t) & B_1(t) \\ C_1(t) & D_2(t) \end{bmatrix} \end{aligned} \quad (3.12)$$

Where the subscripts 1 and 2 indicate the order of the polynomial. For N lines:

$$\begin{aligned} \begin{bmatrix} A & B \\ C & D \end{bmatrix} &= \left[\frac{1}{\sqrt{(1-t^2)}} \right]^2 \cdot \begin{bmatrix} A_N(t) & B_{N-1}(t) \\ C_{N-1}(t) & D_N(t) \end{bmatrix} \quad (\text{for } N \text{ even}) \\ &= \left[\frac{1}{\sqrt{(1-t^2)}} \right]^2 \cdot \begin{bmatrix} A_{N-1}(t) & B_N(t) \\ C_N(t) & D_{N-1}(t) \end{bmatrix} \quad (\text{for } N \text{ odd}) \end{aligned} \quad (3.13)$$

Note that $A(t)$ and $D(t)$ are even polynomials, and $B(t)$ and $C(t)$ are odd polynomials for any value of N . We can immediately obtain the $S_{21}(t)$ expression from

this matrix, using a known relation between $[ABCD]$ and S parameters

$$S_{21} = \frac{2}{A + B/Z_0 + CZ_0 + D} \quad (3.14)$$

In our case we take Z_0 , the reference impedance for the scattering parameters, as unity, for the convenience of the synthesis method. Such unity impedance corresponds to the source impedance. Thus, we obtain

$$\begin{aligned} S_{21}(t) &= \frac{2[1 - t^2]^{N/2}}{A(t) + B(t) + C(t) + D(t)} = \frac{[1 - t^2]^{N/2}}{\varepsilon_t E(t)} \\ &= \frac{\sqrt{P(t)}/\varepsilon_t}{E(t)} \end{aligned} \quad (3.15)$$

where ε_t includes all the constants. As we intended to prove, this equation has the same form as equation (3.10). It is clear that $P(t)$, the numerator polynomial of S_{21} in the t plane, is of degree N , with N transmission half-zeros at $t = \pm 1$, which means that the function is fully canonical in this plane, even though $P(\omega) = 1$, due to the fact that there were no transmission zeros in the real frequency plane. $P(t)$ being fully canonical means that ε_{Rt} is non-unity, like it would happen in the ω plane. It is also interesting to point out that due to the form that $P(t)$ takes, it is impossible to calculate for odd-degree functions, which is actually not a problem for the synthesis procedure.

Due to ε_{Rt} being non-unity, $S_{11}(t) = \frac{F(t)/\varepsilon_{Rt}}{E(t)}$. Using the same approach as with S_{21} , the expression of $S_{11}(t)$ in terms of $[ABCD]$ polynomials is

$$S_{11} = \frac{A + B/Z_0 - CZ_0 - D}{A + B/Z_0 + CZ_0 + D} \quad (3.16)$$

Again, by taking Z_0 as unity, we can establish:

$$S_{11}(t) = \frac{A(t) + B(t) - C(t) - D(t)}{A(t) + B(t) + C(t) + D(t)} = \frac{F(t)/\varepsilon_{Rt}}{E(t)} \quad (3.17)$$

This equation would suffice to build the $[ABCD]$ polynomials in terms of $F(t)$ and $E(t)$, knowing that $A(t)$ and $D(t)$ are even polynomials, and $B(t)$ and $C(t)$ are odd polynomials (see equation (3.13)).

The constants ε_t and ε_{Rt} are obtained using the same principle as in the ω plane, evaluating them at a frequency point where $S_{21}(t)$ and $S_{11}(t)$ are known, such as the cutoff frequency. The cutoff frequency, as seen in previous sections, corresponds to $\theta = \theta_c$, and using $t = j \tan \theta$, we obtain t_c , the point in the t plane at which the transfer and reflection functions are known:

$$\varepsilon_t = \frac{[1 - t^2]^{N/2}}{(\sqrt{1 - 10^{-RL/10}}) \cdot |E(t)|} \Big|_{t=t_c} \quad (3.18)$$

and

$$\varepsilon_{Rt} = \frac{\varepsilon_t}{\sqrt{\varepsilon_t^2 - 1}} \quad (3.19)$$

3.2.2 Network Synthesis

We are now ready to extract, one by one, the unit elements that will form the Stepped Impedance filter, given the $E(t)$ and $F(t)$ polynomials obtained for a certain filter specification, using a Chebyshev or Zolotarev function, or a Chained function based on either of the two. It can be easily proved that the impedance Z_{in} looking at the input of a circuit described by an $[ABCD]$ matrix, loaded with an impedance Z_L , such as our filter, is

$$Z_{in} = \frac{A(t)Z_L + B(t)}{C(t)Z_L + D(t)} = \frac{1 + S_{11}(t)}{1 - S_{11}(t)} = \frac{E(t) + F(t)/\varepsilon_{Rt}}{E(t) - F(t)/\varepsilon_{Rt}} \quad (3.20)$$

where Z_L is the load impedance terminating the output of the network, and, as mentioned earlier, it is assumed that the source impedance $Z_S = 1$. In the synthesis procedure we will be evaluating $A(t)/C(t)$ or $B(t)/D(t)$ ratios, so it becomes unimportant whether Z_L is included in the previous equation, since the ratios will not change.

Knowing that $A(t)$ and $D(t)$ are even polynomials, and $B(t)$ and $C(t)$ are odd polynomials (see equation (3.13)), and looking at equation (3.20), it follows that the $[ABCD]$ polynomials are constructed as follows:

$$\begin{aligned}
 A(t) &= (e_0 + f_0) + (e_2 + f_2)t^2 + (e_4 + f_4)t^4 + \dots \\
 B(t) &= (e_1 + f_1)t + (e_3 + f_3)t^3 + (e_5 + f_5)t^5 + \dots \\
 C(t) &= (e_1 - f_1)t + (e_3 - f_3)t^3 + (e_5 - f_5)t^5 + \dots \\
 D(t) &= (e_0 - f_0) + (e_2 - f_2)t^2 + (e_4 - f_4)t^4 + \dots
 \end{aligned} \tag{3.21}$$

where e_i and f_i are the coefficients of the $E(t)$ and $F(t)/\varepsilon_{Rt}$ polynomials, respectively.

We are finally in a position to start extracting the impedances of the UEs that will form the LPF. First, the overall $[ABCD]$ matrix is decomposed into the first UE and a remainder matrix $[ABCD]'$:

$$\frac{\varepsilon_t}{[1 - t^2]^{N/2}} \cdot \begin{bmatrix} A(t) & B(t) \\ C(t) & D(t) \end{bmatrix} = \frac{1}{(1 - t^2)^{N/2}} \cdot \begin{bmatrix} 1 & Z_1 t \\ t/Z_1 & 1 \end{bmatrix} \frac{\varepsilon_t}{[1 - t^2]^{(N-1)/2}} \begin{bmatrix} A'(t) & B'(t) \\ C'(t) & D'(t) \end{bmatrix} \tag{3.22}$$

In the first step, calculating the open-circuit impedance $z_1 1$ or the short-circuit admittance $y_1 1$ will yield the impedance of the first line element. Using the known $[ABCD]$ matrix expression

$$z_{11} = \frac{A}{C} = \frac{B}{D} \quad (3.23)$$

We can obtain the impedance of the first transmission line Z_1 by evaluating in $t = 1$ (we can use A/C or B/D).

$$Z_1 = \frac{A(t)}{C(t)} \Big|_{t=1} = \frac{B(t)}{D(t)} \Big|_{t=1} \quad (3.24)$$

To complete the first iteration we need to calculate the remaining $[ABCD]'$ matrix for the next iteration:

$$\begin{aligned} \frac{\varepsilon_t}{[1-t^2]^{(N-1)/2}} \cdot \begin{bmatrix} A'(t) & B'(t) \\ C'(t) & D'(t) \end{bmatrix} &= \frac{1}{(1-t^2)^{1/2}} \cdot \begin{bmatrix} 1 & -Z_1 t \\ -t/Z_1 & 1 \end{bmatrix} \frac{\varepsilon_t}{[1-t^2]^{N/2}} \begin{bmatrix} A(t) & B(t) \\ C(t) & D(t) \end{bmatrix} \\ &= \frac{\varepsilon_t}{[1-t^2]^{(N+1)/2}} \cdot \begin{bmatrix} A(t) - tZ_1 C(t) & B(t) - tZ_1 D(t) \\ C(t) - tA(t)/Z_1 & D(t) - tB(t)/Z_1 \end{bmatrix} \end{aligned} \quad (3.25)$$

For the right-hand expression to have the same form as the left-hand side it is necessary to divide top and bottom by $(1-t^2)$, in order for the denominator to change from $[1-t^2]^{(N+1)/2}$ to $[1-t^2]^{(N-1)/2}$, also leaving the polynomials $A'(t)$, $B'(t)$, $C'(t)$ and $D'(t)$ to be one degree less than the original $[ABCD]$ polynomials. With this, the first step is complete, and the process is repeated until all N of the UEs are extracted. The Load termination is calculated by recognizing that at zero frequency, the cascade of UEs is effectively transparent, and $Z_{in} = Z_L$. Thus, we evaluate (3.20) at $t = 0$

$$Z_{in}|_{t=0} = \frac{e_0 + f_0}{e_0 - f_0} = Z_L \quad (3.26)$$

It can be shown that the UE values for odd-degree networks are equal about the center of the network, whereas those of even-degree networks are antimetric.

Having extracted the N unit elements of length θ_c and impedance Z_i , it would be possible to realize the LPF in waveguide, coaxial or planar structure as a series of transmission lines, each with impedance Z_i . In the case of rectangular waveguide realization, this means that the waveguide height (b) varies in proportion to the value of Z_i , as seen in the following expression:

$$Z = \sqrt{\mu/\epsilon} \cdot \frac{2 \cdot \frac{b}{a}}{\sqrt{1 - (\frac{\lambda}{2a})^2}} \tag{3.27}$$

Therefore, with b normalized to the incoming waveguide dimension, the heights of the different waveguide sections could be immediately calculated. However, this means abrupt impedance changes, and performance can be severely degraded from the ideal. Better results are obtained if redundant impedance inverters are introduced at the junctions by using the dual-network theorem on alternate UEs, as seen in Figure 3.5. In waveguide technology, these inverters are usually realized with capacitive irises.

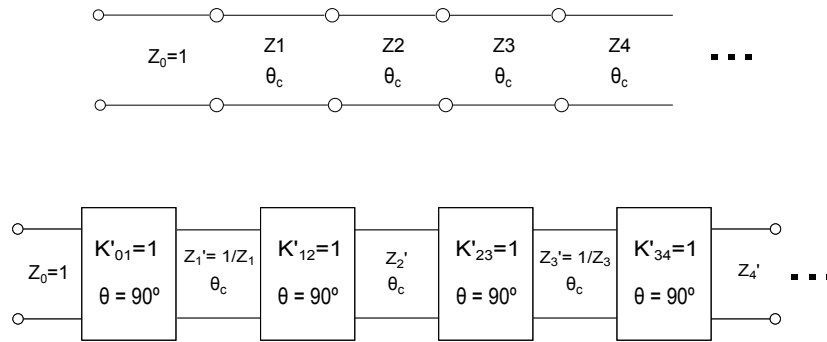


Figure 3.5: Introduction of Impedance Inverters in the Stepped Impedance LPF

Impedances can be given a prescribed value, if the inverters are scaled accordingly to keep the coupling coefficient $k_{i,i+1}$ constant:

$$k_{i,i+1} = \frac{K'_{i,i+1}}{\sqrt{Z'_i Z'_{i+1}}} = \frac{K''_{i,i+1}}{\sqrt{Z''_i Z''_{i+1}}} \tag{3.28}$$

A common practice is to set all Z_i'' to one (same impedance as the source transmission line). In this case, the impedance values of the inverters are given by

$$K''_{i,i+1} = \frac{1}{\sqrt{Z_i' \cdot Z_{i+1}'}}, \quad i=0,1,2, \dots, N \quad (3.29)$$

where $Z_0 = Z_S$ and $Z_{N+1} = Z_L$. The inverters now have nonunity values, and the network becomes symmetric in all cases (it was antimetric for even degree filters). These inverters will be realized as capacitive conducting posts in rectangular waveguide structure in the next chapter.

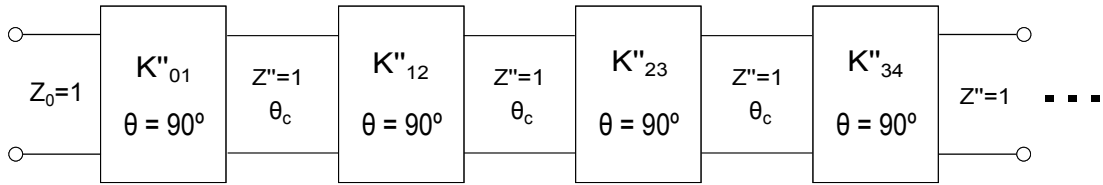


Figure 3.6: Stepped Impedance filter using non-unity Impedance Inverters and transmission lines of constant characteristic impedance

To illustrate the design procedure, we show the computed values of a sixth order Chebyshev filter, with a return loss of 26 dB and cutoff angle of $\theta_c = 30^\circ$. The first step is the synthesis of the Chebyshev polynomials in the s plane, to then transform them to the t plane using the techniques explained in this chapter. The singularities values in the s and t plane are listed in Table 3.1.

s plane		t plane	
Roots of $F(s)$	Roots of $E(s)$	Roots of $F(t)$	Roots of $E(t)$
$\pm 0.9659j$	$-0.1633 \pm 1.1421j$	$\pm 0.5516j$	$-0.1451 \pm 0.6807j$
$\pm 0.7071j$	$-0.4461 \pm 0.8361j$	$\pm 0.3780j$	$-0.2808 \pm 0.4148j$
$\pm 0.2588j$	$-0.6094 \pm 0.3060j$	$\pm 0.1305j$	$-0.3002 \pm 0.1348j$
$\varepsilon = 1.8023$	$\varepsilon_R = 1$	$\varepsilon_t = 76.0993$	$\varepsilon_{Rt} = 1.0001$

Table 3.1: Poles and zeros of a sixth-degree Chebyshev function in the s and t planes

With these values, we form the $[ABCD]$ polynomials and apply the element extraction to obtain Z_i . Then, we introduce the impedance inverters and scale the circuit accordingly. Results are shown in Table 3.2

UE cascade (no inverters)		After introducing Inverters ($Z_i = 1$)	
Z_1	1.7616	K''_{S1}	0.7534
Z_2	0.4247	K''_{12}	0.4910
Z_3	3.0592	K''_{23}	0.3726
Z_4	0.3658	K''_{34}	0.3458
Z_5	2.6351	K''_{45}	0.3726
Z_6	0.6353	K''_{56}	0.4910
Z_L	1.1192	K''_{6L}	0.7534

Table 3.2: Element values of sixth-degree Stepped Impedance Lowpass Filter

In order to realize this filter we would need a structure that presents the element values of Table 3.2 at the desired cut-off frequency, using the Hi-Low impedance cascade or the inverter based implementation. The latter will be covered in chapter 4, using various topologies to implement the impedance inverters in waveguide technology.

3.3 Synthesis of Tapered-Corrugated lowpass filter.

This type of filter, like the stepped impedance circuit seen in the previous section, is composed of a series of UEs, but is different in that they appear in pairs, each pair having the same characteristic impedance Z_i , and at the junction of each pair, a distributed capacitor is located. This structure is shown in Figure 3.7. At the frequency where the length θ_c of the distributed capacitors becomes 90° the open circuits at the ends of the UEs transform to short circuits seen from the main line,

which translates to a transmission zero at this frequency.

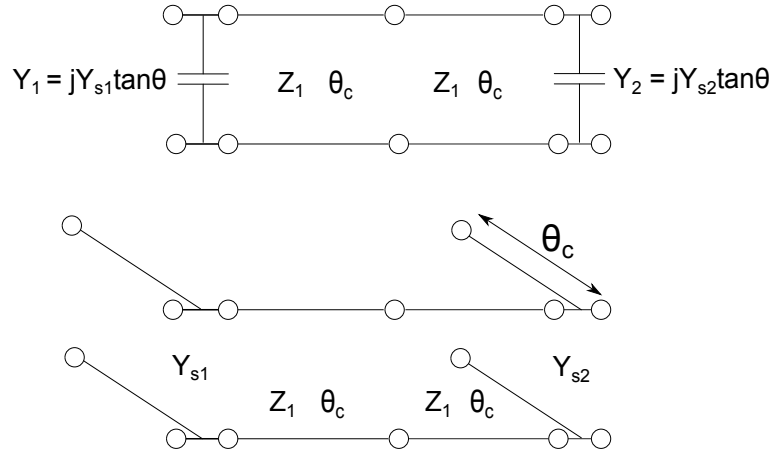


Figure 3.7: Basic element of the lumped/distributed filter

Similarly to what was done with the stepped impedance circuit, it can be shown that the circuit show in Figure 3.7 has the same form of the transfer function as a Chebyshev or Zolotarev function of the second type, with a pair of transmission half-zeros at a frequency of $\omega = \frac{1}{\sin \theta_c}$. Again, θ_c is the chosen cutoff frequency for the distributed prototype, and is transformed with the same mapping formula as the one for the stepped impedance LPF.

The transfer function for the Chebyshev function of the second kind or Zolotarev function with a single half-zero pair, necessary due to the structure itself, has the following form:

$$S_{21}(\omega) = \frac{\sqrt{\omega^2 - a^2}}{\varepsilon E(\omega)} \quad (3.30)$$

applying the transformations seen in the previous section, we obtain

$$S_{21}(\theta) = \frac{\sqrt{a^2 - a^2 \sin^2 \theta}}{\varepsilon_t E(a \sin \theta)} \quad (3.31)$$

where the constants are consolidated into ε_t . The meaning of the transformation is exactly the same as in the stepped impedance filter. In this case, a represents the position of the half-zero pair in the ω plane, which maps to 90° in the θ plane.

Figure 3.8 shows an example of the transformation for an eleventh degree Chebyshev function of the second kind with $\theta_c = 28$, meaning the filter will present a transmission half zero pair at $\omega = \frac{1}{\sin \theta_c} = \pm 2.1301$. It is clearly appreciated that this transmission zero maps to $\theta = 90^\circ$.

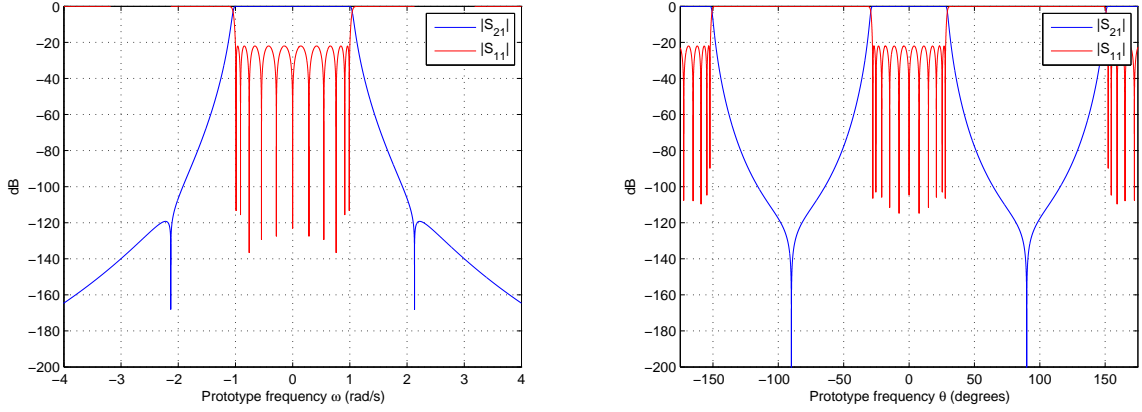


Figure 3.8: Eleventh-degree Chebyshev function of the second kind in the ω and θ plane.

Applying the identities $\sin \theta = \tan \theta / \sqrt{1 + \tan^2 \theta}$ and $\cos \theta = 1 / \sqrt{1 + \tan^2 \theta}$, and the transformation $t = j \tan \theta$, we obtain

$$S_{21}(t) = \frac{1}{\sqrt{1-t^2}} \cdot \frac{1}{\varepsilon_t E(-jta/\sqrt{1-t^2})} = \frac{[\sqrt{1-t^2}]^{N-1}}{\varepsilon_t' E(t)} \quad (3.32)$$

Again, similarly to what was done in the Stepped Impedance case, we must find the expression for $S_{21}(t)$ for the structure shown in Figure 3.7, extended to an arbitrary degree N , in order to proceed with the synthesis. First, we calculate the $[ABCD]$ matrix of the double UE, each of length θ_c , squaring the matrix

corresponding to a single UE (equation (3.5))

$$\begin{bmatrix} A & B \\ C & D \end{bmatrix} = \begin{bmatrix} 1 \\ \sqrt{(1-t^2)} \end{bmatrix}^2 \cdot \begin{bmatrix} 1 & Z_u t \\ t/Z_u & 1 \end{bmatrix}^2 = \frac{1}{1-t^2} \cdot \begin{bmatrix} 1+t^2 & 2Z_1 t \\ \frac{2t}{Z_1} & 1+t^2 \end{bmatrix} \quad (3.33)$$

Now we pre- and postmultiply by the shunt capacitors (see Figure 3.7)

$$\frac{1}{1-t^2} \cdot \begin{bmatrix} 1 & 0 \\ Y_{S1} t & 1 \end{bmatrix} \cdot \begin{bmatrix} 1+t^2 & 2Z_1 t \\ \frac{2t}{Z_1} & 1+t^2 \end{bmatrix} \cdot \begin{bmatrix} 1 & 0 \\ Y_{S1} t & 1 \end{bmatrix} = \begin{bmatrix} A_2(t) & B_1(t) \\ C_3(t) & D_2(t) \end{bmatrix} \quad (3.34)$$

where the subscripts represent the degree of the polynomials. This matrix corresponds to a third degree lowpass filter based on the circuit depicted in Figure 3.7

For a filter of degree N , the $[ABCD]$ matrix of such structure becomes:

$$[ABCD] = \frac{1}{[1-t^2]^{(N-1)/2}} \cdot \begin{bmatrix} A_{N-1}(t) & B_{N-2}(t) \\ C_N(t) & D_{N-1}(t) \end{bmatrix} \quad (3.35)$$

and, using the relation (3.14)

$$S_{21}(t) = \frac{2[1-t^2]^{(N-1)/2}}{A_{N-1}(t) + B_{N-2}(t) + C_N(t) + D_{N-1}(t)} = \frac{[1-t^2]^{(N-1)/2}}{\varepsilon_t E_N(t)} \quad (3.36)$$

which, as intended, has the same form as (3.32).

For the design of this type of filter, we have shown that an odd-degree function with a half-zero pair is required. As a consequence of this, the numerator of $S_{21}(\omega)$ takes the form $P(\omega) = \sqrt{\omega^2 - a^2}$ and the polynomial $P(\omega)$ cannot be formed using the alternating pole method. However, (3.32) shows that in the t plane, the numerator of $S_{21}(t)$ is $P(t) = [1-t^2]^{(N-1)/2}$, which, because N is an odd number, represents

a polynomial in the variable t and thus, we can easily find the polynomials required, as follows:

1. With the desired return loss equiripple level and lowpass cutoff angle θ_c , which will determine the width of the reject band before the second harmonic appears, form the polynomial $F(\omega)$ using the method presented in Section 2.4 for the Chebyshev function of the second kind with a half-zero pair at the position $a = 1/\sin \theta_c$.
2. Transform the roots of the $F(\omega)$ polynomial to the t plane to obtain $F(t)$
3. Form the polynomial $P(t) = [1 - t^2]^{(N-1)/2}$.
4. Calculate the constant ε_t , by evaluation the filtering function at a point where the return loss is known, like the cutoff frequency, where $t = t_c = j \tan \theta_c$

$$\varepsilon_t = \frac{1}{|F(t_c)|} \cdot \frac{[1 - t_c^2]^{(N-1)/2}}{\sqrt{10^{RL/10} - 1}}$$

5. Use the Alternating Pole Method in the t plane. To do this we form the polynomial $E(t) = P(t) \pm \varepsilon_t F(t)$ ($\varepsilon_{Rt} = 1$ since the function is not fully canonical), root it, and reflect any singularities that are in the right half-plane back to the left half-plane to preserve the Hurwitz condition. These will be the roots of the polynomial $E(t)$

At this point we can build the $[ABCD]$ polynomials related to the $E(t)$ and $F(t)$ polynomials, and synthesize the values of the circuit elements using a very similar method to the one used for the stepped impedance filter.

$$\begin{aligned} A(t) &= (e_0 - f_0) + (e_2 - f_2)t^2 + (e_4 - f_4)t^4 + \dots \\ B(t) &= (e_1 - f_1)t + (e_3 - f_3)t^3 + (e_5 - f_5)t^5 + \dots \\ C(t) &= (e_1 + f_1)t + (e_3 + f_3)t^3 + (e_5 + f_5)t^5 + \dots \\ D(t) &= (e_0 + f_0) + (e_2 + f_2)t^2 + (e_4 + f_4)t^4 + \dots \end{aligned} \quad (3.37)$$

where e_i and f_i are the coefficients of the $E(t)$ and $F(t)$ polynomials.

3.3.1 Network Synthesis

The first element to be extracted is the capacitor Y_{S1} , to prepare the network for the extraction of the $2\theta_c$ unit element of characteristic impedance Z_1 . Therefore, as the first step, we assume the overall network to be composed of a capacitor in cascade with the remainder matrix $[ABCD]^{(1)}$:

$$\begin{aligned} \frac{1}{[1-t^2]^{(N-1)/2}} \cdot \begin{bmatrix} A(t) & B(t) \\ C(t) & D(t) \end{bmatrix} &= \begin{bmatrix} 1 & 0 \\ tY_{S1} & 1 \end{bmatrix} \frac{1}{[1-t^2]^{(N-1)/2}} \begin{bmatrix} A^{(1)} & B^{(1)} \\ C^{(1)} & D^{(1)} \end{bmatrix} \\ &= \frac{1}{[1-t^2]^{(N-1)/2}} \cdot \begin{bmatrix} A^{(1)} & B^{(1)} \\ tY_{S1}A^{(1)} + C^{(1)} & tY_{S1}B^{(1)} + D^{(1)} \end{bmatrix} \end{aligned} \quad (3.38)$$

Using known $[ABCD]$ matrix relations and taking the right hand side of (3.38), the short-circuit admittance y_{11} looking into this network is

$$y_{11} = \frac{D(t)}{B(t)} = tY_{S1} + \frac{D^{(1)}}{B^{(1)}} \quad (3.39)$$

To evaluate Y_{S1} we have to make use of the fact that, for the network consisting of a double UE as the leading component, the differential of its input admittance with respect to t is zero at $t = \pm 1$. This can be proved by differentiating the input admittance y_{11R} of the network corresponding to $[ABCD]^{(1)}$, composed of the first double UE and the remainder network (which we will denote as $[ABCD]^{(2)}$).

$$\begin{aligned}
[ABCD]^{(1)} &= \frac{1}{[1-t^2]^{(N-1)/2}} \begin{bmatrix} A^{(1)} & B^{(1)} \\ C^{(1)} & D^{(1)} \end{bmatrix} = \frac{1}{(1-t^2)} \cdot \begin{bmatrix} 1+t^2 & 2tZ_1 \\ \frac{2t}{Z_1} & 1+t^2 \end{bmatrix} \\
&\cdot \frac{1}{[1-t^2]^{(N-3)/2}} \cdot \begin{bmatrix} A^{(2)} & B^{(2)} \\ C^{(2)} & D^{(2)} \end{bmatrix} \\
&= \frac{1}{[1-t^2]^{(N-1)/2}} \cdot \begin{bmatrix} (1+t^2)A^{(2)} + 2tC^{(2)}Z_1 & (1+t^2)B^{(2)} + 2tD^{(2)}Z_1 \\ (1+t^2)C^{(2)} + \frac{2tA^{(2)}}{Z_1} & (1+t^2)D^{(2)} + \frac{2tB^{(2)}}{Z_1} \end{bmatrix}
\end{aligned} \tag{3.40}$$

Therefore, the input admittance of the network corresponding to $[ABCD]^{(1)}$ can be expressed as

$$y_{11R} = \frac{D^{(1)}}{B^{(1)}} = \frac{(1+t^2)D^{(2)} + 2tB^{(2)}/Z_1}{(1+t^2)B^{(2)} + 2tD^{(2)}Z_1} \tag{3.41}$$

It can be proved that the differential of (3.41) evaluated at $t = 1$ is always zero, regardless of the form of the $[ABCD]^{(2)}$ polynomials.

Going back to the input admittance of the overall network y_{11}

$$y'_{11} = \frac{dy_{11}}{dt} = \left[\frac{D(t)}{B(t)} \right]' = Y_{S1} + \left[\frac{D^{(1)}}{B^{(1)}} \right]' \tag{3.42}$$

$$y'_{11} \Big|_{t=\pm 1} = \left[\frac{D(t)}{B(t)} \right]' \Big|_{t=\pm 1} = Y_{S1} \tag{3.43}$$

having obtained the value of the first admittance Y_{S1} , and following equation (3.38), we form the remaining $[ABCD]^{(1)}$ matrix

$$\begin{aligned}
 [ABCD]^{(1)} &= \frac{1}{[1-t^2]^{(N-1)/2}} \begin{bmatrix} A^{(1)} & B^{(1)} \\ C^{(1)} & D^{(1)} \end{bmatrix} = \begin{bmatrix} 1 & 0 \\ -tY_s & 1 \end{bmatrix} \cdot \frac{1}{[1-t^2]^{(N-1)/2}} \cdot \begin{bmatrix} A & B \\ C & D \end{bmatrix} \\
 &= \frac{1}{[1-t^2]^{(N-1)/2}} \cdot \begin{bmatrix} A & B \\ C - tY_s A & D - tY_s B \end{bmatrix}
 \end{aligned} \tag{3.44}$$

The next step is extracting the first double UE. This can be done directly after knowing the value of Y_{S1} , by simply evaluating the admittance of the remaining network y_{11R} at $t = 1$

$$y_{11R}|_{t=1} = \left[\frac{D^{(1)}}{B^{(1)}} \right]' \Bigg|_{t=1} = \frac{1}{Z_1} \tag{3.45}$$

The double UE of impedance Z_1 must now be extracted from the matrix $[ABCD]^{(1)}$, to form the remaining matrix $[ABCD]^{(2)}$, as follows

$$\begin{aligned}
 [ABCD]^{(1)} &= \frac{1}{[1-t^2]^{(N-1)/2}} \begin{bmatrix} A^{(1)} & B^{(1)} \\ C^{(1)} & D^{(1)} \end{bmatrix} = \frac{1}{(1-t^2)} \cdot \begin{bmatrix} 1+t^2 & 2tZ_1 \\ \frac{2t}{Z_1} & 1+t^2 \end{bmatrix} \\
 &\quad \cdot \frac{1}{[1-t^2]^{(N-3)/2}} \cdot \begin{bmatrix} A^{(2)} & B^{(2)} \\ C^{(2)} & D^{(2)} \end{bmatrix}
 \end{aligned} \tag{3.46}$$

joining the matrix corresponding to the double UE with the $[ABCD]^{(1)}$ matrix, we obtain

$$\begin{aligned}
 [ABCD]^{(2)} &= \frac{1}{(1-t^2)} \cdot \begin{bmatrix} 1+t^2 & -2Z_1 t \\ \frac{-2t}{Z_1} & 1+t^2 \end{bmatrix} \cdot \frac{1}{[1-t^2]^{(N-1)/2}} \cdot \begin{bmatrix} A^{(1)} & B^{(1)} \\ C^{(1)} & D^{(1)} \end{bmatrix} \\
 &= \frac{1}{[1-t^2]^{(N+1)/2}} \cdot \begin{bmatrix} (1+t^2)A^{(1)} - 2Z_1 t C^{(1)} & (1+t^2)B^{(1)} + \frac{-2t}{Z_1} D^{(1)} \\ -\frac{2t}{Z_1} A^{(1)} + (1+t^2)C^{(1)} & -\frac{2t}{Z_1} B + (1+t^2)D^{(1)} \end{bmatrix}
 \end{aligned} \tag{3.47}$$

s plane	t plane	
Roots of $F(s)$	Roots of $F(t)$	Roots of $E(t)$
$\pm 0.9901j$	$\pm 0.5250j$	$-0.0289 \pm 0.5532j$
$\pm 0.9115j$	$\pm 0.4734j$	$-0.0790 \pm 0.4950j$
$\pm 0.7594j$	$\pm 0.3816j$	$-0.1124 \pm 0.3945j$
$\pm 0.5449j$	$\pm 0.2646j$	$-0.1301 \pm 0.2709j$
$\pm 0.2845j$	$\pm 0.1348j$	$-0.1378 \pm 0.1371j$
0	0	-0.1398

Table 3.3: Poles and zeros of a eleventh degree Chebyshev function of the second kind in the s and t planes

Shunt Capacitors		UE pairs	
i	Y_{Si}	i	Z_i
1, 11	1.5120	2, 10	1.6340
3, 9	3.0119	4, 8	1.8382
5, 7	3.2919	6	1.8707

Table 3.4: Element values of eleventh degree Corrugated Lowpass Filter

finally, we have to divide and multiply the right-hand side term by $(1 - t^2)^2$ to obtain the correct degree $(N - 3)/2$ for the denominator polynomial, completing the first iteration. The next iteration now begins by extracting the admittance Y_{S2} from $[ABCD]^{(2)}$. The process is repeated until all elements are obtained. To illustrate the design procedure, we synthesize the element values for a eleventh degree filter, with a prescribed return loss of 22 dB and cutoff angle $\theta_c = 28^\circ$. This means that the filter will present a transmission half zero at $\omega = \pm 2.1301$ (normalized frequency).

With these values, we form the $[ABCD]$ polynomials and apply the element extraction to obtain Y_{Si} (admittance of shunt capacitors) and Z_i (characteristic impedance of the transmission lines). Results are shown in Table 3.4

Although chapter 4 is focused on the realization of the Stepped Impedance pro-

prototype using alternative topologies, I also show some examples of the traditional Corrugated filter implementing the prototype network seen in this section, including small modifications to the structure.

Chapter 4

Realization of the Lowpass Filter Using Alternative Topologies

In the preceding chapters, we have studied how to synthesize the prototype network for the distributed Stepped Impedance LPF and the Tapered Corrugated LPF, for any given specification and using different types of filtering functions. In this chapter we explore the realization of the Stepped Impedance filter in waveguide technology using one or multiple conducting posts as impedance inverters. This type of filter would normally be realized using rectangular capacitive irises in the waveguide, which can lead to multipactor breakdown due to the small distances between parallel plates and the strong EM fields in the area. One of the approaches that can be taken to reduce the multipactor breakdown power thresholds is to introduce modifications in such waveguide filter geometry. For these reasons, we have decided to explore the utilization of curved surfaces such as circularly or elliptically shaped posts to realize the microwave filter.

I have used the commercial package HFSS for the design and verification of these filters, controlling its operation (3D design, analyses and storing of results) via scripts generated by MATLAB functions. These functions are sequentially called with the required parameters to create a macro file that can be run by HFSS. When

the script is complete, MATLAB starts HFSS using this file. As a starting point, we have made use of the MATLAB API available at [6], and have expanded it with additional functions following the same structure.

Scripting allows the automation of the design process, making it much faster and less prone to errors. In our particular case, we will be able to build Chebyshev, Zolotarev or Chained function filters of any specification, using any topology to implement each inverter, just by clicking a button of the GUI provided, running one of the scripts already programmed or writing a few lines of MATLAB code. Furthermore, as we will show later in this chapter, we are able to automate the interaction between MATLAB and HFSS, where we use the former to analyze the results produced by the latter and modify the design parameters in an iterative manner, until the prescribed convergence criteria are met. Since the generation of the HFSS scripts is done by MATLAB functions, this can be achieved by a simple cyclic routine.

I will show multiple topologies able to realize the stepped impedance LPF network with impedance inverters presented in the previous chapter, focusing mainly on the utilization of conducting posts along a waveguide of constant dimensions. At the end of the chapter, additional topologies are briefly presented and described, and we give an example of design. All filters have been designed in an automatic fashion using the software developed, and synthesizing new filters would only require a different set of the input parameters.

4.1 Design Technique

The design technique utilized for all filters is explained here, applied to the topology based on circular posts placed parallel to the wide dimension of a waveguide. To realize the network of 4.1, the whole circuit can be sliced in $N + 1$ segments

consisting of an impedance inverter connected to transmission lines of length $\theta_c/2$, as shown in figure 4.2. If we characterize this small circuit, and manage to create an equivalent physical structure for each of the $N + 1$ segments, the final filter can be realized by simply cascading them.

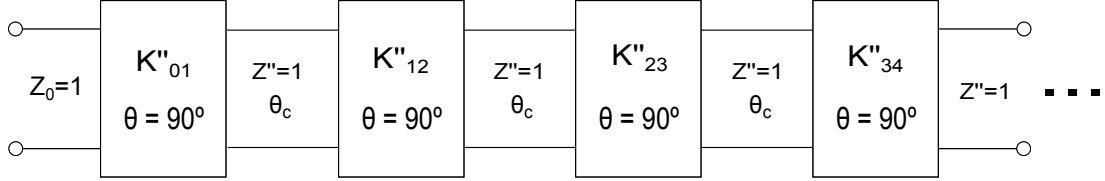


Figure 4.1: Low pass filter network

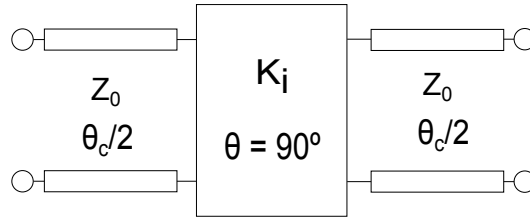


Figure 4.2: Circuit Segment: Impedance inverter with input and output transmission lines

Each of these segments will be realized using a waveguide section of the appropriate length, containing one or more conducting posts (Figure 4.3).

In order to correctly model each of these segments using conducting posts (or any other arbitrary shape), we will work with the scattering parameters, computed using HFSS. We can work with S_{11} or S_{21} indistinctly (there is no need to use both). The design is divided in two steps:

1. Finding the dimensions of the post that give the same $|S_{11}|$ and $|S_{21}|$ as the circuit in Figure 4.2
2. Adjusting the position of the ports (L in 4.3) for the posts obtained in step 1 until the phase conditions are the same as those of Figure 4.2

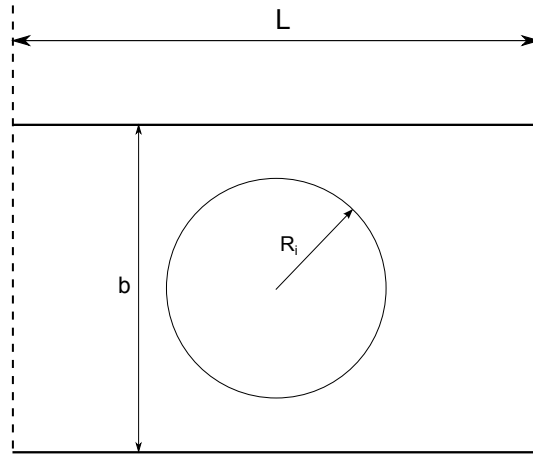


Figure 4.3: Circuit Segment realized using a conducting post

These two conditions have to be computed at the prescribed cutoff frequency (in the prototype network of Figure 4.1 this frequency was 1). The fact that the ideal network was obtained with unity impedance transmission lines does not alter the value of the scattering parameters we have to adjust, as the assumption of unity impedance is done only for clarity purposes and does not imply a loss of generality, since the circuit can be scaled at any time to a different impedance, yielding the same scattering parameters.

Note that the position of the ports does not affect the value of $|S_{21}|$ and $|S_{11}|$, so the length of the waveguide section in step 1 is arbitrary. In step 2, the analysis has to be done using the posts given by step 1, since the dimensions of the post will affect the phase of the travelling wave. Therefore, for each inverter, step 1 has to be done before step 2.

The expression of $|S_{11}|$ and $|S_{21}|$ for each segment can be obtained knowing K_i and the transmission matrix of an impedance inverter

$$[ABCD] = \begin{bmatrix} 0 & jK \\ j\frac{1}{K} & 0 \end{bmatrix} \quad (4.1)$$

If we analyze the circuit consisting of an impedance inverter connected to transmission lines of characteristic impedance Z_0 (Figure 4.2), using (4.1), it can be proved that

$$|S_{11}| = \left| \frac{(K/Z_0)^2 - 1}{(K/Z_0)^2 + 1} \right| \quad (4.2)$$

$$|S_{21}| = \frac{2Z_0}{K + \frac{1}{K}Z_0^2} \quad (4.3)$$

Finding the phase conditions is immediate, knowing that for the capacitive impedance inverter $\angle S_{11} = 180^\circ$ and $\angle S_{21} = -90^\circ$

$$\angle S_{11} = -\theta_c/2 + 180^\circ - \theta_c/2 = +180^\circ - \theta_c \quad (4.4)$$

$$\angle S_{21} = -\theta_c/2 - 90^\circ - \theta_c/2 = -90^\circ - \theta_c \quad (4.5)$$

Assuming we utilize S_{21} (again, the results obtained would be identical using the parameter S_{11}), the approach taken to complete these steps and build the LPF using HFSS is as follows:

1. Create a design consisting of a waveguide section of arbitrary length, containing one or more conducting posts as shown in Figure 4.3
2. For the desired cutoff frequency, run a parametric analysis varying the radius of the post to obtain $|S_{21}|$ as a function of R .
3. For each inverter K_i , calculate $|S_{21_i}|$, and using the data from step 2, interpolate R_i .
4. For each R_i run a parametric analysis varying L (length of the WG section) in order to obtain $\angle S_{21}$ as a function of L , or obtain the phase for an arbitrary, small enough value of L , and analytically calculate the remaining length using well known waveguide equations.

5. Using the data from step 4, interpolate L for each inverter, so that $\angle S_{21} = -90^\circ - \theta_c$
6. Cascade all the sections, with their respective R_i and L_i .

Having completed all steps, the design is finished and the structure can be analyzed to check the frequency response. The software developed automates this task, generating the necessary scripts to build the HFSS designs, run the appropriate simulations and analyze the results. This is done using two MATLAB functions, one for the inverters, to compute R_i and L_i (we call this function twice, indicating what parametric analysis to run) and one to build and simulate the filter with the values obtained, in order to validate the design.

Some of the script-building functions, used to build the scripts used as input to run HFSS, are:

- hfssCreateVariable(...)
- hfssBox(...)
- hfssEllipse(...)
- hfssSweepAlongVector(...)
- hfssAssignMaterial(...)
- hfssAssignWavePort(...)
- hfssAdd(...)
- hfssSubtract(...)
- hfssInsertSolution(...)
- hfssInsertParametric(...)
- hfssCreateReport(...)

- `hfssExecuteScript(...)`

Before using these functions, the different K_i of the inverters must be synthesized with the theory explained in chapters 2 and 3. In order to make the design of multiple filters easy and immediate, even for someone unfamiliar with the software, we have created a simple MATLAB GUI able to complete every step taking the following input parameters:

- Type of filtering function: Chebyshev, Zolotarev, Chained.
- Prescribed Return Loss level in passband.
- Length of the transmission line elements θ_c
- Waveguide dimensions.
- Cutoff frequency.
- Number of posts used to implement each impedance inverter.
- Minor/Major axis ratio: Controls the shape of the posts (circular or elliptical of varying eccentricity).
- Various HFSS parameters.

Due to the modular nature of the software involved in the design, this GUI could be easily expanded to utilize arbitrary topologies, other filter functions, and different prototype circuits such as the corrugated filter studied in the previous chapter.

4.2 Example of filter design

As a first introduction to how the software realizes the previously explained procedure, we will design step by step a lowpass filter with the following parameters

Function type	Chebyshev
Filter degree (N)	6
Prescribed Return Loss	25
θ_c	30°
WG dimensions	$a = 47.55mm, b = 22.5mm$ (WR-187)
WG freq. range	3.95 to 5.85 GHz
Cutoff frequency	5.5 GHz

Table 4.1: Filter specification of the first filter designed

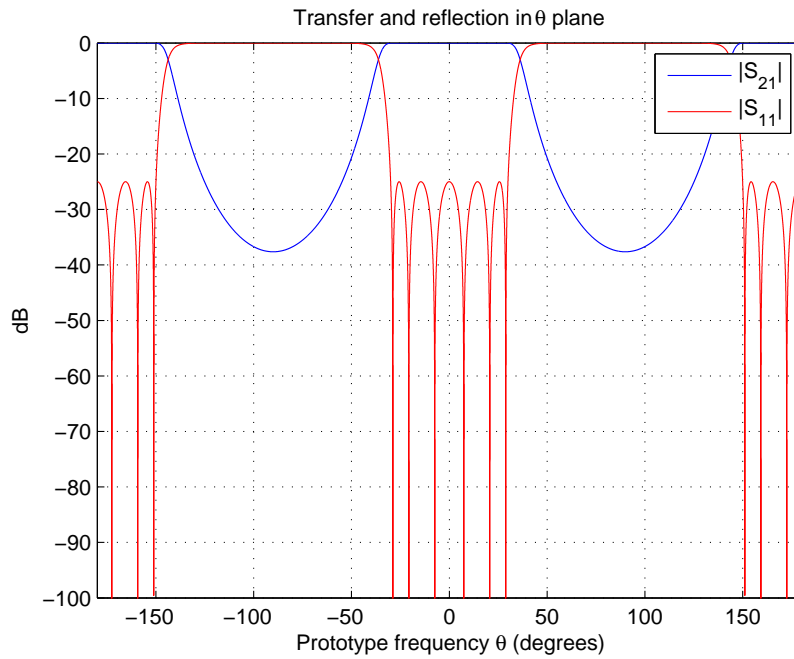


Figure 4.4: Ideal transfer and reflection function of the filter designed

The Stepped Impedance synthesis (see chapter 3) yields the following values for the inverters that implement this filter (7 inverters, connected by transmission lines of length θ_c)

	K	$ S_{21} $ (dB)
K''_{S1}	0.75344	-0.34354
K''_{12}	0.49101	-2.0336
K''_{23}	0.3726	-3.6837
K''_{34}	0.34581	-4.1837
K''_{45}	0.3726	-3.6837
K''_{56}	0.49101	-2.0336
K''_{6L}	0.75344	-0.34354

Table 4.2: Inverter values and associated $|S_{21}|$ for first filter designed

We will implement this filter using two circular posts per inverter. The steps explained here are the same for every topology.

First, a HFSS design consisting of two circular post centered in a WG section of arbitrary length is built, in order to calculate the relation between $|S_{21}|$ and the radius of the posts (as mentioned earlier, the length of the WG section does not affect $|S_{21}|$). Figure 4.5 shows this design

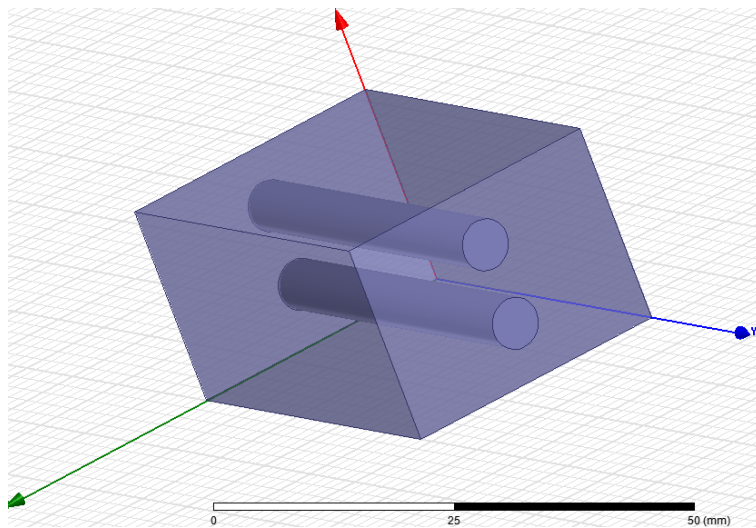


Figure 4.5: Waveguide section containing two conducting posts

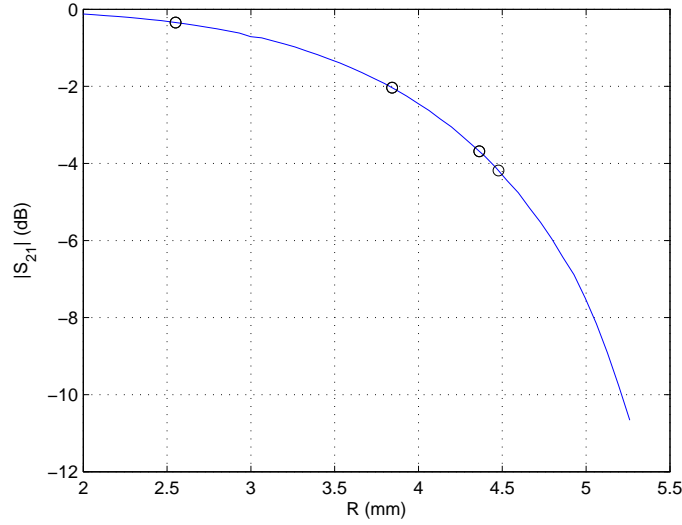


Figure 4.6: Variation of $|S_{21}|$ with R (radius of posts)

After running a parametric sweep for R , we are able to interpolate the value of R to realize each inverter, as shown in Figure 4.6. The points corresponding to the desired levels of $|S_{21}|$ are shown in table 4.3.

Having computed the dimensions of the posts, we must accurately obtain, for each inverter, the waveguide length that gives $\angle S_{21} = -90^\circ - \theta_c = -120^\circ$. This is done by running a sweep on the length parameter for each of the previous values of R (obviously only the first four need to be done, due to the symmetry of the

R_1	2.5512
R_2	3.8422
R_3	4.3623
R_4	4.477
R_5	4.3623
R_6	3.8422
R_7	2.5512

Table 4.3: Radius values (mm) for each of the conducting posts pairs

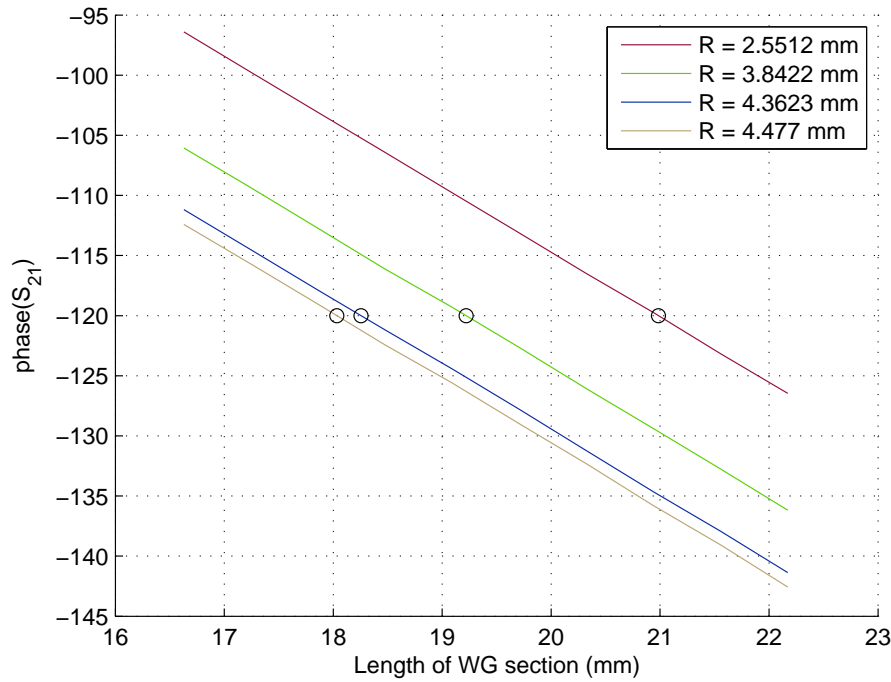


Figure 4.7: Variation of $\angle S_{21}$ with length of WG section for each value of R

network). As stated earlier, we could also calculate the phase for a single length value and obtain the required length using theoretical waveguide propagation equations. When taking this second approach, we need to be careful not to place the ports too close to the posts, where propagation is not correctly modeled by the theoretical equations. Since the parametric sweep only requires a few points (five to ten is more than enough, and it is a very simple 3d structure), in all filter shown here I have opted for the first option. Figure 4.7 and table 4.4 show the results of the parametric sweep. Finally, the filter is constructed by cascading these elements, as shown in Figure 4.8

Figure 4.9 shows the frequency response of this filter. There is no propagation before the waveguide cutoff frequency (3.1546 GHz), which has the effect of moving the entire passband (including the negative frequencies of the theoretical response) to this frequency, as in a bandpass filter. In addition, for frequencies lower than the recommended band (3.95 to 5.85 GHz), due to the strong waveguide dispersion

L_1	20.9641
L_2	19.203
L_3	18.2575
L_4	18.0075
L_5	18.2575
L_6	19.203
L_7	20.9641

Table 4.4: Length of waveguide sections for each inverter

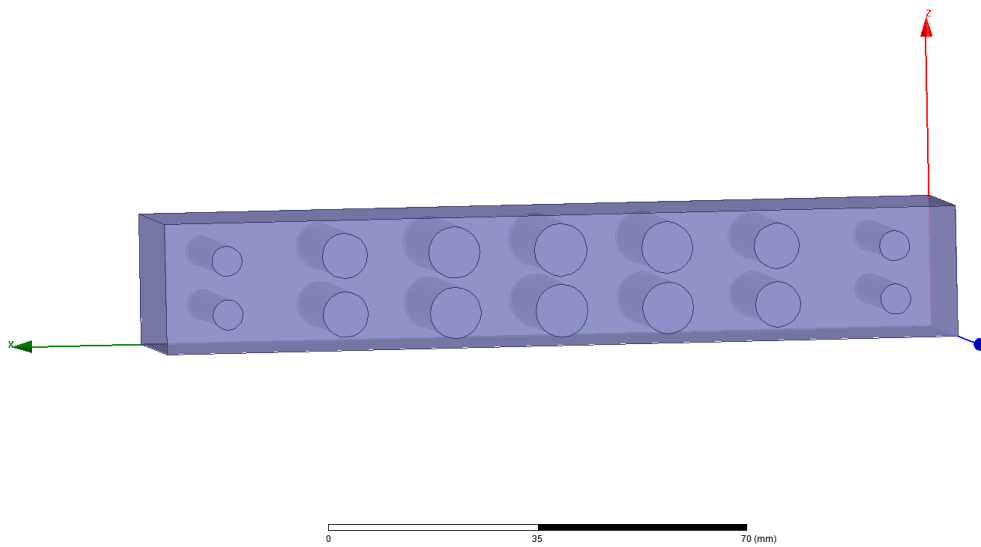


Figure 4.8: Sixth degree LPF realized using conducting posts pairs.

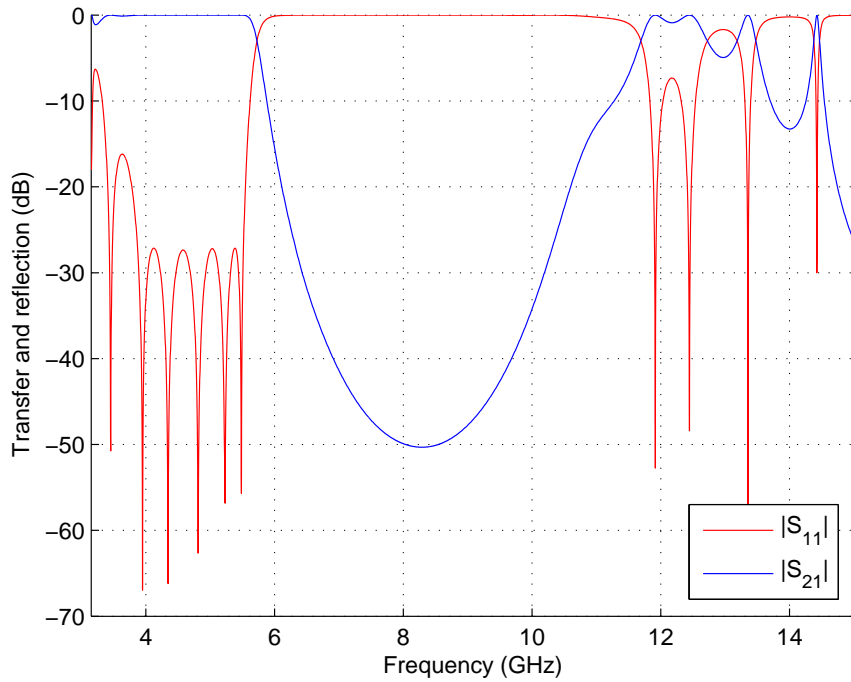


Figure 4.9: Frequency response of sixth degree Chebyshev LPF realized using conducting posts pairs.

near the cutoff frequency of the first mode, it is impossible to obtain an equiripple response. Therefore, the usable frequencies start around 3.95 GHz, as can be seen in figures 4.9 and 4.10. Note that the in-band return loss and rejection are better than that of the theoretical polynomials, due to the frequency dependence of the impedance inverters, making the filter behave as if it were of higher degree (S_{11} does cross 5.5 GHz at precisely 25 dB though, if the design is perfectly done)

In chapter 3 we saw that the position of the spurious band in the ideal prototype network depended on the value of the Commensurate Lines length, θ_c , since it is the parameter that controls the periodicity of the frequency response (shorter lines make the spurious band appear further away). There is a limit, however, to how small θ_c can be made in practice:

1. As we make θ_c smaller, the inverters will start presenting increasingly lower values of K , which translates in greater values of R for this particular topology,

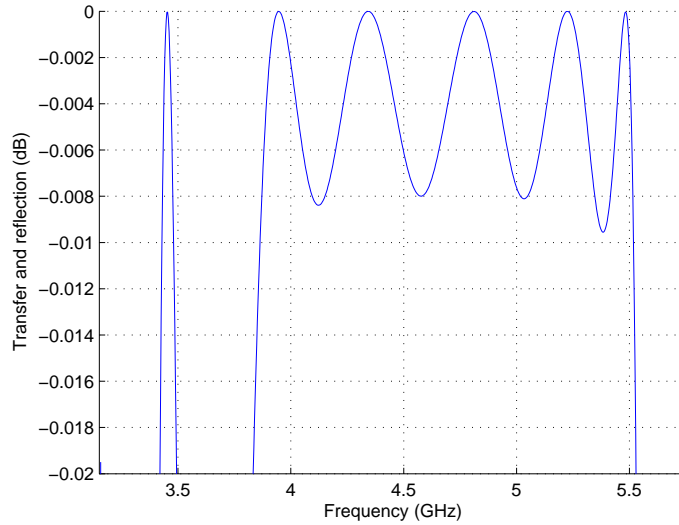


Figure 4.10: Pass band of sixth degree Chebyshev LPF realized using conducting posts pairs.

leaving very small gaps between the posts and the waveguide walls, which could be detrimental to the high power performance of the filter. Note that the value of K also depends on the other parameters, like the type of filtering function, the cutoff frequency or the prescribed return loss.

2. The filter might become impossible to realize using a certain topology (depending on the factors mentioned and the shape of the posts), due to the phase condition $\angle S_{21} = -90^\circ - \theta_c$, which may result in a situation where posts would have to overlap.

In the actual implementation using conducting posts, the spurious free range also depends on the dimension of the posts along the propagation axis, which will vary depending on the particular topology used, even for the same theoretical filtering function. For example, using single post inverters instead of post pairs results in the first spurious band appearing earlier, since the posts have to be bigger along the direction of propagation. Using elliptical posts widens the spurious free range, with the downside of requiring smaller gaps to obtain the same $|S_{21}|$. We compare the

filter designed with a possible equivalent using capacitive irises (Figure 4.11). This filter has been synthesized using the design technique and software described here, to show that it can be adapted to any structure. To design this filter, we just had to modify the two MATLAB functions mentioned earlier (one for the inverters and one to construct the filter) to draw this particular topology in the HFSS modeler. The aperture of the irises and the length of the waveguide sections are adjusted to implement the required values of $|S_{21}|$ and $\angle S_{21}$ respectively, as was done for the post topology. The performance of both filters is almost identical, since they're implementing the same function at the design frequency. The small difference in the spurious free range is due to the actual dimension of the impedance inverters, which could be adjusted to obtain exactly the same filter.

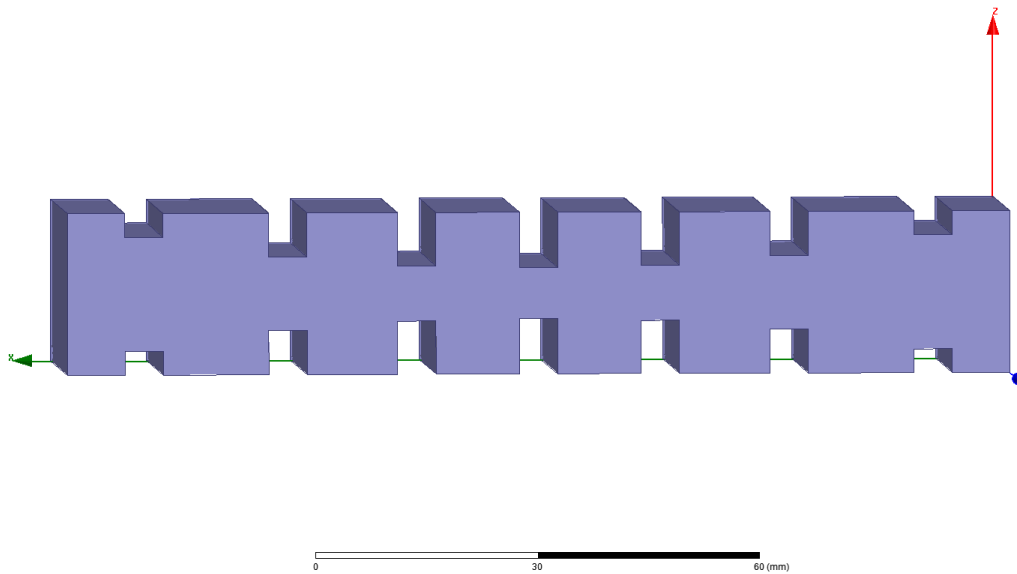


Figure 4.11: LPF using traditional capacitive irises

All the filter of the next section, where we study the effect of various design parameters, are of sixth degree. For illustrative purposes, I have designed a 12th degree filter designed with elliptical posts (Figure 4.13), for a prescribed value of return loss of 20 dB and $\theta_c = 22^\circ$. Figure 4.14 shows the frequency response of this filter.

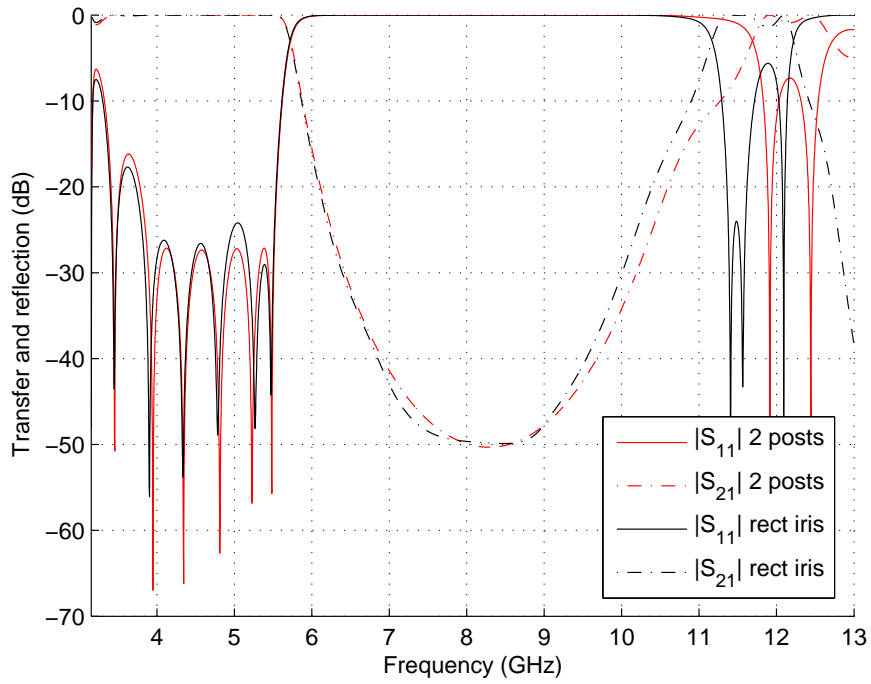


Figure 4.12: Comparison of double post based filter and capacitive iris filter

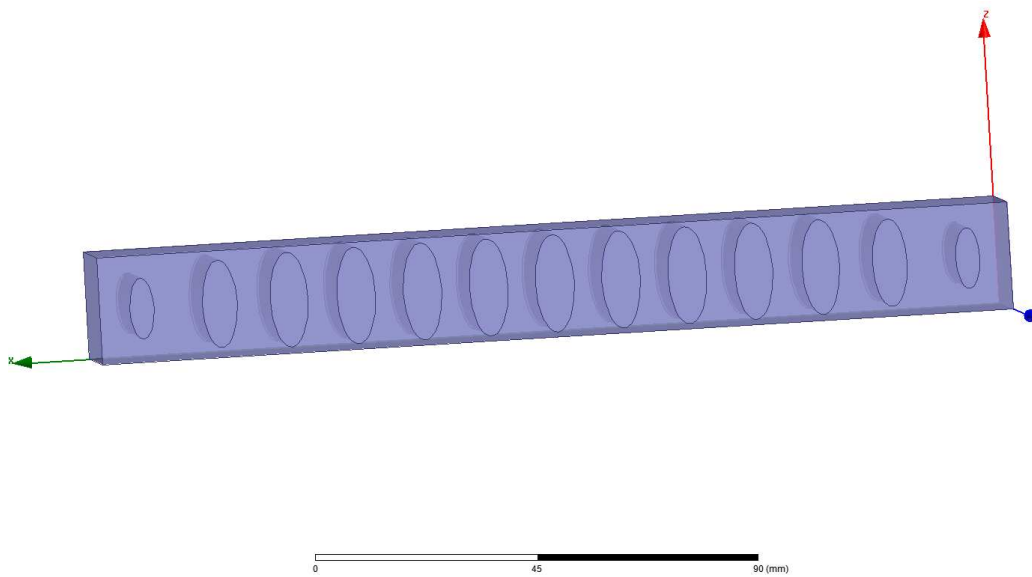


Figure 4.13: Twelfth degree LPF using elliptical posts

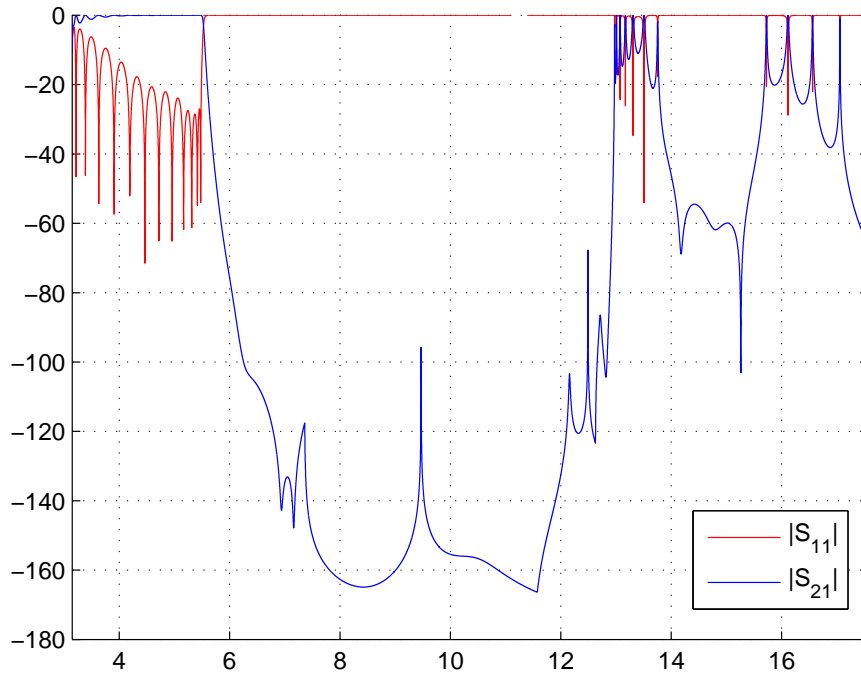


Figure 4.14: Frequency response of twelfth degree LPF using elliptical posts

4.3 Analysis of Results

In this section we study the effect that each of the input parameters has on the final frequency response of the filter, and compare the different post shapes and function types. To fully describe each filter designed we give two sets of values, defining the post dimensions and positions inside the waveguide. Differently to what was done in the previous section, we give the position of the posts by listing the distance between the centers of adjacent posts (d), instead of the computed waveguide length associated to each post plus transmission lines. Obviously the conversion between these two values is immediate. Each value of R and d is numbered sequentially, and the vertical position of the posts is always such that the gaps dimensions are uniform at each inverter (the placement of the posts could be different, as long as the design technique is executed as explained). All dimensions are given in millimeters.

4.3.1 Variation of the prescribed Return Loss level.

This parameter controls the ripple level in the passband. For higher values of this parameter, the ripple will be lower, at the cost of slightly worse rejection in the stopband. We will take the filter specification of the previous section, realized with post pairs, and vary RL . The specifications of the original filter are shown table 4.5

Function type	Chebyshev
Filter degree (N)	6
Prescribed Return Loss	25
θ_c	30°
WG dimensions	$a = 47.55mm, b = 22.5mm$ (WR-187)
WG freq. range	3.95 to 5.85 GHz
Cutoff frequency	5.5 GHz

Table 4.5: Filter specification of the first filter designed

We will design two additional filters for Return Loss levels of 22 dB and 28 dB.

	$RL = 25$	$RL = 22$	$RL = 28$
$K''_{1,7}$	0.75344	0.72018	0.78392
$K''_{2,6}$	0.49101	0.46182	0.5218
$K''_{3,5}$	0.3726	0.35535	0.39209
K''_4	0.34581	0.33251	0.36109

Table 4.6: Inverters values for filter designs with different prescribed Return Loss

As we see, the prescribed Return Loss level affects the value of the impedance inverters obtained in the synthesis in a quite simple manner, giving higher values of K_i (smaller posts) for higher values of RL and viceversa, as seen in table 4.7

	$RL = 25$	$RL = 22$	$RL = 28$
$R_{1,7}$	2.5517	2.7426	2.3738
$R_{2,6}$	3.8414	3.9634	3.6966
$R_{3,5}$	4.3623	4.4366	4.2803
R_4	4.4762	4.5331	4.4128

Table 4.7: Radius values (mm) for filter designs with different prescribed Return Loss

With these values, as always, we compute the position of the ports for each post pair that gives the phase condition $\angle S_{21} = -90^\circ - \theta_c$ and finally cascade the elements to obtain the final structure. The computed distance in millimeters between the centers of consecutive post pairs is shown in table 4.8 and Figure 4.15 compares the three filter responses. The difference in return loss is clear, and it also results in a variation of the rejection performance of the filter.

	$RL = 25$	$RL = 22$	$RL = 28$
$d_{1,6}$	20.1023	19.8764	20.3018
$d_{2,5}$	18.7375	18.5547	18.9476
$d_{3,4}$	18.1441	18.0207	18.2983

Table 4.8: Computed distance between posts (mm) for filter designs with different prescribed Return Loss

4.3.2 Variation of the Commensurate Line length θ_c

This is the parameter that most directly affects the spurious free range of the filter, since it controls how the ideal frequency response is transformed to the θ plane (see chapter 3, section 2), with higher values of θ_c making the first spurious band appear closer and viceversa. As we make θ_c smaller, the posts required become larger, and the length of the waveguide section associated to each post becomes smaller due

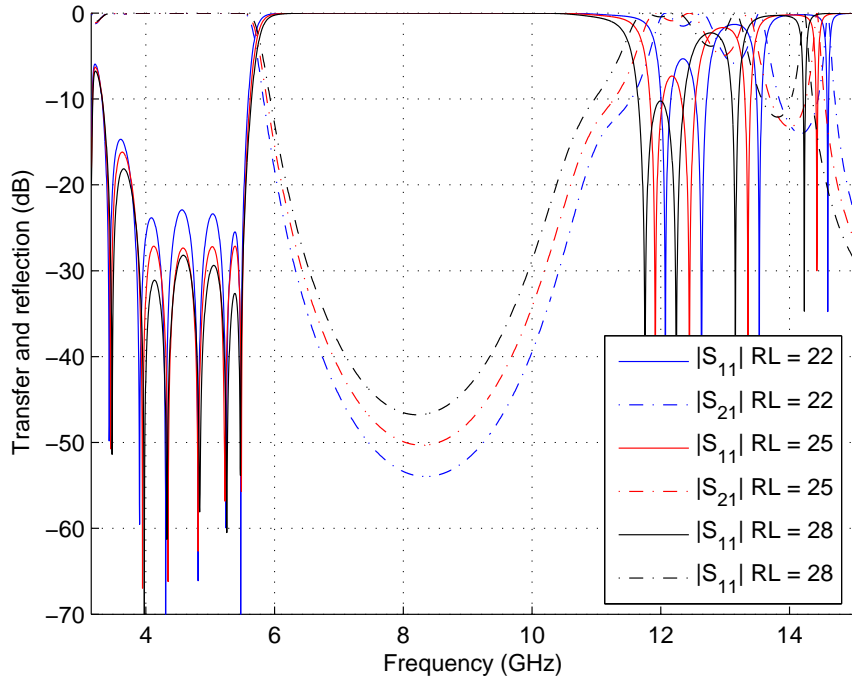


Figure 4.15: Comparison of frequency response varying the prescribed Return Loss

to the phase condition $\angle S_{21} = -90^\circ - \theta_c$, thus making the posts be closer, making the filter unrealizable if the value is too low. For these reasons, this parameter has to be chosen carefully for each design, depending on the specific requirements. Since the type of post also affects the spurious response, filters that may not be realizable using for example a single circular post, may be achievable using elliptical posts, post pairs, or any other topology.

Taking the filter specification of the first filter (see table 4.5), we compare the element values and the frequency response for various values of θ_c . The filters are designed using circular post pairs. Tables 4.9, 4.10 and 4.11 show the values of K_i , R_i and $d_{i,i+1}$ obtained in the synthesis of three filters with $\theta_c = 30^\circ, 26^\circ$ and 34° .

	$\theta_c = 30$	$\theta_c = 26$	$\theta_c = 34$
$K''_{1,7}$	0.75344	0.71101	0.79029
$K''_{2,6}$	0.49101	0.42634	0.55488
$K''_{3,5}$	0.3726	0.31578	0.43293
K''_4	0.34581	0.2934	0.4022

Table 4.9: Inverter values for filter designs with different prescribed transmission line length θ_c

	$\theta_c = 30$	$\theta_c = 26$	$\theta_c = 34$
$R_{1,7}$	2.5517	2.7856	2.3352
$R_{2,6}$	3.8414	4.1247	3.5522
$R_{3,5}$	4.3623	4.6051	4.0963
R_4	4.4762	4.6907	4.2338

Table 4.10: Radius values (mm) for filter designs with different prescribed transmission line length θ_c

	$\theta_c = 30$	$\theta_c = 26$	$\theta_c = 34$
$d_{1,6}$	20.1023	18.9757	21.1698
$d_{2,5}$	18.7375	17.5089	19.9607
$d_{3,4}$	18.1441	16.9650	19.3811

Table 4.11: Computed distance between posts (mm) for filter designs with different prescribed transmission line length θ_c

Figure 4.16 shows the frequency response of the three filters. As expected, the spurious free range is the main difference between the three designs, with the pass-band response being very similar.

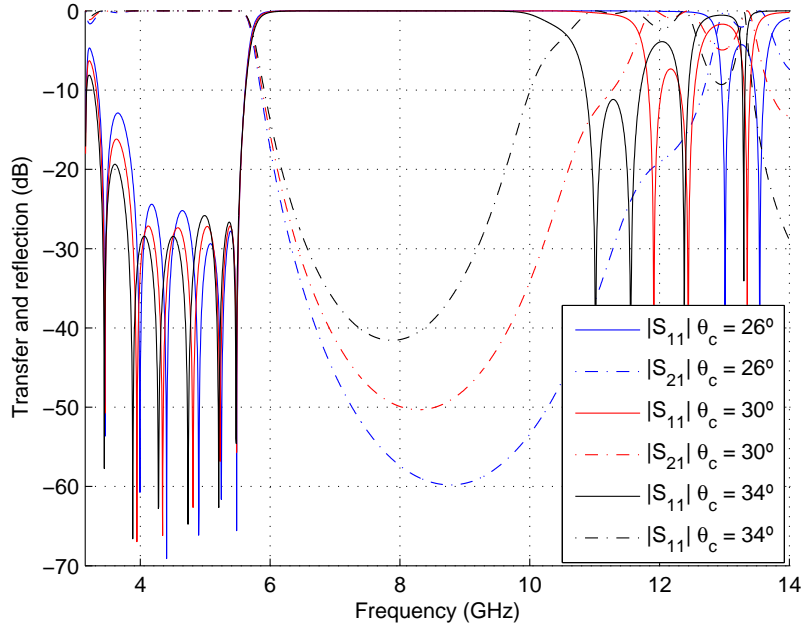


Figure 4.16: Comparison of frequency response varying the Commensurate Line length θ_c

4.3.3 Comparison of different post topologies

We have mentioned multiple times that different topologies can be used as long as the conditions to realize the network elements are fulfilled. The small GUI developed allows the automatic design of these filters using any number of posts (circular or elliptical) aligned vertically to realize each inverter. I show some examples using the filter specification of table 4.5, using the basic topologies depicted in Figure 4.17: a single circular post, an elliptical post of axial ratio 0.75, a post pair (done earlier), and a group of three posts. The physical dimensions computed for each topology are shown in tables 4.12 and 4.13. Figures 4.18, 4.19, 4.20 and 4.21 show the filters designed, and Figure 4.22 compares their frequency responses. The pass-band performance is almost identical, but the spurious free range varies for each implementation, as we cannot force the structure to realize the theoretical circuit at every frequency (the filters are identical at 5.5 GHz, the design frequency). Topolo-

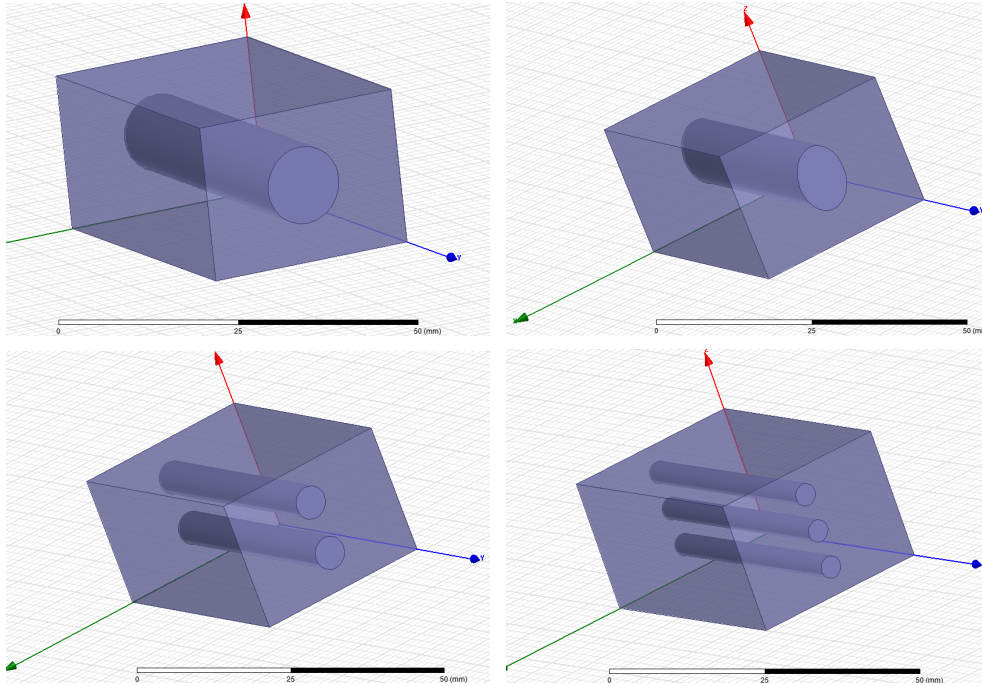


Figure 4.17: Different post topologies to realize the LPF

gies that have a wider spurious free range, due to a smaller post dimensions along the propagation axis, will generally require smaller gaps between the posts and the waveguide walls.

	Circ. Post	Ellip. post	2 Circ. Posts	3 Circ. Posts
$R_{1,7}$	3.821	4.1009	2.5517	1.999
$R_{2,6}$	6.3575	6.6109	3.8414	2.8648
$R_{3,5}$	7.6504	7.7824	4.3623	3.1628
R_4	7.9621	8.0607	4.4762	3.2248

Table 4.12: Radius values (mm) for filter designs using different topologies

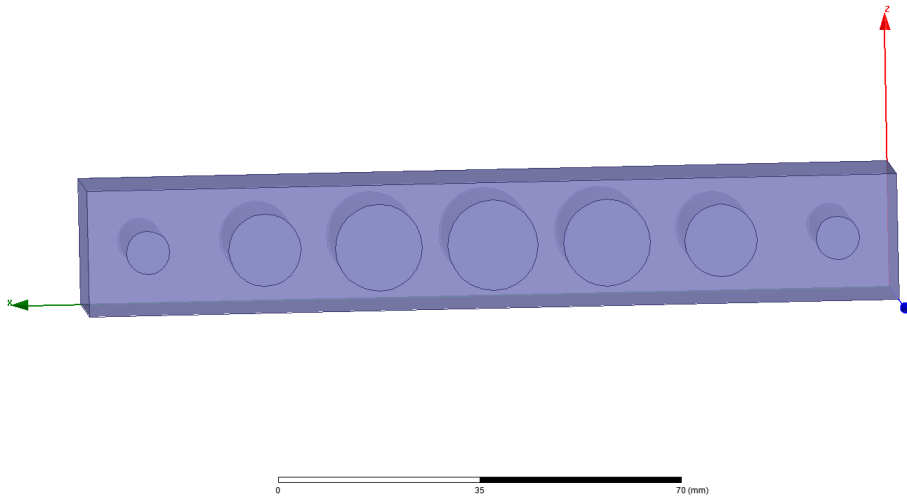


Figure 4.18: Low pass filter using single circular posts as impedance inverters

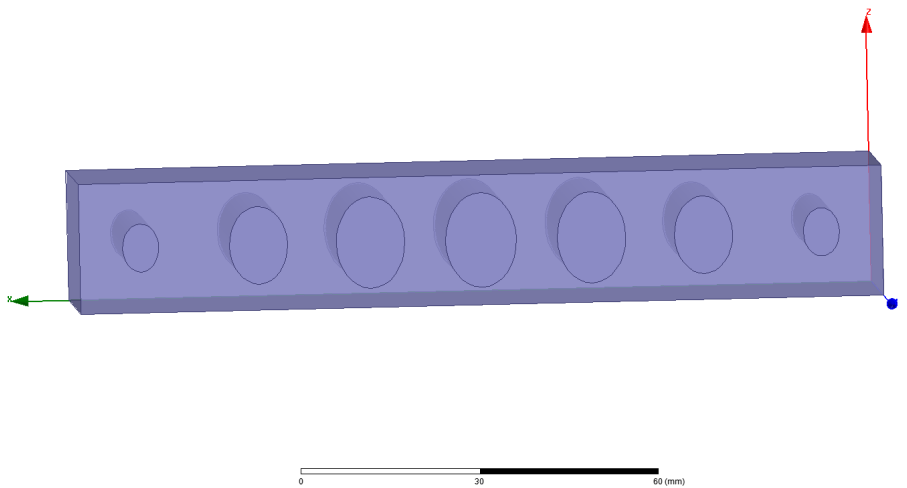


Figure 4.19: Low pass filter using single elliptical posts (axis ratio 0.75) as impedance inverters

	Circ. Post	Ellip. post	2 Circ. Posts	3 Circ. Posts
$d_{1,6}$	20.5822	19.9152	20.1011	19.7261
$d_{2,5}$	20.0737	18.6052	19.1153	17.8959
$d_{3,4}$	20.1171	18.0816	18.8466	17.0437

Table 4.13: Computed distance between posts (mm) for filter designs using different topologies

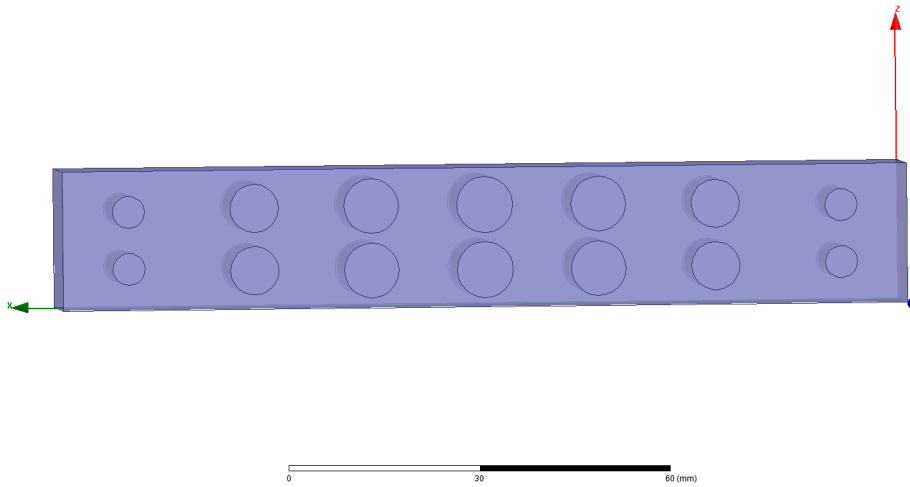


Figure 4.20: Low pass filter using circular posts pairs as impedance inverters

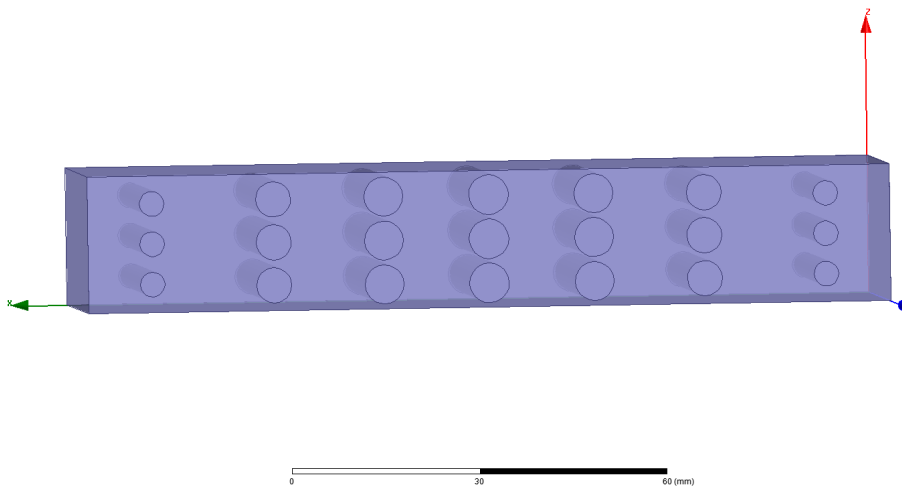


Figure 4.21: Low pass filter using three circular posts as impedance inverters

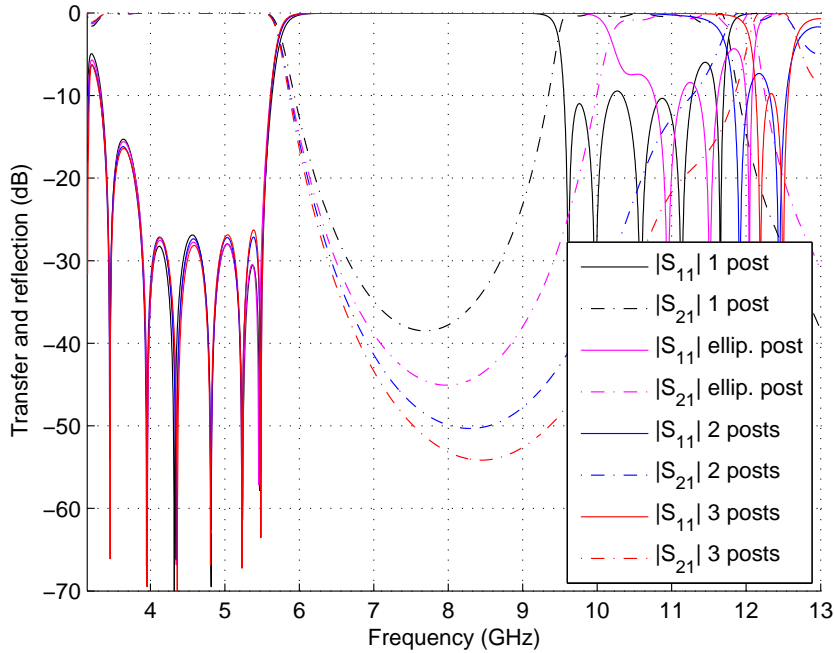


Figure 4.22: Comparison of frequency responses using different topologies

Note that the filters have simply been designed with the theoretical filtering function, to see how the frequency response varies (mainly the spurious-free range). This means that the in-band response is in theory identical and they all present the same scattering parameters at the cutoff frequency of 5.5 GHz. In a practical application, we would have tried to obtain the same frequency response for all the topologies, varying the synthesis parameters (mainly θ_c , since the difference lies in the spurious band). Having done this, the filters would be compared using other criteria, such as power handling or sensitivity to manufacturing errors.

4.3.4 Comparison of the different types of filtering functions

We compare the Chebyshev, Zolotarev and Chained function responses of the same degree, using the same theoretical transmission line length θ_c and the same maximum allowed return loss and utilizing the double post topology. This is done

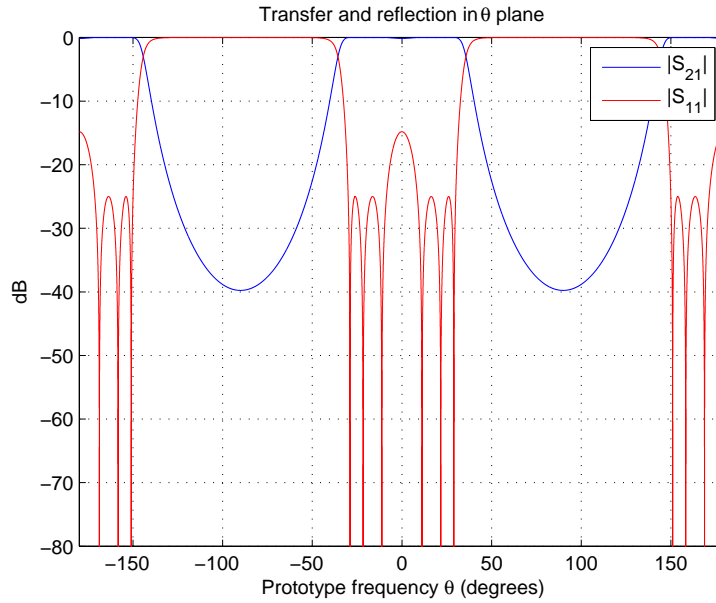


Figure 4.23: Ideal frequency response of sixth-degree Zolotarev filter

	Chebyshev	Zolotarev	Chained
$K''_{1,7}$	0.75344	0.71795	0.86317
$K''_{2,6}$	0.49101	0.47682	0.63021
$K''_{3,5}$	0.3726	0.35612	0.45811
K''_4	0.34581	0.34553	0.41648

Table 4.14: Inverter values for filter designs using different filtering functions types

simply for illustrative purposes, and a proper comparison, where we adjust the return loss to obtain the desired response in all three cases is done later. For the Zolotarev filter we have chosen $x_1 = 0.3$, and the Chained filter is a cubed second-degree Chebyshev function. Figures 4.23 and 4.24 show the ideal response of the Zolotarev and Chained filters. The element values and dimensions corresponding to these filters are shown in tables 4.14, 4.15 and 4.16.

As expected, the Chained filter yields notably smaller posts, since its based on lower degree functions. The Zolotarev filter presents posts of dimensions similar to those of the Chebyshev filter. Figures 4.25 and 4.26 show the frequency response of

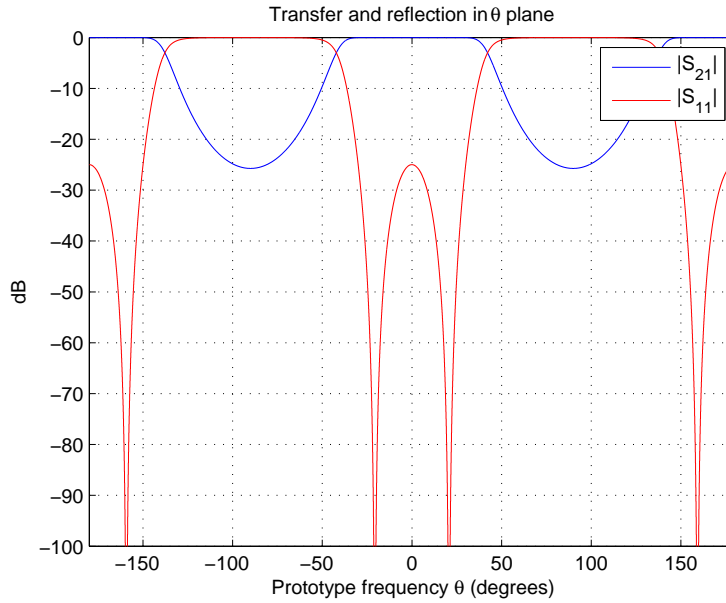


Figure 4.24: Ideal frequency response of sixth-degree (2^3) Chained Chebyshev filter

	Chebyshev	Zolotarev	Chained
$R_{1,7}$	2.5517	2.758	1.8603
$R_{2,6}$	3.8414	3.9122	3.2014
$R_{3,5}$	4.3623	4.4352	3.9814
R_4	4.4762	4.4744	4.1749

Table 4.15: Radius values (mm) for filter designs using different filtering functions types

	Chebyshev	Zolotarev	Chained
$d_{1,6}$	20.1023	19.9152	20.8760
$d_{2,5}$	18.7375	18.6052	19.5847
$d_{3,4}$	18.1441	18.0816	18.7968

Table 4.16: Computed distance between posts (mm) for filter designs using different filtering functions types

the Zolotarev and Chained filters respectively, and Figure 4.27 compares the three responses. Obviously all three filters present the prescribed return loss at the design frequency (5.5 GHz), but the differences between the three functions are depicted clearly. In the Zolotarev response we can clearly appreciate the higher reflection lobe around the center of the passband, before the equiripple frequencies start. As was seen in chapter 2, the width of this lobe is controlled by the parameter we have denoted as x_1 (if $x_1 = 0$ we obtain a Chebyshev response). As for the Chained filter, due to the highly dispersive nature of the waveguide near the cutoff frequency of the first mode, the ideal response of two reflection zeros cannot be achieved, but the effect of placing the reflection zeros together is evident in the second half of the passband, around 5 GHz. If the utilized frequencies are in this area, the return losses are very low. When comparing the three responses, it is clear that the rejection of the Chained filter is notably worse, with the Chebyshev and Zolotarev filter presenting very similar performance. It is interesting to note that as the value of x_1 increases, the rejection improves, with the obvious downside of less utilizable bandwidth.

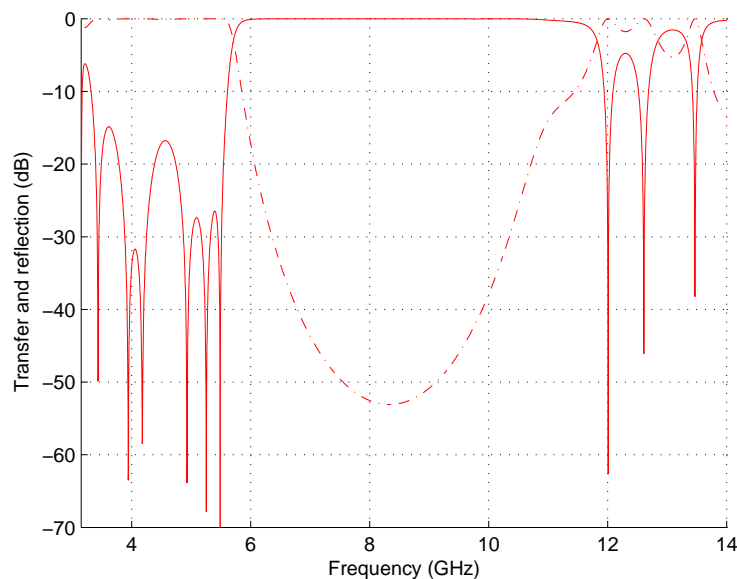


Figure 4.25: Frequency response of sixth-degree Zolotarev filter

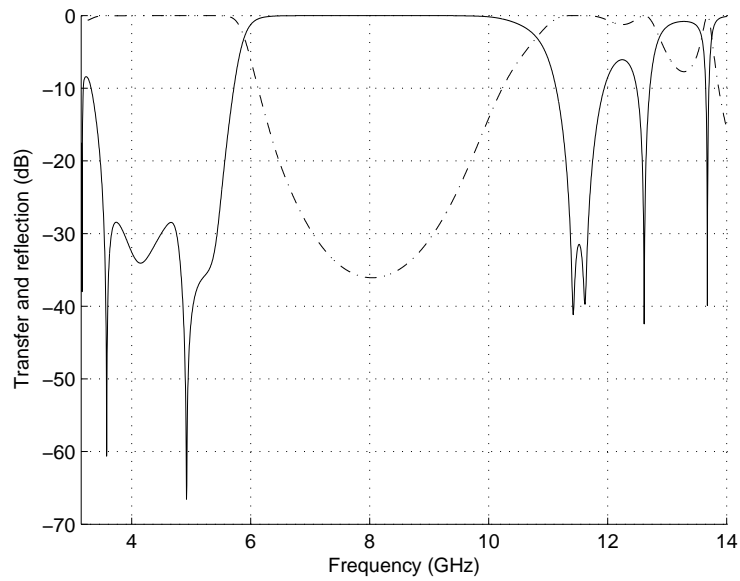


Figure 4.26: Frequency response of sixth-degree (2^3) Chained Chebyshev filter

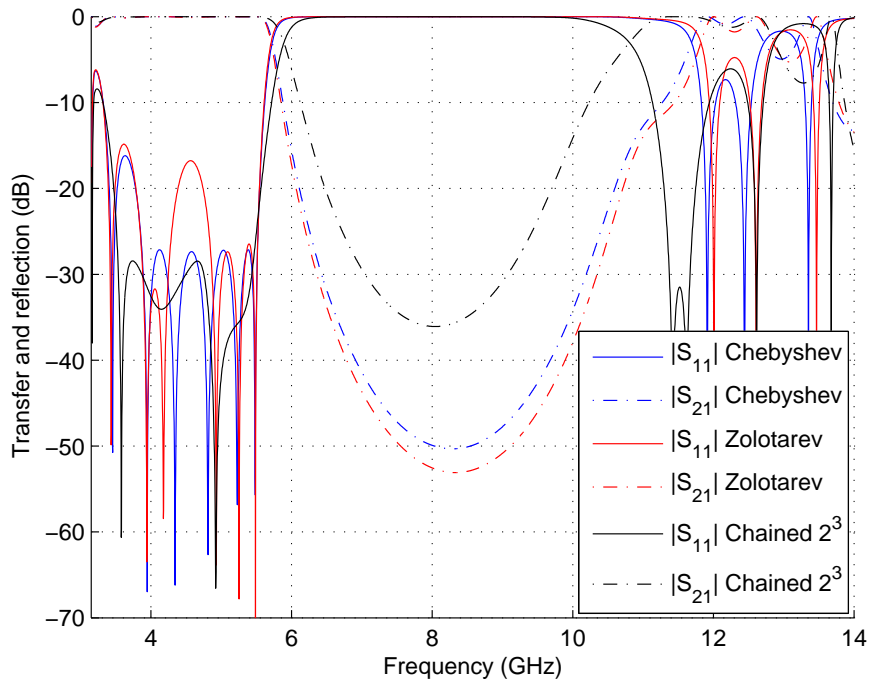


Figure 4.27: Comparison of frequency response using different filtering function types

4.3.5 Using MATLAB-HFSS interaction to optimize the filter design

When designing a microwave filter, we will most likely have to comply to a set of specifications that cannot be immediately translated into a set of values for the design parameters we have seen, at least not with absolute precision, due to various factors like waveguide dispersion and frequency dependance of the impedance inverters. For example, we may require a certain attenuation at a given frequency, a prescribed spurious-free range or a maximum gap dimension we cannot surpass.

One advantage of using scripting to control the HFSS designs and simulations is that we can iteratively create a design, analyze the results, and modify one or more of the input parameters depending on this data until we obtain a design that satisfies the specification, all done by a MATLAB script. We will show a simple example of this application, where we modify the prescribed return loss level in the passband for the three filters based on the three different function types we have seen: Chebyshev, Zolotarev and Chained 2^3 (using *2nd* degree Chebyshev polynomials as seed) until they all present a set attenuation at a certain frequency. This will also serve as a better comparison between the different filtering functions.

I have arbitrarily chosen to design a filter that presents an attenuation of 20 dB at frequency 6.4 GHz with a cutoff frequency of 5.5 GHz, implemented using a single post topology. We have seen that the rejection of the Chained filters is substantially worse than that of Chebyshev and Zolotarev filters, meaning it will require a lower value of RL (higher maximum loss in the passband) to achieve the same level of rejection. After convergence, the values of RL obtained for each filter are shown in table 4.20. Results are as expected: Zolotarev requiring slightly lower maximum return loss to achieve the desired rejection, and Chained requiring a much higher value. Tables 4.18 and 4.19 list the radii and positions of the posts, and Figure 4.28 presents the frequency response of each filter.

	Return Loss (dB)
Chebyshev	30.5969
Zolotarev	32.5643
Chained Chebyshev	18.9508

Table 4.17: Computed values of Return Loss to achieve a prescribed value of attenuation

	Chebyshev	Zolotarev	Chained
$R_{1,7}$	3.2967	3.3944	3.2122
$R_{2,6}$	5.7682	5.7641	5.6071
$R_{3,5}$	7.2171	7.237	7.3248
R_4	7.6108	7.555	7.6331

Table 4.18: Radius values (mm) for filter designs using different filtering functions types, after iterative optimization

	Chebyshev	Zolotarev	Chained
$d_{1,6}$	20.7827	20.7612	20.8286
$d_{2,5}$	20.1221	20.1281	20.1562
$d_{3,4}$	20.0422	20.0392	20.1466

Table 4.19: Computed distance between posts for filter designs using different filtering functions types, after iterative optimization

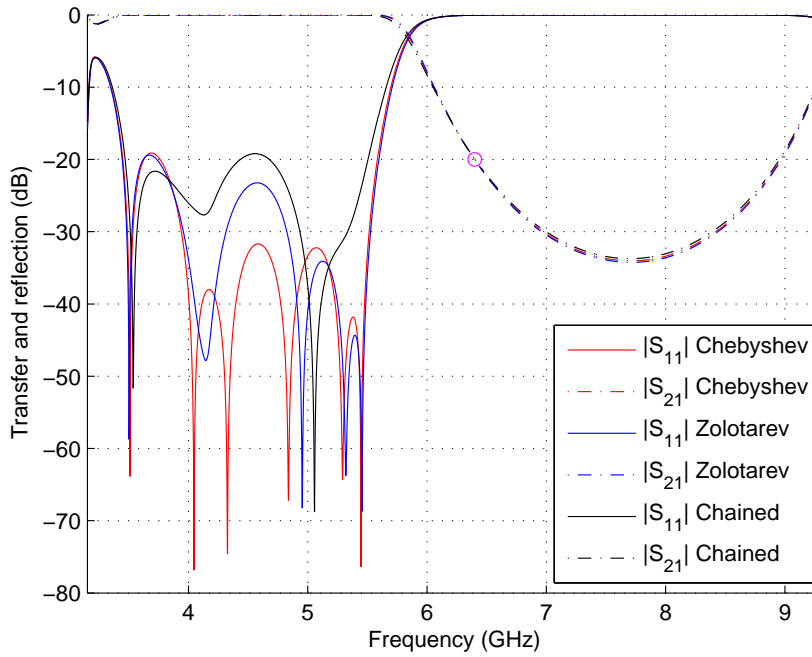


Figure 4.28: Frequency response of three filters with the same rejection performance

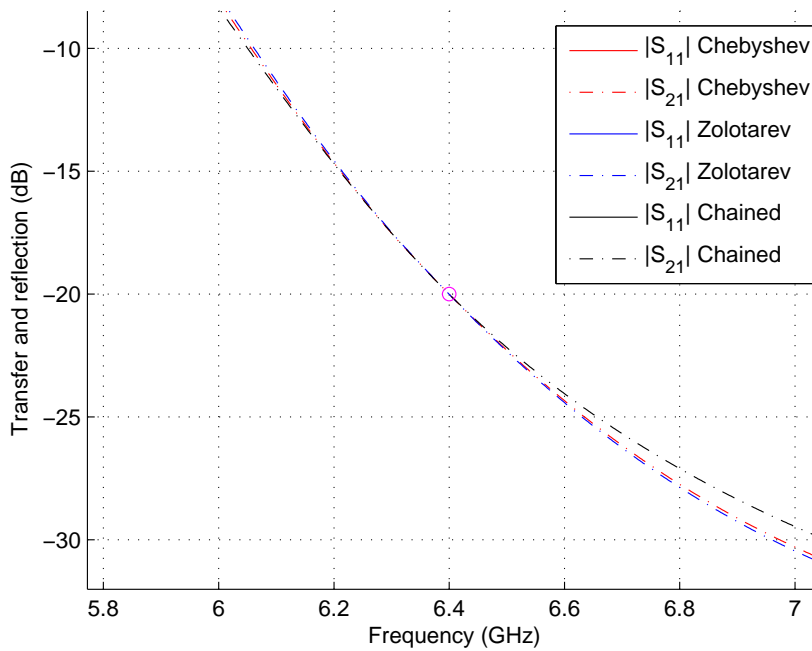


Figure 4.29: Designated frequency point of equal rejection for the three filters

The post dimensions are very similar in all three designs, and they present almost exactly the same out of band response due to the iterative process. The fact that the Zolotarev function naturally presents slightly better rejection than the other two functions here translates into less return loss in the reduced passband and a smaller maximum post dimension, since we forced the rejection to be the same. Also, by increasing the value of x_1 , which controls the start point of the equiripple zone for Zolotarev polynomials (see chapter 3), we could increase the rejection of the filter. This comes at an obvious cost: we would be making the usable passband narrower by increasing the width of the high-reflection lobe. In a real application, this lobe could be made to be as wide as the required bandwidth allows. In this regard, the Chained filter stands in a similar position to the Zolotarev: if we look at the entire passband, the performance is worse around the center, but if we are interested only in the frequencies around the reflection zero, the return loss is also very low for several hundreds of megahertz. If the center of the band does not matter, we could design a filter with very high return loss as long as the necessary frequencies are near the reflection zero, in order to build a filter with better rejection. Depending on the maximum return loss allowed, the bandwidth at which the Chained filter will be better may or may not be wide enough to meet the application needs.

To illustrate this we have designed Zolotarev and Chained filters where the required return loss is 20 dB, a typical value. For the Chained filter, we have chosen only 2 dB of return loss in the synthesis of the polynomials (an arbitrarily low value), and for the Zolotarev filter x_1 has been set to 0.55, leaving in both cases a narrow usable passband. Figure 4.30 shows the frequency response of these two filters. Figure 4.30 compares these responses with a Chebyshev filter with constant 20 dB of RL, showing that the out of band performance is slightly improved. The Chained filter can be designed to have a wider 20 dB bandwidth by increasing the value of the prescribed RL in the synthesis of the polynomials, but the advantage obtained in rejection would quickly disappear, as it already stands in a very small advantage over the Zolotarev and Chebyshev filters.

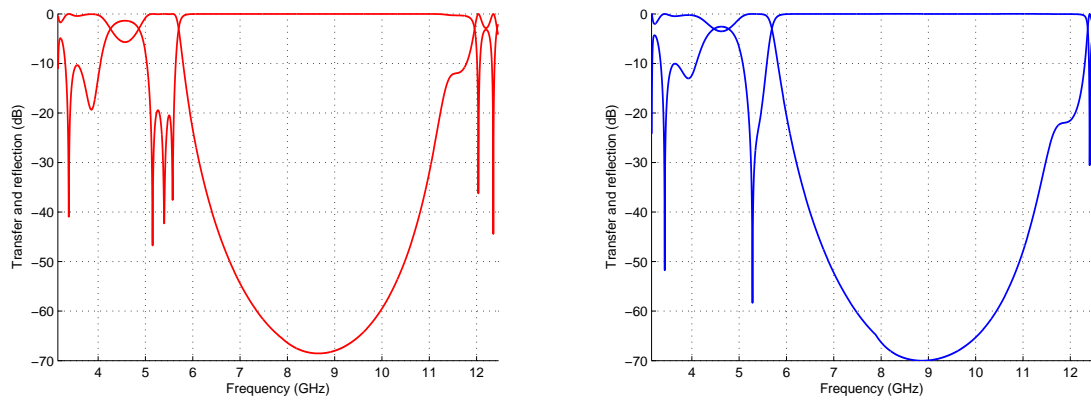


Figure 4.30: Zolotarev and Chained filters with reduced usable bandwidth to achieve better rejection than a Chebyshev filter

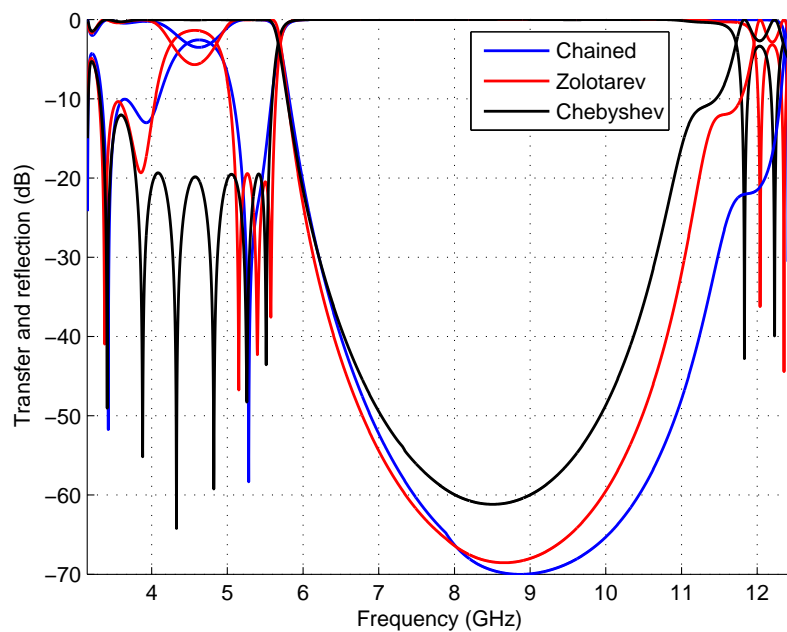


Figure 4.31: Regular Chebyshev filter compared to reduced-bandwidth Zolotarev and Chained filters

It is clear that when designing a filter for a real application, a specific comparison

20 dB bandwidth (MHz)	
Zolotarev	490
Chained	295
Chebyshev	1700

Table 4.20: Usable bandwidth (return loss of 20 dB) for each type of filtering function

would be needed, taking into account the required bandwidth, maximum return loss allowed, spurious-free band and power handling capabilities, to determine the optimal type of filtering function, although the margin of improvement over the traditional equiripple Chebyshev has resulted to be quite low.

4.3.6 Effect of manufacturing errors

To get an idea of how these filters will perform when manufactured, I have run a number of experiments where the geometry of the filter is corrupted by a random error with an uniform distribution. This will also serve to compare the sensitivity to manufacturing errors of the different function types and topologies. The results presented have been obtained by independently introducing a random variation to each of the posts radius and position coordinates, given a maximum manufacturing error.

The experiment has been done with the filters designed in the previous section, where we compared the different functions by adjusting the return loss until all three filters presented the same rejection performance. Figure 4.32 shows the results, for a maximum error of $\pm 20 \mu m$ in the radius and position of each post. In this case, the Chebyshev and Zolotarev filters present a very similar deviation from the nominal design, with the Chained filter being slightly more robust. As seen in the previous section, depending on the bandwidth required for a particular application, it could be better to utilize the Chained or Zolotarev filters, since for a limited range of frequencies inside the passband it presents less return loss. Figure 4.33 shows the yield analysis corresponding to the dual post filter of 4.9. Note that this filter cannot be compared to those of Figure 4.32, as it presents a different frequency response.

It is seen that, for the variability introduced, the filters designed in C band are resistant to manufacturing errors. I have also run this experiment for a K band filter in the standard WR-42 (same maximum error of $\pm 20 \mu m$), with a cutoff frequency of 24 GHz. Fig. 4.34 shows the results of this analysis. Despite the reduction in filter dimensions (much higher frequency), keeping the same magnitude of error, the in band return loss remains at an acceptable level, barely surpassing 20 dB in the worst case, for a filter with a specification of 25 dB. This gives us an idea of the precision that would be required to fabricate these filters.

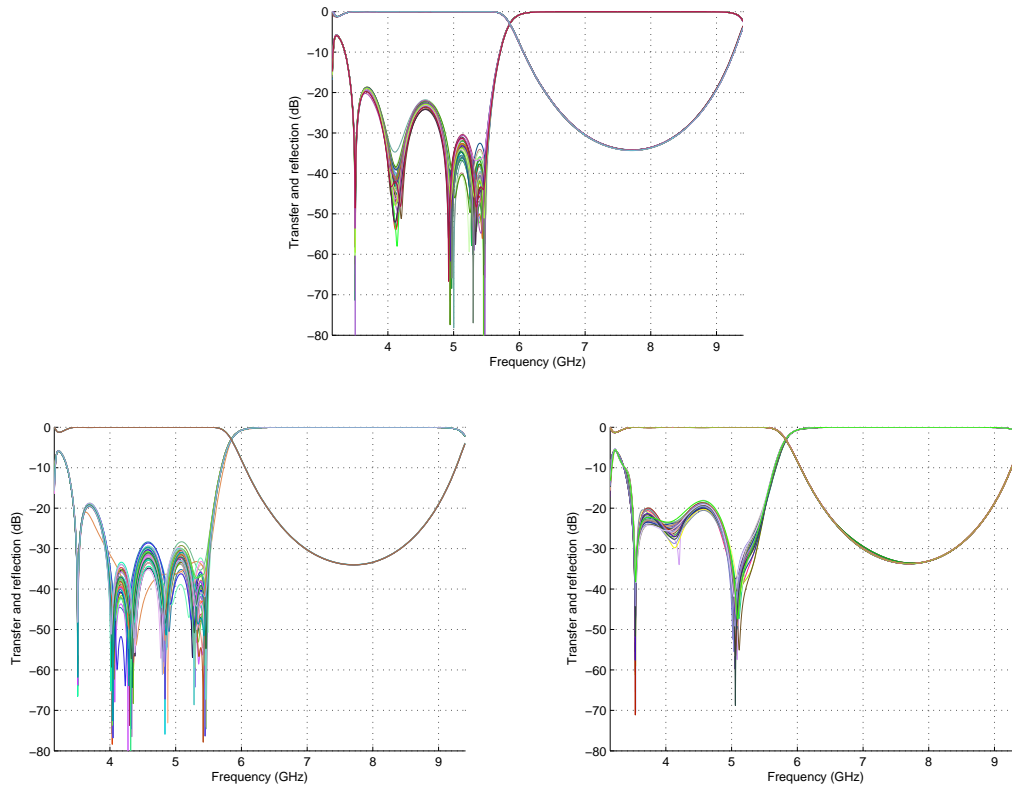


Figure 4.32: Yield analysis of sixth degree Zolotarev, Chebyshev and Chained filters with the same rejection performance (different prescribed Return Loss).

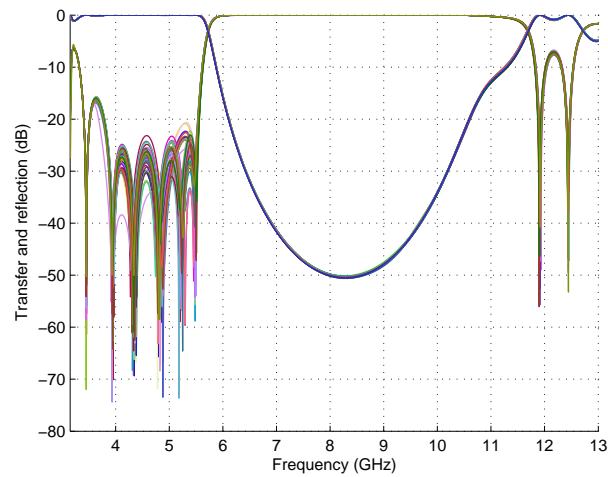


Figure 4.33: Yield analysis of sixth degree Chebyshev filter using circular posts pairs

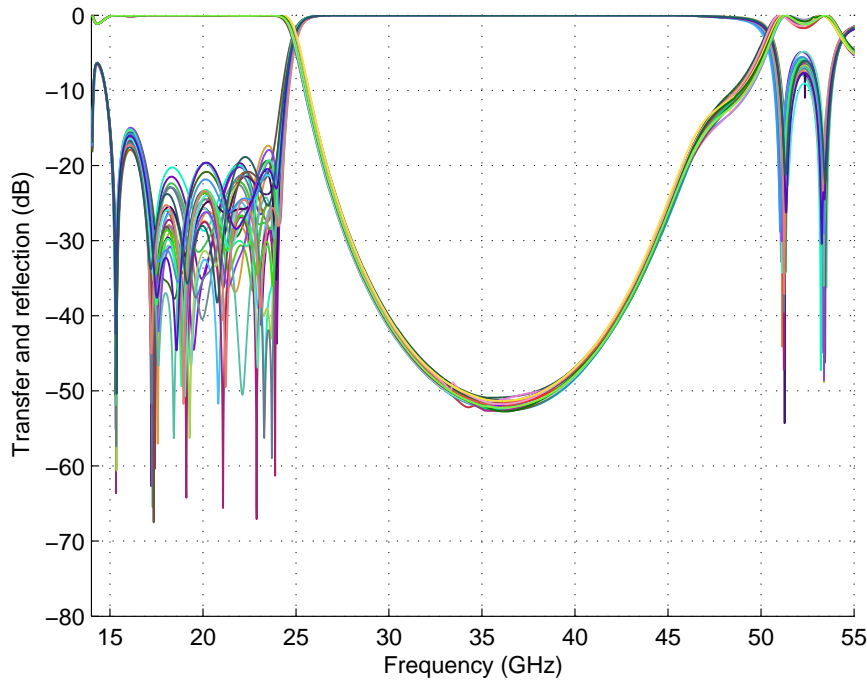


Figure 4.34: Yield analysis of sixth degree K-band filter

4.4 Additional topologies using conducting posts

In this section we briefly present additional topologies to realize the lowpass filter, based on applying certain modifications to the previous designs. All designs presented here have been yet again done with help of the MATLAB software developed in an automated fashion and they can be reproduced.

4.4.1 Post-based filter with reduced waveguide heights

In these filters, by progressively reducing the waveguide height, a wider spurious free range is obtained. To illustrate this, we have designed a filter with the same specifications of Table 4.5. The final design is shown in Figure 4.35. The input waveguide height is the same as in all designs, following the standard WR-187, $b = 22.15$ mm. This height is reduced to $0.75b$, $0.5b$ and $0.35b$ at the center of the filter. In Figure 4.36 this filter is compared to its equivalents using single circular

post inverters and double post inverters, designed in the previous section.

When designing these filters, due to the asymmetry of the network, we cannot use the parameter S_{21} to adjust the position of the ports of each inverter. This means that we have to use the reflection parameters S_{11} and S_{22} to independently adjust the phase in each port. The reflected wave phase we have to adjust is the same for both ports, $180^\circ - \theta_c$, but the lengths of the input and output sections that realize this condition will be different. We proceed as follows:

- Set a static value for the output waveguide, and adjust the length of the input waveguide until $\angle S_{11} = 180^\circ - \theta_c$.
- Set a static value for the input waveguide, and adjust the length of the output waveguide until $\angle S_{22} = 180^\circ - \theta_c$.

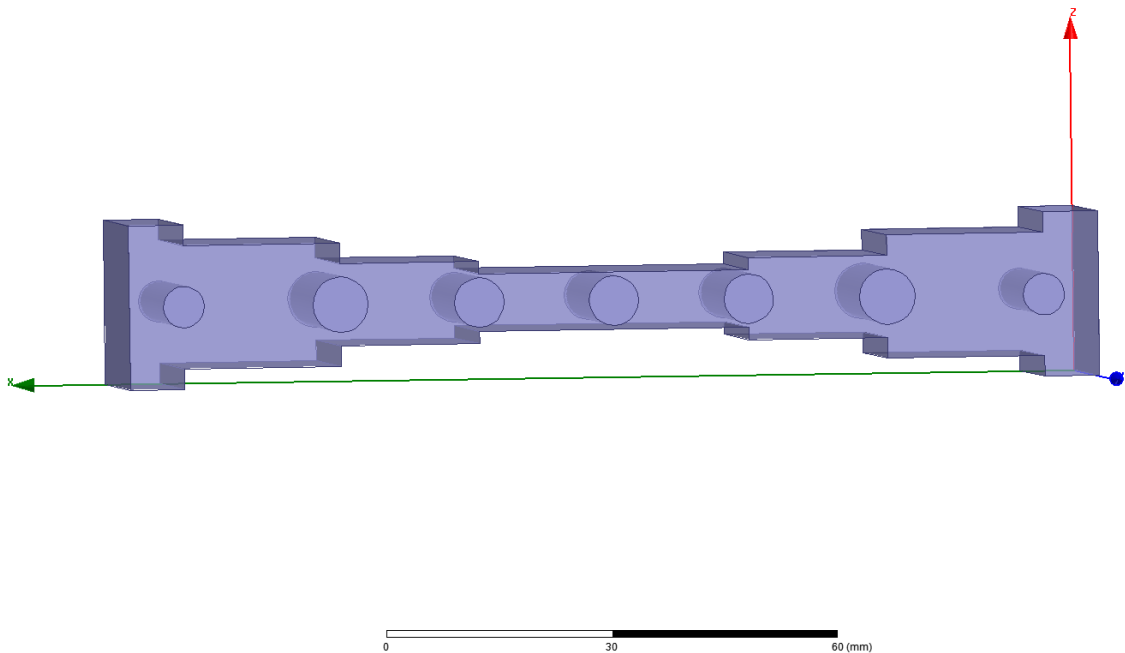


Figure 4.35: Lowpass filter using reduced waveguide height

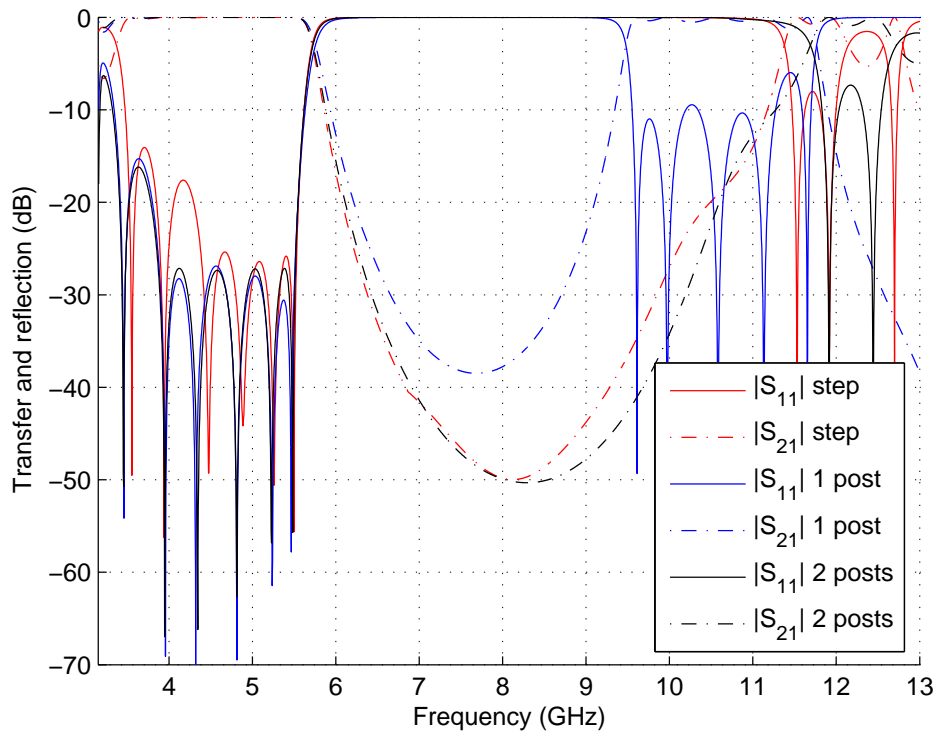


Figure 4.36: Frequency response of reduced waveguide height filter, compared with single post and double post filters in constant height waveguide.

The spurious free range of the new filter is better than the standard single post filter, and almost identical to that of the double post filter. Obviously, a filter designed combining post pairs and reduced waveguide heights would perform even better in this regard. The downside is that the lower part of the passband has been deteriorated, with a wider range of frequencies presenting higher return losses. This type of filter would also allow the utilization of fixed size posts (for example all posts having the same diameter), adjusting the height of the waveguide sections.

4.4.2 Multiple post implementation introducing a displacement to some of the posts

The variation introduced here consists of introducing a certain displacement to one (or more) of the posts implementing the impedance inverters. Doing this we have

found that transmission zeros appear at higher frequencies. The filter of Figure 4.37 has been designed with a static offset of 4mm to the central post of each inverter, which has caused the appearance of transmission zeros at frequencies near the first spurious band, making it narrower while not affecting the inband performance and barely degrading the rejection, as seen in Figure 4.38.

These transmission zeros could be very useful if we were able to control their position in order to make the spurious bands narrower, or even eliminate them by using the right offsets in each inverter. Since the entire design is automated, this possibility could be explored very efficiently, using the MATLAB functions developed.

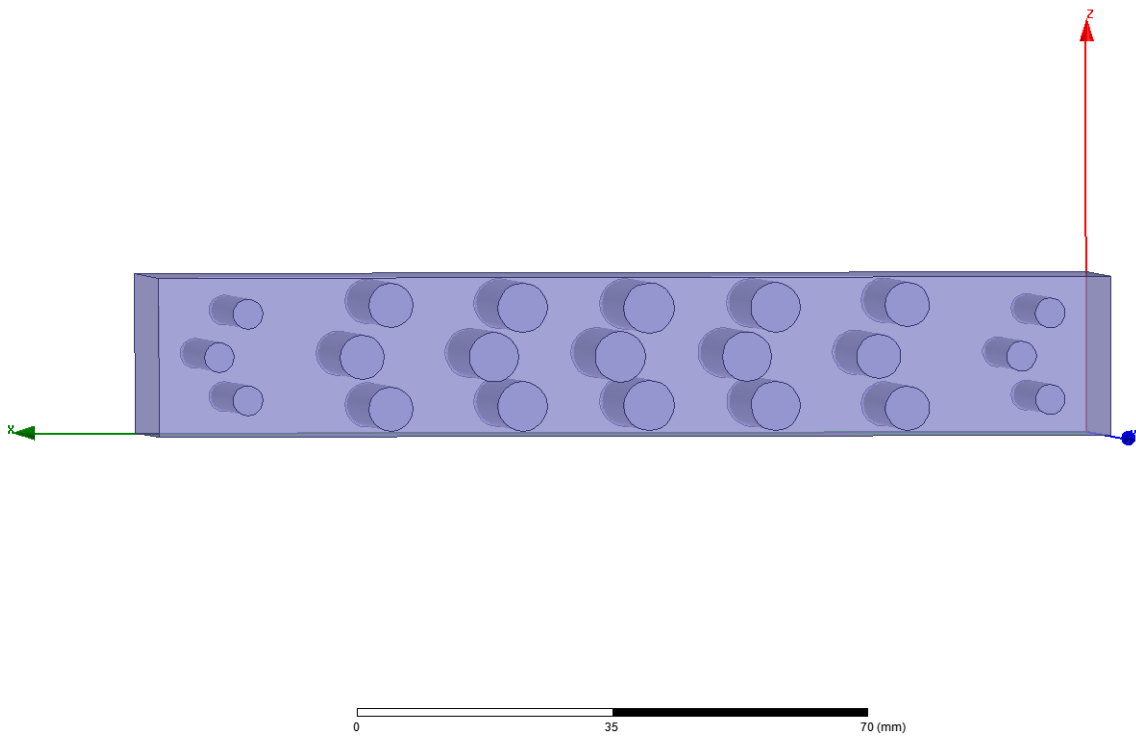


Figure 4.37: Lowpass filter using non-aligned posts

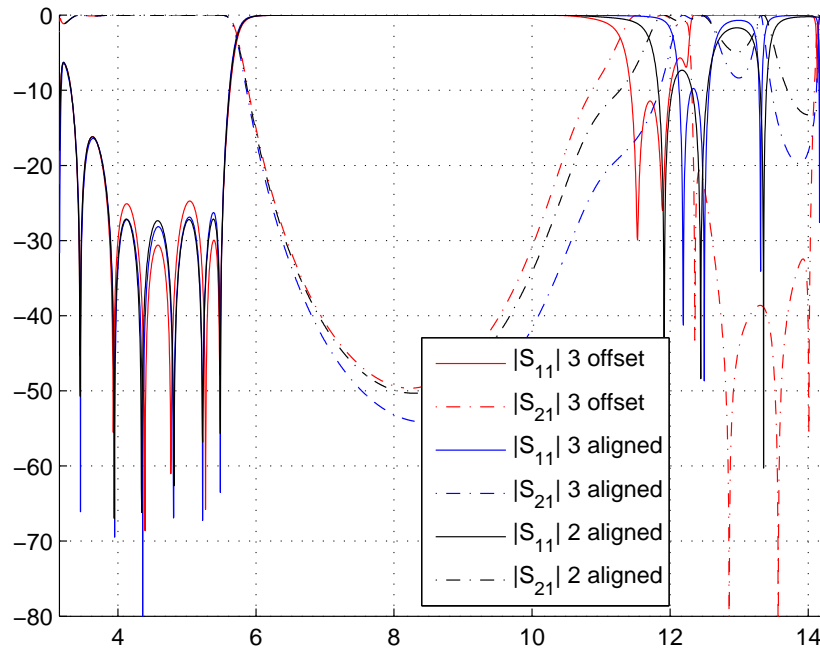


Figure 4.38: Frequency response of filter with non-aligned posts, compared with aligned double and triple post equivalent.

4.5 Realization of the Tapered-Corrugated LPF using the proposed design technique

In the previous chapter, two well known distributed low pass filter prototype circuits were described and their synthesis implemented. All the filters realized until now are based on the Stepped Impedance prototype with impedance inverters, due to it being more convenient for the topologies utilized. The only goal of this section is to adapt the design technique to the Tapered-Corrugated filter, by finding the adequate scattering parameters equations. Figure 4.39 shows an example of the network to be realized. This circuit is sliced in sections consisting of a shunt capacitance plus two transmission lines of electrical length θ_c , as shown in Figure 4.40. If this circuit is terminated in Y_{i+1} , it is immediate to obtain:

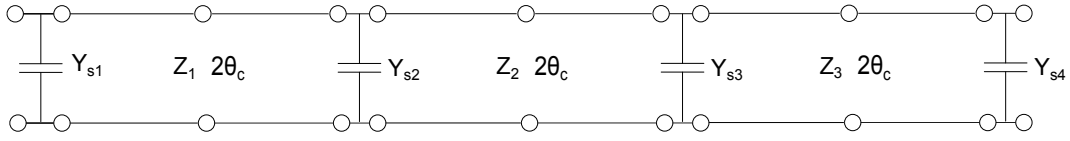


Figure 4.39: Tapered Corrugated prototype network

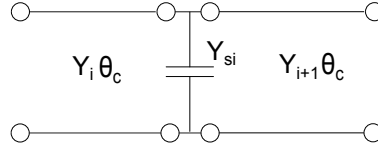


Figure 4.40: Basic network element of the tapered-corrugated filter

$$S_{11} = \frac{Y_i - (jY_s + Y_{i+1})}{Y_i + (jY_s + Y_{i+1})} \quad (4.6)$$

Obviously the expression of S_{22} is analogous, and the absolute value and phase, necessary in the two-step design technique used in this work, are found immediately using this equation. The phase corresponding to the transmission lines is $2\theta_c$. We work with the reflection parameters, and not S_{21} , because due to the asymmetry of the network the phase of the traveling wave behaves differently at each side of the capacitance, the same way it occurred in the post based filter with reduced waveguide heights. Note, however, that the aperture of the iris can be computed using any of the scattering parameters. The traditional structure that implements this small circuit is depicted in Figure 4.41. The heights of the waveguide sections corresponding to the transmission lines are obtained immediately from the synthesis (they are directly proportional to their characteristic impedance) and the aperture of the gap is adjusted to obtain the right value of S_{11} . Then, in the second step, the length of the waveguide sections is adjusted independently according to $\angle S_{11}$ and $\angle S_{22}$. We have to keep in mind that in this case, the phase condition is not constant, it depends on the value of the admittance Y_i .

If we try to design this type of filter using a WR or WG standard, the filter obtained will present a much worse frequency response than expected, both in terms of in-band return loss and spurious-free range. For this reason, the height of the

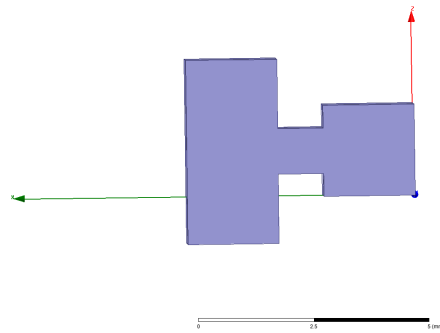


Figure 4.41: Basic network element of the tapered-corrugated filter (HFSS)

incoming waveguide has to be reduced using transformers. The amount by which this height is reduced will affect the frequency response, mostly the spurious free range, and is limited by factors such as the reflection produced by the transformer or the power handling requirements (a smaller waveguide device will be more likely to trigger multipaction). Note that this reduction of the dimensions cannot be effectively applied to the filters of the previous section, as the improvement is almost nonexistent and it results in very small gaps.

I have designed two C-band filters, with the specifications of table 4.21, using the traditional structure consisting of capacitive irises and a slightly modified topology to introduce curved surfaces (input and output transformers are not included in the design). The filters designed are shown in Figures 4.42 and 4.43. The design of these filters is automated, as it only required adapting the MATLAB scripts and functions developed to a new 3d model and using equation 4.6 instead of the expressions used previously. The second filter requires smaller minimum distances in the irises, but due to the curved surfaces it will present a much higher multipaction threshold.

Figure 4.44 shows the frequency response of both filters. They are almost identical, and the transmission zero in the rejected band is clearly appreciated (see chapter 3). The green line indicates the maximum return loss specified in the theoretical polynomials, 26 dB, showing that the filters designed barely surpass this level at any point in the passband. An interesting thing to note about these filters is that the entire passband presents roughly the same Return Loss, in contrast to all the filters

Function type	Chebyshev
Prescribed Return Loss	26
θ_c	26°
Cutoff frequency	5.5 GHz

Table 4.21: Filter specification of Tapered Corrugated Filter

of the previous section, which had a higher reflection zone at low frequency.

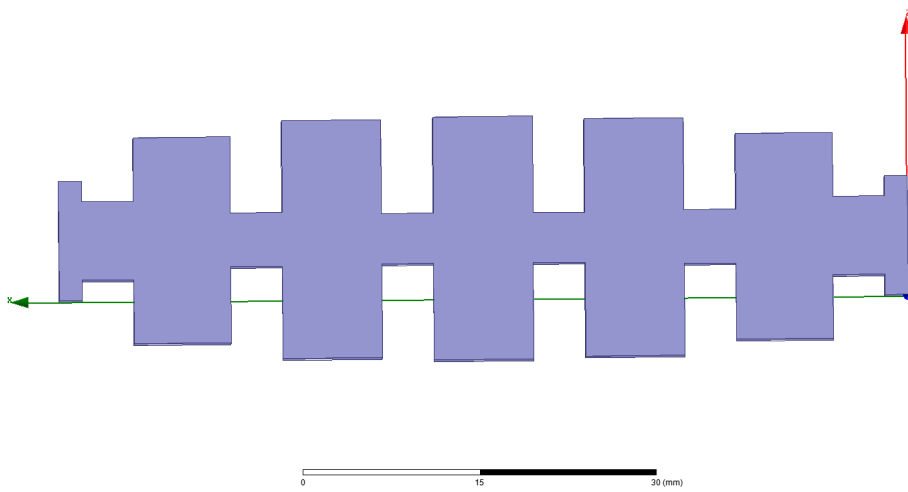


Figure 4.42: Tapered Corrugated filter using standard capacitive irises

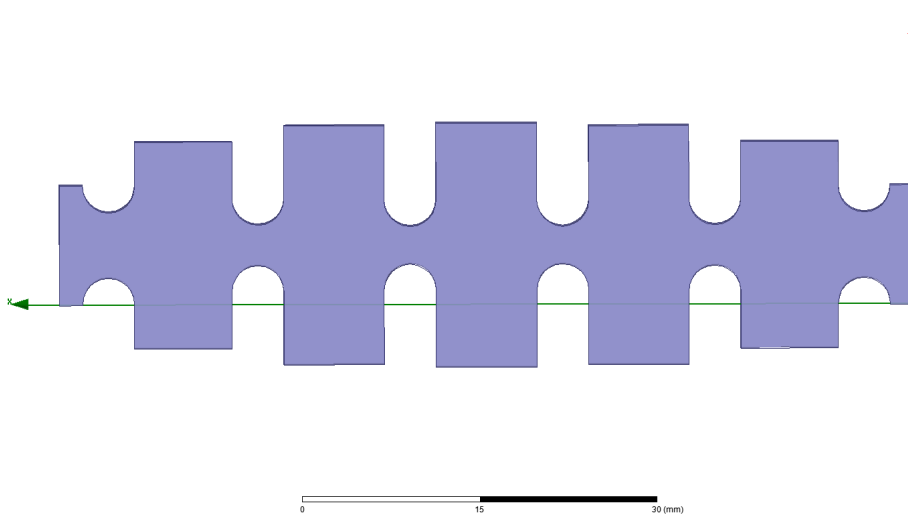


Figure 4.43: Tapered Corrugated filter using curved capacitive irises

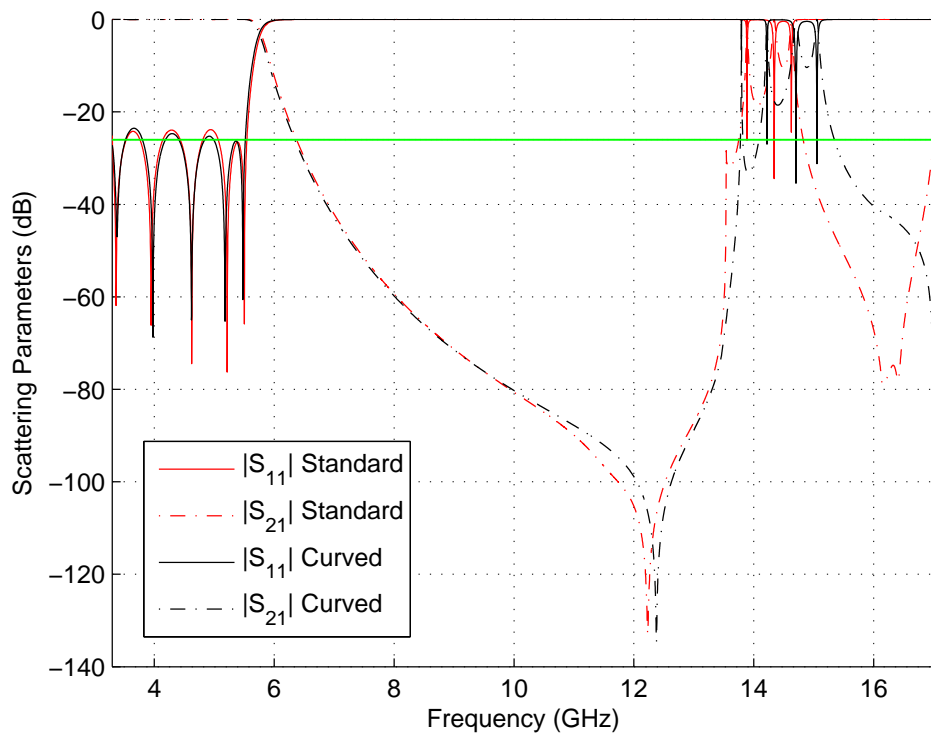


Figure 4.44: Frequency response of the Tapered Corrugated filters designed

Chapter 5

Conclusions and Future Lines of Research

Throughout this project we have covered the entire design process of lowpass microwave filters using distributed elements. These filters are necessary in space applications to suppress the harmonics generated by the high-power amplifiers, and require bandwidths in the GHz range. As a first step in the realization of the lowpass filter, in chapter 2, we have reviewed some important scattering parameter relationships (particularly the unitary conditions) and explained the synthesis method for the most commonly used polynomials, programming the required MATLAB functions to obtain them using recursive techniques. Note that even though this project has been focused on lowpass filters, these polynomials are also the basis of other types of filters.

In chapter 3 we detailed the transformations required to utilize the transfer and reflection polynomials (originally in the s or ω plane) in the synthesis of the lowpass filters based on distributed elements, working in the transformed frequency variable $t = j \tan \theta$, where $\theta = \beta l$, the electrical length of the transmission lines utilized. This transform is done to account for the periodicity in the frequency response of these distributed elements every π radians. Then, we reviewed the synthesis procedures of two possible implementations of distributed lowpass filters: the Stepped Impedance filter and the Lumped/Distributed filter.

Finally, in chapter 4 we have explored new topologies able to implement the aforementioned filters, focusing mainly on the Stepped Impedance filter using conducting posts as impedance inverters. Obviously, the software developed for chapters 2 and 3 is used here to obtain the network element values. Then, HFSS is used to match the real elements with the ideal network using a technique based on comparing the absolute value and phase of the scattering parameters. The process is explained in detail and we give multiple examples of full designs comparing multiple topologies and varying each of the parameters that control the response of the filter, and perform various yield analyses to prove that the filters are resistant to random manufacturing errors.

All the HFSS operations are controlled via scripts generated by various MATLAB functions, which not only allows the automation of the process, but also permits the interaction between MATLAB and HFSS to iteratively synthesize and analyze filters in order to obtain a design that perfectly matches the application needs. The knowledge acquired and the software developed are combined in a MATLAB GUI that implements all the design process (synthesis of filtering polynomials, synthesis of ideal filter network, and realization of physical structure using full wave simulations) for the post based filters, producing a final design in HFSS in a few minutes. To do this, the user simply has to introduce the required parameters and click a button. To design the multiple filters not included in the GUI's possibilities we have programmed separate MATLAB scripts that basically perform the same operations for each particular structure, in a completely automated, fast and precise fashion. All in all, we have proved that these topologies work and have provided useful tools for their design, even for someone unfamiliar with the synthesis techniques or the theory behind them. The realization technique presented, based on independently computing the dimensions of each impedance inverter using the absolute value and phase of the scattering parameters in two separate steps, allows a straightforward and fast design without need of any optimization, and we have showed that it can

be applied to basically any structure.

Some lines of research that open with this project include:

- Studying the power handling capabilities of the filters designed, to compare them with the standard low pass filters built with rectangular windows, and find the most optimal configurations among the topologies proposed. Some prototypes will be fabricated, and we expect an improvement in the multi-pactor threshold, due to the curved surfaces of the posts.
- Further studying the topologies presented at the end of chapter 4. We introduced the possibility of reducing the height of the waveguide along the filter in order to improve the spurious free range, and showed a design proving this concept. We also found that if a displacement is introduced to some of the posts that realize each inverter (for multi-post implementations) so that they are not vertically aligned, transmission zeros appear at higher frequencies, which could be used to reduce or even eliminate some of the spurious bands. This research could be done very efficiently using the automating software developed.
- Exploring the use of dielectric or magnetic materials in these filters.
- Exploring additional, innovative topologies to realize the Tapered-Corrugated filter. At the end of chapter 4, the design technique used throughout this work was applied to the design of these filters, including small modifications that could serve as the basis for further research.

References

- [1] F. Q. Pereira, V. Boria, B. Gimeno, D. C. Rebenaque, J. P. García, and A. A. Melcón. Investigation of multipaction phenomena in inductively coupled passive waveguide components for space applications. Technical Report TU4A-05, IEEE MTT-S International Microwave Symposium Digest, San Francisco, California, USA, 11-16 June 2006.
- [2] J. Rasch, D. Anderson, Joakim F. Johansson, M. Lisak, J. Puech, Elena Rakova, and V. E. Semenov. Microwave multipactor breakdown between two cylinders. *IEEE Transactions on Plasma Science*, vol. 38, NO. 8, August 2010.
- [3] J. Rasch, V. E. Semenov, E. Rakova, D. Anderson, J. F. Johansson, M. Lisak, and J. Puech. Simulations of multipactor breakdown between two cylinders. *IEEE Transactions on Plasma Science*, vol. 39, NO. 9, September 2011.
- [4] Richard J. Cameron, Chandra M. Kudsia, and Raafat R. Mansour. *Microwave Filters for Communications Systems*. Wiley, 2007.
- [5] Marco Guglielmi and Graham Connor. Chained function filters. *IEEE Microwave and Guided Wave Letters*, vol. 7, NO. 12, December 1997.
- [6] HFSS script generation using MATLAB. <https://www.cresis.ku.edu/~rvc/projects/hfssapi/doc/hfss-matlab-api.html>.